Technische Universität München
Fakultät für Informatik
Lehrstuhl für Informatikanwendungen in der Medizin

Computer-Assisted Navigation Methods for Screw Placement in Slipped Capital Femoral Epiphysis Surgery

Bamshad Azizi Koutenaei

Vollständiger Abdruck der von der Fakultät für Informatik der Technischen Universität München zur Erlangung des akademischen Grades eines

Doktors der Naturwissenschaften (Dr. rer. nat.)

genehmigten Dissertation.

Vorsitzende(r): Prof. Dr. Stephan Jonas

Prüfende(r) der Dissertation: Prof. Dr. Nassir Navab
Prof. Dr. Kevin Cleary
Prof. Sean Tabaie

Die Dissertation wurde am 06.10.2020 bei der Technischen Universität München eingereicht und durch die Fakultät für Informatik am 15.03.2021 angenommen.

Abstract

In the last decades, progresses in medical imaging, robotics and computational science have resulted in a move from open surgery to minimally invasive ones resulting in less morbidity, faster recovery, and therefore dramatic improvement in patient outcome. However, In Minimally Invasive Surgery (MIS) the thorough visual of the target area is not as available for surgeons as in traditional open surgery sometimes jeopardizing the precision, speed, and reliability, in particular for less-experienced surgeons. A large number of Computer-Aided Surgery (CAS) and Image-Guided Intervention (IGI) techniques have been introduced to remedy such problems by using computer technology before and during the surgery to increase accuracy and reduce invasiveness.

For orthopedic procedures, surgeons utilize intra-operative medical images such as fluoroscopy to navigate the surgical tools and confirm the position and the orientation of implants and other surgical tools. The number of fluoroscopic images needed depends on the complexity of the case and skill of the surgeon. Among orthopedic procedures, one of the most widespread hip disorders is Slipped Capital Femoral Epiphysis (SCFE). SCFE is a common precursor to hip pathology in adolescence and causes a deformity in the proximal femoral epiphysis. Currently, CAS techniques could alleviate the challenges exist in the conventional SCFE surgery duo the intricate geometry of the proximal femur. However, to perform a successful surgery using these techniques; some critical issues should be still addressed including limitation of current methods and real-time navigation and tracking.

This thesis introduces the design and validation of different novel navigation methods and techniques for screw placement during SCFE procedure taking advantage of Inertial Measurements and Robotic technologies. These methods provide projection and visualization of the surgical tool trajectory during the SCFE procedure, introducing different novel navigation solutions. The first method uses an integrated software platform and a robotic arm to guide the surgeon based on pre-operative CT images and optical tracking by aligning the drill orientation with the planned trajectory. The second method uses an Inertial Measurements Unit (IMU) to navigate the surgical tool based on two orthogonal fluoroscopic images. In the third methodology, the navigation system is designed based on two IMU devices attached respectively to the surgical tool and the imaging system. Together the IMUs provide the information needed for recovering the orthopedic tool trajectory visualized on two arbitrary orthogonal X-ray images in real-time.

After conducting more than 10 phantom studies on more than 500 bone models, these techniques resulted in faster and more efficient pre-operative calibration and set up times compared to other intra-operative navigation systems and traditional SCFE surgery. The proposed approaches improve the accuracy of surgical tool navigation, decrease the number of required X-ray images without changing the clinical workflow and addresses the limitation of existing navigation and tracking in current CAS systems. This thesis therefore position itself in the research field of Computer Assisted Surgery as one of the step stones towards better surgical guidance for more accuracy and reproducibility in minimally invasive orthopedic surgery.

Zusammenfassung

Die Fortschritte der letzten Jahrzehnte in der medizinischen Bildgebung, der Robotik und in den Computerwissenschaften führten zu einem Übergang von offener zu minimalinvasiver Chirurgie, was wiederum zu einer geringeren Morbidität, einer schnelleren Genesung und damit zu einer signifikanten Verbesserung des Ergebnisses bei Patienten führte. Im Vergleich zur herkömmlichen, offenen Chirurgie haben die Chirurgen bei einem minimalinvasiven Eingriff (Minimally-Invasive Surgery, MIS) jedoch häufig nicht die vollständige Sicht des Zielbereiches, was manchmal besonders für die weniger erfahrenen Chirurgen eine Gefährdung der Präzision, Geschwindigkeit und Zuverlässigkeit darstellt. Es wurde eine nicht geringe Anzahl von verschiedenen computergestützten Eingriffen (Computer-Aided Surgery, CAS) und bildgesteuerten Eingriffstechniken (Image-Guided Interventions, IGI) zur Behebung derartiger Problematik bei der Verwendung von Computertechnologie vor und während des Eingriffs eingeführt, um damit die Präzision zu erhöhen und die Invasivität zu reduzieren.

Für orthopädische Eingriffe verwenden Chirurgen zur Führung der chirurgischen Instrumente und zur Überprüfung der Position und Ausrichtung von Implantaten und anderen chirurgischen Instrumenten intraoperative medizinische Bildgebung wie beispielsweise die Fluoroskopie. Die Anzahl der benötigten fluoroskopischen Bilder hängt von der Komplexität des Falls und den Fähigkeiten des Chirurgen ab. Unter den orthopädischen Eingriffen ist eine der am weitest verbreiteten Hüfterkrankungen die gelöste Wachstumsfuge des Oberschenkels (slipped capital femoral epiphysis, SCFE). Eine gelöste Wachstumsfuge des Oberschenkels ist häufig der Vorläufer eines Hüftleidens im Jugendalter. Es verursacht eine Deformität in der proximalen Wachstumsfuge des Oberschenkels. Gegenwärtig könnten durch CAS-Techniken die bestehenden Herausforderungen der konventionellen SCFE-Chirurgie, nämlich die komplizierte Geometrie des proximalen Oberschenkelknochens, erleichtert werden. Um jedoch mit diesen Techniken erfolgreich operieren zu können, sollten einige der kritischen Probleme einschließlich der Einschränkung der aktuellen Methoden sowie der Echtzeitnavigation und –verfolgung angegangen werden.

Diese Arbeit ist eine Einführung in das Design und die Validierung verschiedener neuartiger Methoden und Techniken für das Positionieren von Schrauben während eines SCFE-Eingriffs unter Nutzung von Inertialmessungen und Robotertechnik. Die folgenden Methoden sind verschiedene neuartige Navigationslösungen. Sie können währen des SCFE-Eingriffs zur Projizierung und Visualisierung des Trajektorie des chirurgischen Instrument verwendet

werden. Bei der ersten Methode wird eine integrierte Software-Plattform und ein Roboterarm zur Führung des Chirurgen anhand präoperativer CT-Bilder und optischer Nachverfolgung zur Ausrichtung der Bohrung mit der geplanten Trajektorie genutzt. Bei der zweiten Methode wird eine inertiale Messeinheit (Inertial Measurements Unit, IMU) zur Navigierung des chirurgischen Instruments anhand zweier orthogonaler fluoroskopischer Bilder genutzt. Bei der dritten Methode werden zur Navigation zwei IMU-Geräte, die jeweils am chirurgischen Instrument und am Bildgebungssystem angebracht sind, genutzt. Zusammen liefern die IMUs die Informationen, die zur Wiederherstellung der auf zwei beliebigen orthogonalen Röntgenbildern visualisierten orthopädischen Instrumententrajektorie in Echtzeit erforderlich sind.

Nach mehr als 10 Phantomstudien an über 500 Knochenmodellen führten diese Techniken im Vergleich zu anderen intraoperativen Navigationssystemen und der traditionellen SCFE-Chirurgie zu einer schnelleren und effizienteren präoperativen Kalibrierung und Rüstzeiten. Die vorgeschlagenen Ansätze verbessern die Genauigkeit der Navigation von chirurgischen Instrumenten. Sie verringern die Anzahl der erforderlichen Röntgenbilder, ohne Änderung des klinischen Arbeitsablaufs und sie beheben die Einschränkung der vorhandenen Navigation und Nachverfolgung in aktuellen CAS-Systemen. Diese Arbeit liegt daher im Forschungsbereich der computergestützten Operation als ein wichtiger Schritt zur besseren chirurgischen Führung durch mehr Präzision und der Reproduzierbarkeit in der minimalinvasiven orthopädischen Chirurgie.

To my mother

With love and eternal appreciation

Acknowledgment

Firstly, I would like to express my sincere gratitude to my advisor Prof. Nassir Navab for the continuous support of my Ph.D study and related research, for his patience, motivation, and immense knowledge. I remember the night around 15 years ago when I was in my last year of high school and hopelessly sent him an email and got the most encouraging response the day after. He then invited me to visit his lab in Germany and helped me enormously to build the character who I am today. His guidance helped me in all the time of research and writing of this thesis. I could not have imagined having a better advisor and mentor for my Ph.D study.

Also, I express my utmost appreciation to my mentor and advisor Prof. Kevin Clearly for his efforts in guiding and motivating me for my thesis. He gave me the freedom to explore my interests and think outside of the box. That was the main reason I was able to finish this thesis.

My sincere thanks also goes to Dr. Matthew Oetgen, Dr. Javad Fotouhi, and Prof. Farshid Alambeigi, who provided me an opportunity to join their team, and who gave access to the laboratory and research facilities. They also helped me to conduct various experiments. Without they precious support it would not be possible to conduct this research.

I thank my fellow labmates in for the stimulating discussions, for the sleepless nights we were working together before deadlines, and for all the fun we have had in the last few years. In particular, I am grateful to Dr. Ozgur Guler, Emmanuel Wilson and Prof. Monfaredi.

I thank my good friends Dr. Faghihroohi and Sina Rezagholizade for their enormous help and motivation.

Last but not the least, I would like to thank my family: my sister, my brother and my parents for supporting me spiritually throughout writing this thesis and my life in general. In particular, I would like to thank my mother who was the most important character in my life and without her support I would not be standing where I am today.

Contents

List of Figures

List of acronyms

AR	Augmented Reality
CAMC	Camera Augmented Mobile C-arm
CAS	Computer Aided Surgery
CAOS	Computer Assisted Orthopedic Surgery
CBCT	Cone Beam Computed Tomography
CT	Computed Tomography
DOF	Degree Of Freedom
EMT	Electro Magnetic Tracking
FG	Field Generator
FLE	Fiducial Localization Error
FOV	Field Of View
FRE	Fiducial Registration Error
HMD	Head Mounted Display
ICP	Iterative Closest Point
IGS	Image Guided Surgery
IMN	Intra-Medullary Nailing
IMU	Inertial Measurement Unit
IR	Infra-Red
MIP	Maximum Intensity Projection
MIS	Minimally Invasive Surgery
MR	Mixed Reality
MRI	Magnetic Resonance Imaging
OST	Optical See Through
OT	Optical Tracking
RAS	Robotic Assisted Surgery
SCFE	Slipped Capital Femoral Epiphysis
SSE	Sum of Squared Error
THA	Total Hip Arthroplasty
TKA	Total Knee Arthroplasty
TOF	Time Of Flight
TRE	Target Registration Error
VR	Virtual Reality
VST	Video See Through

Chapter 1 – Introduction

Surgery is defined in the Cambridge dictionary as "the treatment of injuries or diseases by cutting open the body and removing or repairing the damaged part, or operation of this type" [1]. Surgeries are categorized by several factors, including the type of damaged organ, the surgical instruments used and the surgical procedure. For example, surgeries that are categorized by injured organ are neurosurgery (nervous system) and orthopedic surgery (musculoskeletal system).

Generally, surgical procedures are also classified by the degree of invasiveness, from minimally-invasive to open surgery. Minimally-invasive surgery (MIS) has a faster recovery, and less pain and damage than open surgery due to the reduction of the incision size and related clinical trauma. In a study of 233,984, patients underwent seven common surgical operations, and both the rate of complication and the medical expenses were lower after MIS for 5 and 4 of the 7 procedures examined [2]. While there are demonstrated benefits to patients, for surgeons a thorough visual of the target area, which is required for precision, is not as available with MIS. Promising recent developments in visualization, display equipment, and medical imaging compensate for this drawback [3].

Computer-Aided Surgery (CAS) or Image-Guided Intervention (IGI) is an active medical field which aids and improves the performance of the surgeon in MIS [4]. CAS is defined as using computer technology before and during the surgery to increase accuracy and reduce invasiveness [5]. Recent advances in medical image analysis, computer graphics and robotics have assisted surgeons by affording more detailed and accurate surgical planning and navigation. In the following section, major steps of CAS and some of its application are described.

1.1 What is Computer-Aided Surgery: From Planning to Post-operational Measurement

From the technical view, CAS utilizes suitable software and hardware to track the surgical instruments with respect to the patient's target area in real-time for various surgical operations. It helps clinical experts plan, perform and monitor the surgery. To achieve this, medical images of the target tissue are acquired before or during the surgery and the tracked position of the instrument is superimposed on them. A schematic of a CAS system is shown in Figure 1-1.

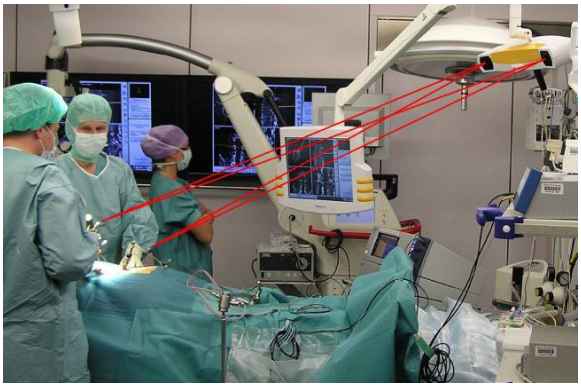

Figure 1-1. A schematic of a CAS system which tracks the patient and the surgical instrument in real time [6].

There is a high similarity between the main components of CAS and the Global Positioning System (GPS). As seen in Figure 1-2, the main components of CAS are as follows:

1- Localizer: similar to the satellite in the GPS.
2- Surgical instrument: plays the same role as a GPS device.
3- Patient images: shows the position of the instrument relative to the patient, similar to the road map in the GPS.

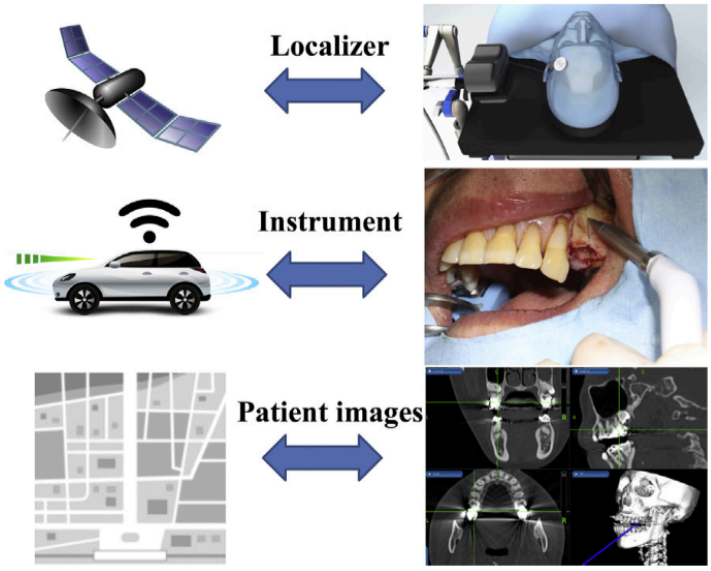

Figure 1-2. Comparison of a surgical navigation system with the Global Positioning System (GPS) [7].

Computer-assisted surgery is a general term which comprises some other expressions such as Surgical Navigation, Image-Guided Surgery (IGS), or Robotic Assisted Surgery (RAS). Surgical navigation and IGS indicate the intervention and using medical images before and during the surgery, while RAS considers the applications of the robotics in CAS. The role of robots in RAS is to augment surgeons' skills by enabling them to perform complex and subtle surgeries with more control and dexterity [8]. Some of most famous surgical robotic technologies have been presented by Peters et al [9]. In this review, several components such as degree of freedom (DOF), number of robotic segments, surgical purpose, FDA status, and commercial availability have been investigated.

To become more familiar with a CAS system, it would be valuable to examine its advantages. Some of main benefits of a CAS system are that [10]:

1- CAS reduces the area of the surgical region around the treated organ and accordingly reduces morbidity, surgery time, and post-operative hospitalization.
2- Using advanced surgical navigation techniques and real-time feedback greatly improves the accuracy and control of surgical procedures. Particularly, it enables surgeons to know where they are during the surgery and how they can safely reach the target using the tracked surgical instruments.

In the next sections, we investigate several phases and components of a CAS system and introduce some of its most prominent applications, including the concept of Augmented Reality and its use in CAS.

1.1.1 Various Phases of CAS

To be more acquainted with a CAS system, it is necessary to understand the general phases of its use during the surgical process. As observed in Figure 1-3, the navigation planning in CAS happens in three phases [11]:

1- Pre-operative planning: the process for CAS begins before surgery and typically includes data collection and modeling based on acquired pre-operative images.
2- Intra-operative navigation or execution: the most vital phase of CAS which enables navigation during the surgical operation. The main components of this phase are registration, tracking, and visualization.
3- Post-operative validation or evaluation: evaluation and assessment after the surgical procedure to assess the accuracy of CAS.

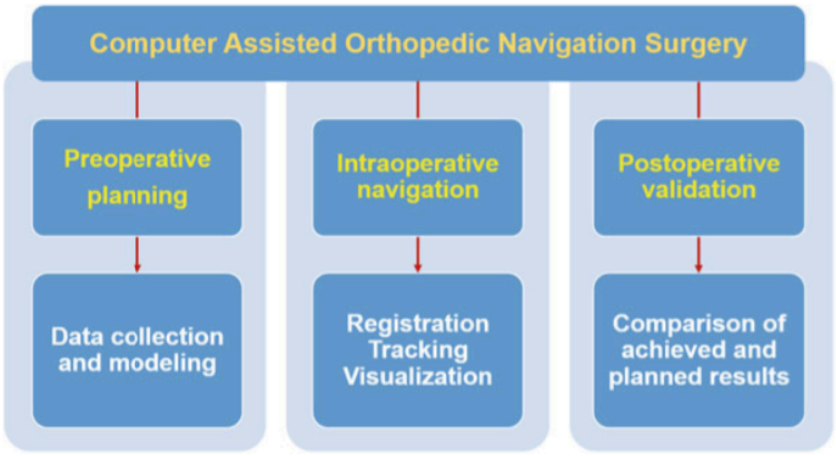

Figure 1-3. Various steps of CAS during the surgical procedure and the main works in each step [11].

In clinical practices, the surgical workflow consists of the first phase, the second phase, or a combination of them [12]. The first phase is mostly applicable to the tissues which do not have significant deformation during surgery, such as total knee arthroplasty [13]. However, most CAS systems need the second phase due to tissue deformations caused by the intervention. Each of these steps has several key components that will be discussed in the next section.

1.1.2 Main Components of a Surgical Navigation System

The first commercial CAS system to contain all essential elements of a surgical navigation system was the StealthStation [14]. Despite the variety in surgical navigation systems that followed, some main components are common. These components (shown schematically in Figure 1-4) are as follows [15]:

1- Image acquisition: Imaging studies are obtained during all phases of surgical navigation planning. Several factors should be considered when choosing the image modality in CAS, such as the type of injured tissue [16]. Various imaging methods used in surgical navigation are investigated in more detail in Section 1.2.
2- Registration: In a typical CAS system, it is essential to overlay acquired intra-operative images on the pre-operative model [17]. Registration performs the overlay process by aligning the space coordinates of the images with the model. The current registration methods utilized in CAS are reviewed in Section 1.4.
3- Tracking: One of the most important elements of a surgical navigation system during the intra-operative phase is the tracking component. The pose and orientation of the surgical instruments related to the patient and acquired images are determined in real time using the tracking system [18]. Therefore,

both efficient speed and accuracy should be considered as vital parameters in the tracking method. We will investigate the basic concepts of tracking in section 1.3, and then review existing methods of tracking in detail in section 1.6.

4- Visualization: This plays a crucial role in all steps of a surgical navigation system. The surgical organ should be visualized precisely from the acquired images before and during the surgery [5]. To achieve this, efficient preprocessing and segmentation techniques are vital. The main visualization techniques for the CAS application are explored in Section 1.7.

5- Display: Various techniques have been proposed to present the reconstructed image acquired from the surgical area [5]. Tang et al. divided the display techniques to video-based, projection-based, and see-through displays [19]. In a video-based display, the surgical field of view and the reconstructed image are presented on the monitor, while the projection-based and see-through displays show images without any video screen. The technology utilized in display methods and their benefits and disadvantages will be discussed in Section 1.8.

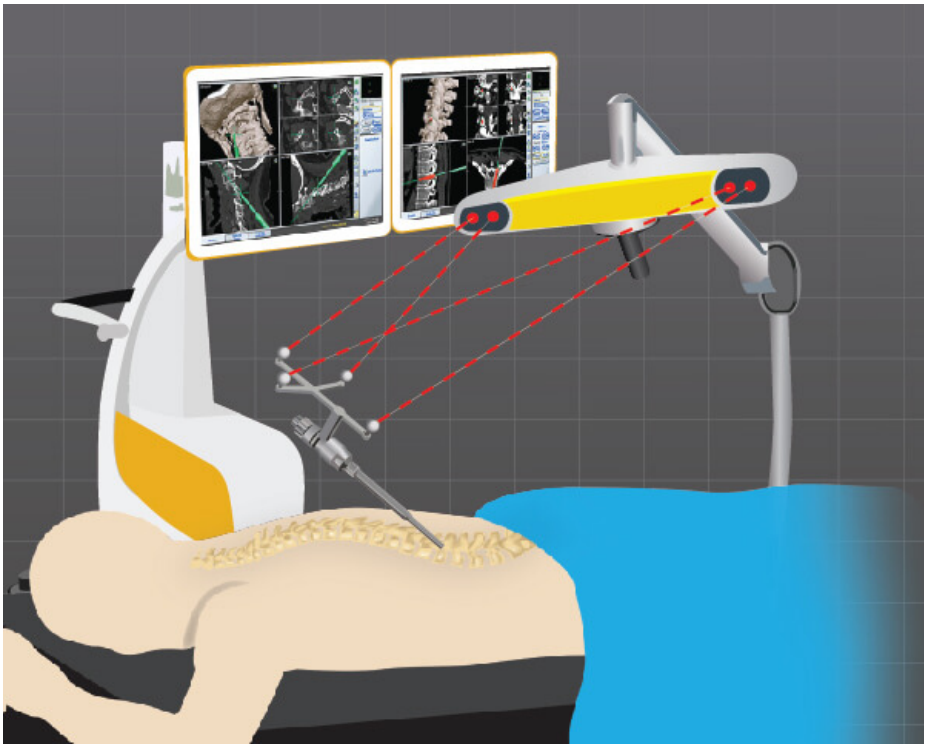

Figure 1-4. Main components of a surgical navigation system including image acquisition, registration, tracking, visualization, and display [20].

1.1.3 Augmented Reality and its Usage in CAS

Display components of a surgical navigation system show the position of surgical instruments related to the acquired images and visualized organs on a monitor, the real world, or the surgical area. This problem is addressed efficiently by Augmented Reality (AR) [21]. AR has been exploited in several applications across medical fields including treatment, surgery, rehabilitation, training, and education [22]. It enables the surgeon to visualize targets that are not directly visible during the intervention.

Augmented reality is a technology that has similarities to virtual reality (VR) and mixed reality (MR), but each interpretive technology has fundamental differences, and those differences are in the degrees of immersion and interaction. Immersion defines the degree of being in a virtual setting, while interaction refers to the user's degree of modification. In virtual reality, the real person or object is fully immersed in the virtual world. As can be seen in Figure 1-5, mixed reality comprises all possible mixtures of the real and virtual worlds. AR is a mixed reality between extremes of virtual reality and reality. AR allows users an expanded understanding of reality by superimposing computer-generated artificial elements onto real structures [23]. An example of abdominal CAS system illustrates the concept of AR, AV and VR in Figure 1-6.

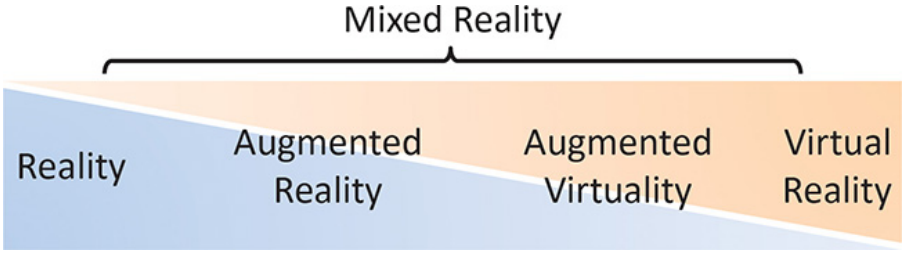

Figure 1-5. The relation between AR, VR and MR compared to the reality [24]. AR is closer to the reality than augmented virtuality and VR.

Various types of augmented reality in medical surgery have been reviewed by Sielhorst et al. [25]. They have also mentioned the potential benefits of AR in surgical navigation, such as extra value from image fusion and improved hand-eye correction. There are also some issues regarding AR methods in CAS such as depth perception and in-attentional blindness [23]. The current AR methods in surgical navigation are discussed in Section 1.8.

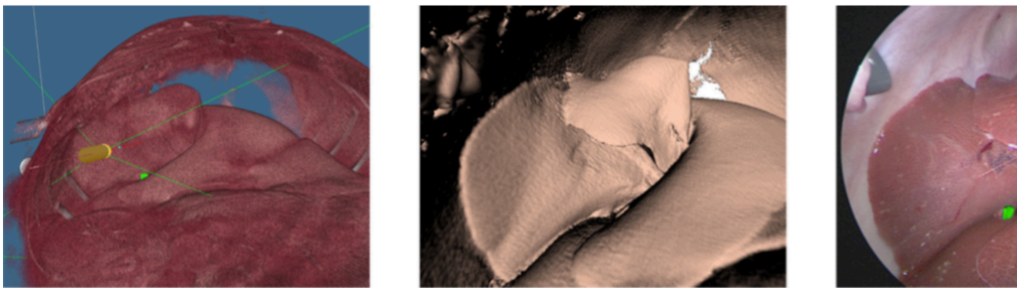

Figure 1-6. Examples of AV (left), VR (middle), and AR (right) in an abdominal CAS system. In the left picture, the virtual endoscope and segmented tumor (green) are shown in the visualized abdominal area. In the middle picture, the surface-rendered image is visualized from the actual view of the endoscope. In the right picture, the segmented tumor (green) is shown on the laparoscopic image [26].

1.1.4 Applications of CAS

CAS has been applied to surgery of several organs in the body. To build an effective surgical navigation system, it is essential to have an accurate and comprehensive knowledge of the anatomical structure in question. Any surgical navigation technology can be used for various tissues; however, there would be some difference due to the inherent characteristics of the organ such as rigidity, structure, or shape.

In this section some of the most well-known applications of CAS are briefly described. The benefits, drawbacks, and issues encountered in the main components of a surgical navigation system are discussed in the following sections. Computer Assisted Orthopedic Surgery (CAOS) as the main application of this thesis is investigated in more detail at the end of this section.

1.1.4.1 Dental and plastic surgery

Two main applications of CAS in dentistry are dental implant placement and orthognathic surgery [27]. The maxillofacial and oral structures have a complex anatomy which would be precisely positioned during computer assisted surgery using augmented reality techniques (Figure 1-7). Several works have been reported for mandibular reconstruction [28] and orthognathic surgery [29] using CAS. In these surveys, various pre-operative planning and post-operative evaluation methods have been reviewed. It has been shown that reconstruction performed with CAS yields higher accuracy compared to the conventional surgical methods. Another review paper has reported the main limitations and inaccuracies of CAS in maxillofacial surgery [30].

Figure 1-7. CAS in dental surgery [31]. The real-time position of the drill is shown on the screen which aids the accurate placement of the implant.

From a more general point of view, CAS is used extensively in the field of plastic surgery. A comprehensive review of previous works has been done [32]. Kim et al. categorized previous works in this field to 3 main groups including surgical planning, navigation, and training [33].

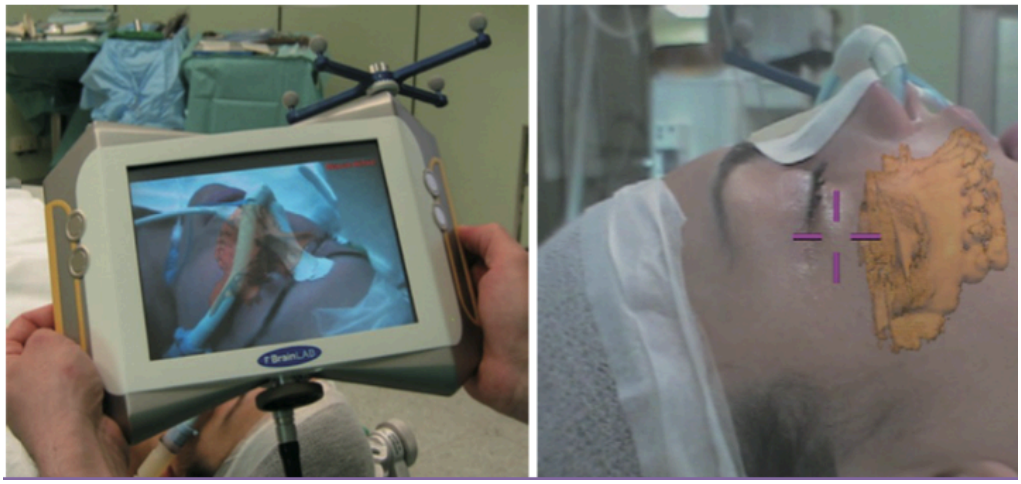

Figure 1-8. Application of CAS in plastic surgery. The segmented virtual maxilla has been show on patient using augmented reality technique (right image) [33]. The whole procedure is also visible on the screen (left image).

1.1.4.2 Neurosurgery

One of the most common uses of CAS is in neurosurgery. Roberts et al. utilized AR for the integration of CT images in a surgical microscope [34]. A great survey of previous works on neurosurgery was done by Lopez et al. in 2018 [35]. According to this review, the fields of neuro-vascular and neuro-oncological surgery are the most widespread applications of AR technology in neurosurgery. In another review paper, these applications have been compared based on the main components of a surgical navigation system including acquired images, registration, tracking, and display [36].

Figure 1-9. CAS in neuro surgery [35]. The reconstructed model of the brain has been shown on an ipad and has been utilized during the surgery.

1.1.4.3 Abdominal surgery

One of the most significant uses of CAS in MIS is in abdominal surgery. Bernhardt et al. did a comprehensive review of previous works on AR in the field of laparoscopic surgery [26], in which they considered the main advantages and challenges of AR in laparoscopic surgery and investigated various techniques of registration, tracking, and visualization utilized by other AR-based laparoscopic methods. There are other reviews of the broad application of laparoscopic surgery in abdominal organs, specifically liver surgery [19] and urology [37]. An example of a CAS system for abdominal surgery can be seen in Figure 1-10.

Figure 1-10. A typical CAS system for kidney surgery [37].

1.1.4.4 Computer-Assisted Orthopedic Surgery

The musculoskeletal system is an organ system in the human body consisting of muscles, bones, ligaments, cartilages, tendons, and other connective tissues. These structures work together to provide posture, shape, and movement of the body. Injuries and diseases in the musculoskeletal system have a considerable impact on public health as the leading cause of disability and pain [38]. When tasked with repair, orthopedic surgeons should treat any malfunction as accurately as possible to reduce post-operative risks. However, orthopedic surgeries have inherent difficulties, including the limited visibility of surgical tissue. Computer technology can be a valuable tool to avoid or minimize surgical risks, which can include infection, bleeding, blood coagulation, and re-injury of the joint or soft tissue. Other benefits of using computer technology include reduced operation time and cost, decreased radiation doses, and for training less experienced orthopedic surgeons [18].

Over the last three decades, surgeons have used Computer-Aided Orthopedic Surgery (CAOS) to assist in performing precise orthopedic surgeries. ROBODOC was the first robotic-assisted system used for total hip replacement in 1992 [39]. Navigation technology followed, with the 1994 introduction of a hip cup replacement system [40]. Since then, various clinical trials and commercial systems have been embraced by orthopedic specialists. Some examples of the robotic technologies used in orthopedics are MAKO/Stryker [41], ROSA [42], and NavioFPS [43]. Existing CAOS systems are mainly categorized into four groups: image-guided, positioning system, passive robotic system, and active robotic system [44]. All of these systems have a standard pre-operative planning system.

CAOS systems have been developed for a wide range of precise operations in the field of orthopedic surgery. The most frequently used are [18]:

- Pedicle screw insertion: Spinal fusion is a critical treatment of various conditions related to degenerative disease or trauma, in which two or more vertebrae in the spine are fused together [45]. This is a typical technique for spinal fusion that encounters significant challenges and risks, including neural and vascular damage. Nolte et al. initially examined the CAOS system for the fixation of spinal implants in 1995 [46]. Several studies have since examined the effect of computer-aided surgery (CAS) on precise spinal fusion [47].
- Hip arthroplasty: Osteoarthritis is a common degenerative disease of the hip joint, which often happens in older adults. Hip resurfacing and Total Hip Arthroplasty (THA) are typical treatments depending on the level of deterioration. Both methods are accomplished more precisely using CAS. Hip arthroplasty can be performed on either the femoral or pelvic side. In total hip arthroplasty, both femoral head and acetabulum are replaced. The orientation and position of the hip should be accurately defined to prevent post-operative dislocation. Sugano has made a review of recent works on hip arthroplasty [48].
- Knee Arthroplasty: The reconstruction and replacement of deteriorated knee joints with metal and plastic components is delineated as knee arthroplasty. Total Knee Arthroplasty (TKA) is one of the most common orthopedic surgeries. The number of TKA surgeries is estimated to increase by 673% from 2005 to 2030 [49]. Similar to THA, CAS is beneficial for accurate TKA and reducing pain and disability. The review of the state of the art in knee arthroplasty using CAS has been performed by Jones et al. [50].
- Bone fracture repair: One of the most prevailing applications of orthopedic surgery is the repairing of bone fracture. The repair process consists of relocating the bone fragments to their normal alignment and fixing the position using particular implants. Several challenges exist in conventional methods: they require high degrees of precision and physical strength from the surgeon, and they are time intensive. CAS and robotics can effectively overcome the drawbacks to traditional bone fracture surgeries [51]. Two examples of CAS in bone fracture repair are intramedullary nail fixation for femur fracture [52], and maxillofacial fracture [30].
- Bone tumor resection: In orthopedic oncology, the surgeon resects the bone sarcoma and some extra healthy tissue near the tumor. Pre-operative planning and medical imaging play a vital role in accurately defining the position of the tumor and surrounding healthy tissue. Intra-operative surgical planning would also make CAS useful in defining the sufficient marginal border [48].

Figure 1-11 shows some applications of Computer-aided Orthopedic Surgery in hip resurfacing [53], fracture reduction [54], pedicle screw placement [55], and knee replacement [56].

(a) Hip Resurfacing

(b) Fracture Reduction

(c) Pedicle Screw Placement

(d) Knee Replacement

Figure 1-11. Some examples of Computer-Aided Surgery in orthopedic surgery: (a) hip resurfacing [53], (b) fracture reduction [54], (c) pedicle screw placement [55], (d) knee replacement (using MAKO/Stryker robot) [56].

1.2 Imaging Methods

Various methods of imaging have been classified based on the level of real-time enhancement of the surgeon's eye in [16]. Figure 1-12 shows various imaging methods incorporated in each phase of the CAOS including pre-, intra-, and post-operative phases [57]. Several critical issues should be addressed by the imaging

methods during the surgical navigation such as image quality, and the timeliness. The main imaging modalities currently utilized in orthopedic surgery are as follows:

1. 2D X-ray: It is widely used in orthopedic surgery due to the high contrast of bones. Using some appropriate contrast material, it also can be used in angiography. However, one major drawback of X-ray imaging is that it affords a single projection through the patient. Therefore, in order to acquire the 3D information of the patient, the imaging should be performed from different orientations related to the patient.
2. Computed Tomography (CT): has a very nice spatial resolution and provides good details of the bony structures. Cone Beam CT (CBCT) images produced by the big motorized C-Arm systems, are broadly used in surgical navigation. However, the quality of the CBCT images are not as good as high-quality CT scanners. One of the most breakthrough works in using X-ray and CT images in the intra-operative phase is the work of Navab et al. named Camera Augmented Mobile C-arm (CAMC) [58], [59]. They integrated a mobile C-arm, optical camera and a double mirror to fuse the optical and X-ray images in real-time.
3. Magnetic Resonance Imaging (MRI): MRI affords a suitable contrast between the soft and hard tissues and can be acquired from arbitrary directions. Moreover, it has almost no risk of ionizing radiation. However, there are some critical issues in exploiting this imaging for the intra-operative phase, including MR compatibility within surgical environment. Although, the open-MRI scanners have been invented for the interventional purpose, their acquired image resolution is less than the closed-tunnel scanners [60].
4. 2D/3D Fluoroscopy: is the most frequent imaging method using during the intra-operative phase. It utilizes X-ray to generate images. However, in contrast to the CT and X-ray imaging, it produces live images during the surgery. Mobile fluoroscopic C-Arm is widely used for the interventional purposes.

In recent years some other imaging methods have been employed increasingly for the surgical navigation purposes, including ultrasound, optical, and nuclear imaging. Table 1 of a study made by Alam et al. has mentioned the pros and cons of each method [61]. Optical imaging is a low-cost, contact-free method which lights up the tissue during the surgery. Ultrasound imaging is a non-ionizing and inexpensive method that provides images with the high temporal resolution. Some examples of US imaging methods in CAS which employed by free-hand or robots are photo-acoustic, or elastography. A review of previous works on robotic-assisted sonography has been performed by Swerdlow et al. [86].

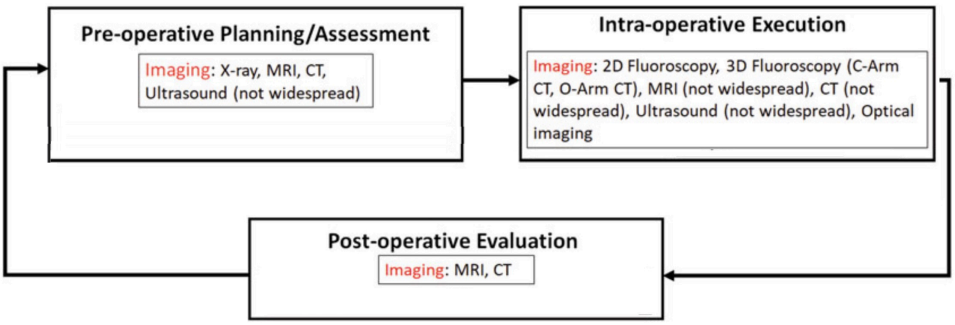

Figure 1-12. Various methods of imaging have been utilized in each phase of the surgical navigation system for orthopedics [57].

1.3 Basics of Tracking

Tracking is one of the most critical components of a CAS system. It is responsible for determining spatial position and orientation of entities, including patient body, surgical instruments, and acquired images during the intra-operative phase. It is essential to computing the entities continuously and in real time. In the context of surgical navigation, three concepts are related to the alignment of objects. These concepts, which have some overlap in their definitions, are as follows:

Tracking: This term describes the dynamic behavior and measurements of the augmented reality system. The position and the orientation of real and virtual objects should be computed continuously in real time. In computer-assisted surgery, these measurements are considered in 3D space, which needs more calculations than 2D tracking performed in image space with traditional computer vision applications.

Registration: is the alignment of spatial properties. To register with each other, they should be aligned in some coordinate system. In tracking systems, the real-world and virtual objects are aligned with each other using registration techniques.

Calibration: is the offline adjustment of measurements. This term is often utilized when the measurement of an instrument or sensor is adjusted with some predefined standard. Calibration is associated with the static registration and many nonspatial parameters of the tracking system.

Figure 1-13 illustrates the overlap areas of these concepts , and how they relate to each other [24]. As can be seen in this figure, the static registration is more related to the calibration, and the dynamic registration is associated with the tracking. Calibration is responsible for the adjustment of nonspatial parameters of tracking devices.

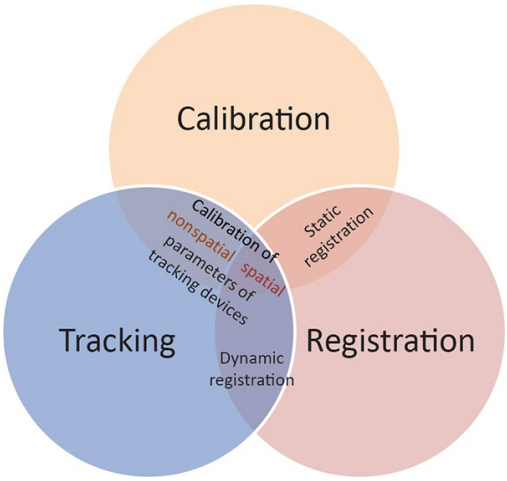

Figure 1-13. Three important concepts adopted with alignment of objects in an AR system are tracking, registration, and calibration [24]. These concepts have some overlap in their definitions which describe their relation to each other.

This section explores the basics of tracking in more detail and describe its vital role in surgical navigation. The registration and calibration concepts are investigated in the following sections. We then review earlier tracking methods in CAS and compare their advantages and disadvantages. Finally, we investigate their use and limitations in CAOS.

1.3.1 Coordinate Systems

The relationship of the main components of a tracking system is the most fundamental issue that should be addressed in CAS. In a surgical navigation system, these components are patient, surgical instrument, camera, tracking sensor, and display. These components can be seen in Figure 1-14. Using tracking sensors and the camera, the positions of the surgical instrument, and the patient are defined related to each other and visualized virtually in the display of the surgical navigation system.

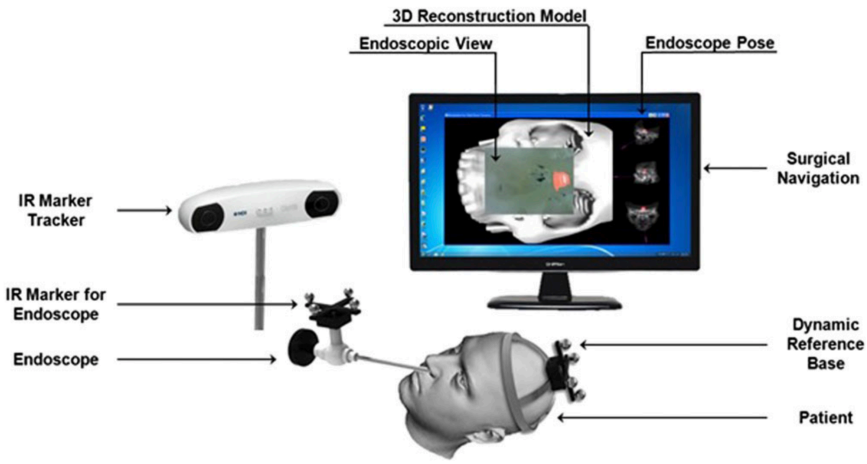

Figure 1-14. Tracking components of a surgical navigation system [62].

In order to explore the relationship of elements in a tracking system, a standard computer graphic pipeline is adopted [63]. This pipeline consists of various transformations, including model transformation, view transformation, and perspective transformation. These transformations describe world, object, and eye coordinate systems. They also identify the position of components related to each other and the global world coordinates [24]. Figure 1-15 illustrates three transformations and their relation to the main components of the tracking system.

1.3.1.1 Model transformation

The primary role of model transformation is to determine the position of objects such as patient and surgical instruments in the real world. To be more precise, model transformation defines the relationship between global world coordinates and local object coordinates. This transformation is not usually used for the virtual object or real static scenes as they don't need tracking in most circumstances.

As illustrated in Figure 1-15, the model transformation is mainly used for tracking moving real objects if there are static objects as well. However, there are some situations that do not require an explicit global coordinate system, for example, in AR settings where we want to augment only tracked objects, but not untracked static ones. In these situations, a separate view transformation can be utilized for every tracked real object.

1.3.1.2 View transformation

View transformation is another critical transformation in the tracking system which defines the relationship between 3D camera or eye coordinates and the world coordinates. The main roles of this transformation are to track for moving

observers, and for moving objects if there are no static objects in the scene [24]. Typically, each available display of the user, tracking sensor and the camera in the AR system needs distinct viewing transformation. Moreover, the camera and the displays should be calibrated before the tracking. The calibration is particularly vital for the system with more than one camera such as systems using stereoscopic displays.

1.3.1.3 Perspective transformation

The perspective transformation converts 3D eye coordinates to 2D screen coordinates. The main goal of this transformation is to project a 3D field of view (FOV) of the camera on the 2D display. The whole process consists of mapping the FOV to a unit cube and projecting onto the 2D screen by removing the Z component and applying a viewport transformation. An important issue to consider in projective transformation is the offline and separate calibration of each camera and display.

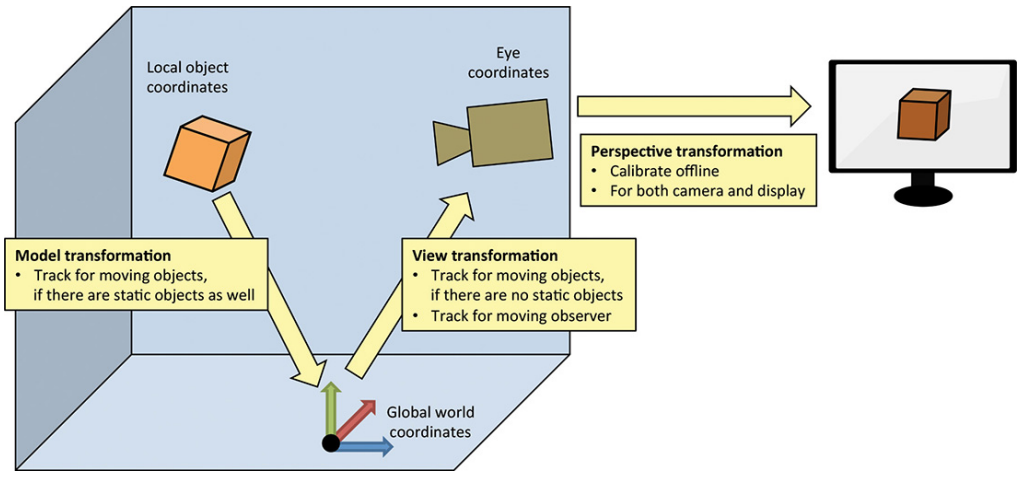

Figure 1-15. Three different transformations, including model, view, and perspective transformations, should be considered in the tracking system [24]. The model and view transformations define the relation of local moving objects and camera to the global world coordinates. Perspective transformation describes the relationship between cameras and the 2D display.

As shown in Figure 1-16, each transformation can be represented by a transformation matrix. For example, the transformation matrix from the camera, surgical tool, and the patient coordinates to world coordinates is shown by T_c^w, T_t^w, and T_p^w. The inverse transform for each of these transformations is achieved by computing the inverse of the corresponding matrix. Moreover, the other conversions can be calculated by multiplying these matrices. For example, the transformation from the camera coordinates to the surgical tool (T_c^s), is computed

by multiplying T_c^w, and T_w^s. This transformation is crucial for surgical tool tracking and should be processed in real-time. However, some transformations, such as T_w^p , require the registration techniques which are acquired in the pre-operative phase. In the next section, we will investigate the various registration methods utilized in the surgical navigation systems.

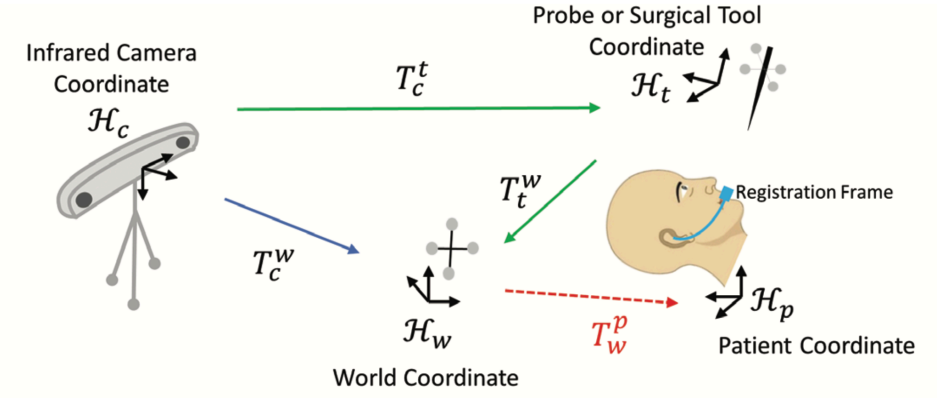

Figure 1-16. Transformations used for the tracking of main components of the surgical navigation system, including the camera, patient, surgical tool. The conversion of these component and the world coordinates is computed by a transformation matrix. T_c^t is the transformation matrix from the camera to the surgical tool coordinate, T_w^p is the transformation matrix from world to patient coordinate, and T_t^w is the transformation matrix from the surgical tool to world coordinate [64].

1.4 Registration

1.4.1 Definition and Basics

Image registration matches separate images into one coordinate system so that the corresponding features of registered images are related to each other. To achieve this goal, one or more images are deformed to optimally aligned with other images. The unchanged image that different dataset is matched to during the registration is called the reference or target image. The image that is deformed to align with the target image is called the moving image or source image. Registration is routine in many clinical applications of medical imaging including multimodal registration, statistical shape modeling, image fusion, atlas-based segmentation, and temporal image registration [65].

Image registration is critical for image-guided surgery. The images acquired before and during the operation should be aligned to convey essential information such as insertion points or other measures of treatment plans. This data is registered with the position of patient and surgical instruments at the beginning of the intra-operative phase [66]. A fundamental transformation of the pre-operative image to the intra-operative image is vital for the correct intervention during the surgical navigation. The registration process is intramodal or

multimodal if the pre-operative and intra-operative image types are the same or different, but all registration methods consist of fundamental components, which will be examined in the following sections [67]. The schematic of image registration is shown in Figure 1-17.

1.4.1.1 Transformation type

Transformations are either global or local. Global transformation alters the whole image at once and is categorized as rigid or affine based on the desired geometric transforms. 3D rigid transformation comprises 3 translation and three rotational parameters, while 3D affine transformation contains three more shear and three scale features. On the other hand, local or nonrigid transformation performs separately in each local region of the image. Nonrigid registration methods can be nonparametric (e.g., fluid-based algorithm) or parametric (e.g., free-form deformation) [68].

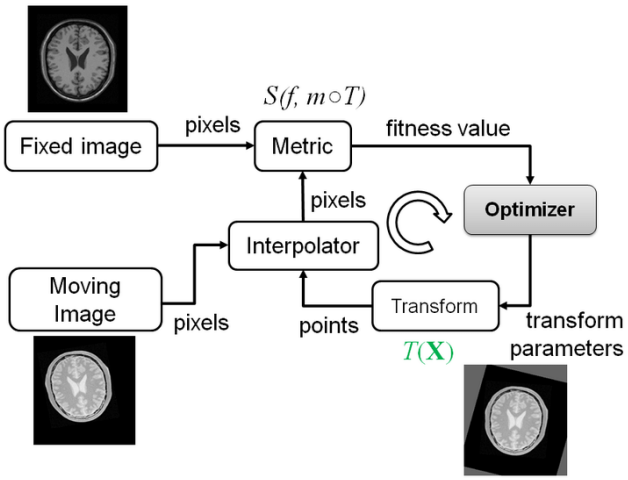

Figure 1-17. Main components of an image registration method include transformation type, metric or similarity measure, optimization method, interpolator, reference, and moving images [67]. The similarity measure between the transformed moving image and the fixed image is optimized in an iterative process. The interpolator recomputes the intensity values of the transformed voxels at integer coordinates.

Nonrigid registration methods are more precise but more time-consuming than global registration methods. This issue is so crucial and should be considered in the surgical navigation systems. To gain the most benefit in surgical navigation, nonrigid registration should be performed with the coarser level of image resolution.

1.4.1.2 Similarity measure

This measure is necessary for evaluating the quality of registration and demonstrates similarities between the target and the registered moving image. The similarity measure is based on either the intensity of image elements or the geometry features of the image. In intensity-based measures, the gray value of the registered image is matched with the target in one of three ways:

- Voxel-based: A well-known measure in this category is the sum of squared error (SSE) of the voxel intensities. Both target and transformed images must have the same resolution and intensity level to use this measure.
- Statistics: An important measure in this group is the normalized cross-correlation of two images, which would be equal to one for two completely similar data.
- Entropy-based: These measures are defined based on the similarity concepts in information theory. One well-known example is normalized mutual information. These measures frequently give more accurate registration results. However, its computation is more time consuming.

In geometry-based measures, the position of voxels in two images is compared. Geometry-based criteria are usually defined based on the corresponding landmark point. Landmarks can be determined automatically or by the user. They can be extracted from the specific features of the anatomy or shape of the organ such as corners or branching points in the vascular structures. However, for many orthopedic surgeries, defining the precise location of anatomical landmarks is a tedious task. Transformation type dictates the required number of corresponding landmarks. For example, rigid registration requires at least four corresponding landmarks, and for affine transformation requires a minimum of six.

1.4.1.3 Optimization method

As shown in Figure 1-17, image registration is an iterative process, in which a similarity measure should be optimized at the end. Several optimizers are employed for the registration processes, but they are divided into continuous variable and discrete variable methods [69]. Continuous variable optimizers include the conjugate gradient method, Quasi-Newton method, and Levenberg-Marquardt method. Discrete variable optimizers use Markov random fields to perform the optimization.

1.4.1.4 Interpolator

The interpolator is required to compute the intensity of voxels at integer-value coordinates in the transformed moving image; in order of accuracy the most commonly used are the nearest neighbor, bilinear and bicubic interpolation functions. The more precise the interpolator function, the more time-consuming

it is. Therefore, the most suitable interpolator should be selected based on the required accuracy and processing time.

1.4.2 Registration for IGS

The registration of data in pre-operative and intra-operative phases for the IGS system is divided into several classes [17]:

- Manual registration: geometric transformations are manually matched to target and moving images.
- Point-based (Fiducial-based) registration: incorporates a set of natural or artificial fiducial landmarks located intra-operatively on the patient and pre-operatively in the acquired images by attaching markers to the patient (in orthopedic surgery, this may involve screwing markers into the bone, which makes the registration method more accurate but invasive.) This established registration technique uses either distance-based, filter-based or probability-based methods [69]. Fiducial markers allow us to efficiently match some favorable regions of the target and the source image, and identifying them in many acquired imaging modalities such as CT or MRI is quite straightforward. However, one critical issue to address is the intervention area that is tracked by the surgical navigation system: for accurate registration, the markers should span an adequate area of the surgery. A schematic of the fiducial-based registration method is shown in Figure 1-18 (a).
- Shape-based (surface-based) registration: uses a point cloud or surface mesh extracted from the intra-operative images aligned to the surface mesh of pre-operative data. Iterative Closest Point (ICP) is a prominent algorithm for surface-based registration. An example of this method is shown in Figure 1-18 (b).
- Volume-based registration: uses the information of the subsurface intensity and geometry to match the moving and target images. Due to the usage of rich information existing in the volume, the volume-based registration method is more accurate and time-consuming than other methods.

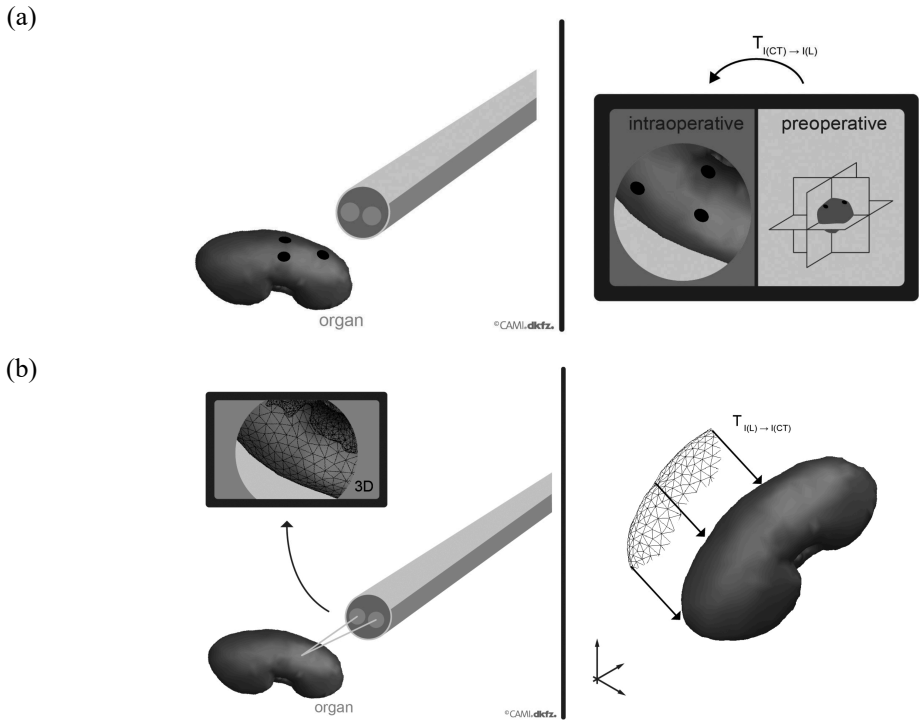

Figure 1-18. A schematic of (a) point-based and (b) surface-based registration methods employed for aligning the pre-operative and intra-operative data in the surgical navigation system [17]. Frequently, some part of the organ's surface which is made apparent by the camera in the intra-operative phase would be useful for the registration method. The pictures on the left demonstrate the intra-operative phase and the pictures on the right show the transformation to pre-operative data.

1.4.3 Error Analysis

Critical in surgical navigation, analysis of the registration error stops the iterative optimization process and informs the surgeon about the quality of registration. Errors are generated due to some intrinsic or extrinsic factor [70]. Intrinsic errors are related to localization errors of the surgical navigation components. Extrinsic errors are generated due to the incorrect setup of the tracking system or some undesired motion of it.

Several measures have been proposed for the error examination of point-based and other registration methods. Prominent measures developed for point-based registration methods include [70]:

1. Fiducial Localization Error (FLE): is associated with inadequate localization of fiducial markers. This intrinsic error would be made by the imaging or the tracking system and can occur in both image domain (FLE_{rad}) or physical domain (FLE_{OR} or FLE in the operating room as be shown in Figure 1-19).It cannot be measured in the IGS systems and should be indirectly estimated [71].

2. Fiducial Registration Error (FRE): is defined as the distance between fiducial markers in the operating room during the intervention and their corresponding points in the registered pre-operative image. One effective measure of this error is the root mean squared of the distance between corresponding landmarks in both spaces. If $g(.)$ is the registration function, N number of landmarks x_i the landmarks in the source image, and y_i the corresponding landmark in target image. The value of FRE is as follows:

$$FRE = \sqrt{\frac{1}{N}\sum_{i=1}^{N}\|g(x_i) - y_i\|^2} \tag{2.1}$$

3. Target Registration Error (TRE): is defined as the distance between a point of interest or target on the patient during the intervention and their corresponding points in the registered pre-operative image. The target points are usually inside the patient and not visible in the physical space. Several methods have been proposed for estimating TRE [72].

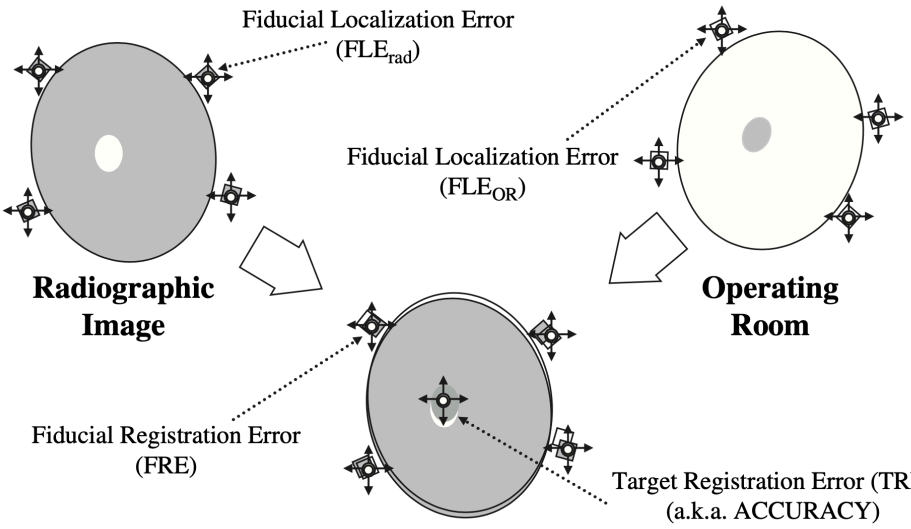

Figure 1-19. The registration errors classified as the Fiducial Localization Error (FLE), Fiducial Registration Error (FRE), and Target Registration Error (TRE). FLE can occur in the image domain (FLE_{rad}) or the operating room (FLE_{OR}) [73]. The surgical target is shown in the center of each ellipsoid.

1.5 Calibration

Some components of a CAS system, including the surgical instrument and the camera, should be calibrated offline to be useful for the tracking system [17]. Calibrating the instrument is necessary to define the location of its tip in the patient's body. Calibrating the intrinsic parameters of the camera is crucial for accurately tracking all CAS components. In the next two sections, we will investigate the calibration of the instrument and the camera.

1.5.1 Instrument Calibration

Instrument calibration is an essential step for accurate tracking in which the direction and distance of the tip of the instrument to the markers are computed. This information enables us to locate the surgical instrument by tracking the attached array of markers. A few examples of the equipment used for determining the tooltip are pivot block or checkerboard pattern (Figure 1-20). Pivot block is a cube with the small cavity for fixing the tip of the instrument and used for the calibration of rigid instruments. The checkerboard pattern is used to calibrate flexible catheters.

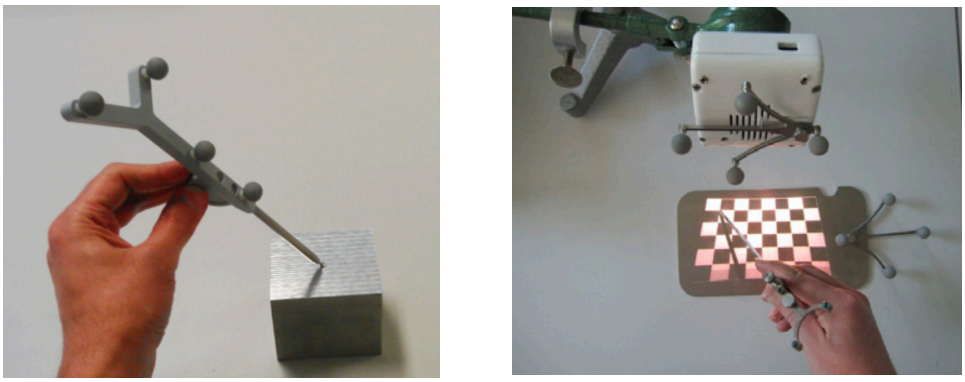

Figure 1-20. Different types of equipment used for calibrating the surgical instrument: (left) pivot block, (right) checkerboard pattern [5].

1.5.2 Camera Calibration

Another important calibration issue that should be address in a surgical navigation system is camera calibration, or learning the intrinsic camera parameters including principle point and focal length. They should be adaptively calibrated for the camera with variable focus ability. The camera calibration is usually performed by attaching a reference array of markers to the camera and verifying the geometric relationship between camera image and the reference array (Figure 1-21). However, computing this geometric relationship is not straightforward. Several algorithms have been proposed to tackle this problem.

For example, ARToolkit, a famous vision-based tracking toolkit, solves this problem by searching a special pattern in the image and the camera image [74].

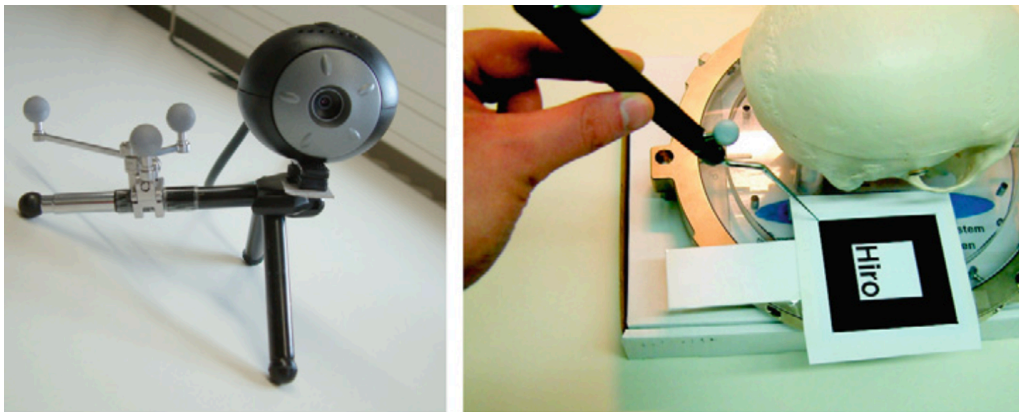

Figure 1-21. Camera calibration using (left) special reference array of markers attached to the camera, and (right) special pattern with the camera and its reference marker in the surgical workspace [5].

1.6 Different tracking systems in CAS

In this section, we will investigate marker-based and marker-less tracking methods. In marker-based tracking methods, artificial visual markers are attached to the surgical tool and employed for tracking. Marker-less tracking methods exploit computer vision algorithms to obtain tracing features from the intra-operative images. Several conditions should be considered for the vision-based methods including robustness and accuracy of the tracking algorithm [75].

Apart from this classification, prominent tracking methods in surgical navigation are divided into types including mechanical, ultrasonic, electromagnetic and optical tracking [76]. Among these, the electromagnetic and optical tracking methods are the most well-known. We will review basics and critical issues of each method and compare their pros and cons in the CAS system.

1.6.1 Mechanical Tracking

One of the earliest tracking methods used for the CAS system is mechanical tracking. It consists of rigid mounting frames that are fixed to the patient organ. The pose and orientation of the surgical instrument is tracked by employing a mechanical connection between the target and reference points. Figure 1-22 shows one of the first mechanical tracking systems introduced by Horsley and Clarke for surgery on an animal's brain [77]. A stereotactic frame attached to a monkey's head with some external markers to define the coordinate system of its brain. The surgical instrument is attached to the frame and navigated during the surgery. The mechanical tracking system has the advantage of high tracking

accuracy, but its significant drawbacks include the difficulty of setting up the stereotactic frames and the invasive nature of the frame attachment to the head. With the advent of other tracking systems, the mechanical tracking is rarely employed for surgical navigation.

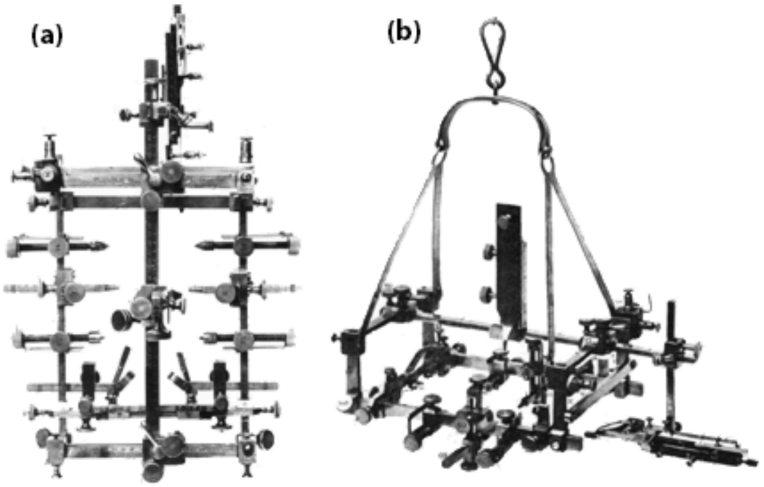

Figure 1-22. The mechanical tracking system utilized by Horsley and Clarke for navigating an insulated needle. (a) Top and (b) side view [77].

1.6.2 Ultrasonic Tracking

This method exploits ultrasonic waves with frequencies higher than 20 kHz. Time-of-flight (TOF), or the difference between a reference signal and an emitted signal, is utilized for tracking [78]. The ultrasonic, or acoustic, tracking system was first proposed by Roberts and colleagues [34]. As shown in Figure 1-23, the target is tracked in real time using an acoustic tracker system fixed to an operative microscope. In order to locate the surgical tool, the transmission time of a sound wave from the source to receivers is computed. Although this method addresses the invasiveness of mechanical tracking methods, it still suffers from critical issues in working volume including noise and reflections.

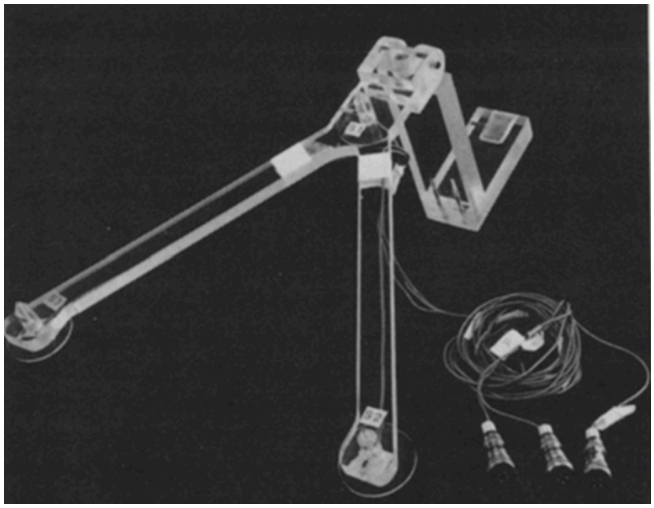

Figure 1-23. An example of ultrasonic tracking device [34]. The acoustic tracker is attached to an operative microscope

1.6.3 Electromagnetic Tracking

One of the most widespread tracking methods in surgical navigation systems is Electromagnetic (EM) tracking, which measures the strength of a magnetic field at a specific location. In this section we will consider the main components and approaches of EM tracking and various sources of error.

1.6.3.1 Main components and techniques of electromagnetic tracking system

An EM tracking system consists of following main components [79]:

- Field Generator (FG): generates a magnetic field consisting of three orthogonal fields. It acts as a transmitter and is positioned at a fixed location.
- EM sensors (electromagnetic tools): contain several small coils and are attached to the surgical instrument. The magnetic field generated by FG induces a voltage to EM sensors which is utilized for the pose estimation. Categories of EM sensors include search coils, fluxgate sensors, Superconducting Quantum Interference Devices (SQUIDs), and Hall-effect Sensors. Search coils measure the magnetic flux density over time and fluxgate sensors measure static or low frequency alternating fields.
- Control unit: controls the modulation of the field generator and the data acquisition of the EM sensors.
- Workstation

A schematic of an EM tracking system with its main components is shown in Figure 1-24. Generally, EM tracking systems are categorized based on the magnetic field type [80]:

1. DC-driven: the magnetic field is provided by alternating current.
2. AC-driven: the magnetic field is generated by quasi-static direct current.
3. Passive system: an RF signal is produced by a permanent magnet for localization.

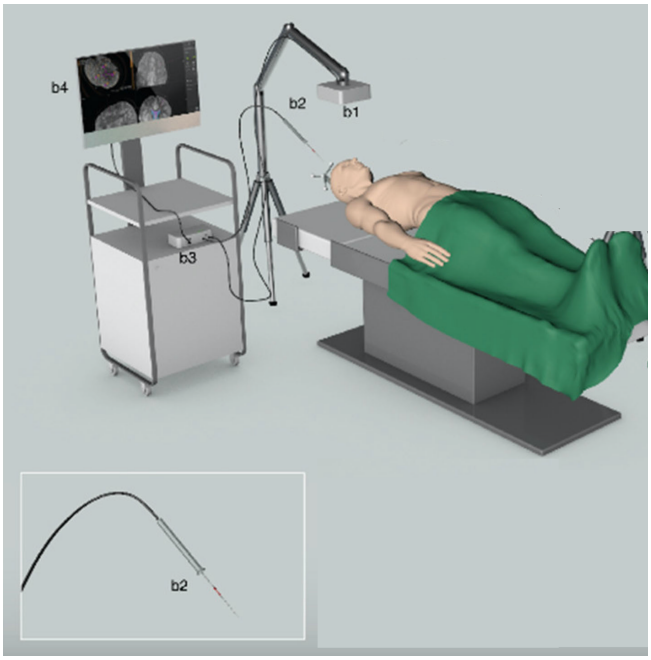

Figure 1-24. A schematic of an electromagnetic tracking system and its main components including (b1) a field generator, (b2) an electromagnetic tool, (b3) a control unit, and (b4) a workstation [80].

The order of the magnetic field at any point in the neighborhood of the FG is specified based on its distance from the generator. Several field generator topologies have been used for EM tracking system including triaxial generator design and multiple planar coils. The triaxial field generator comprises three orthogonal windings on a cube former and provides a unique magnetic field distribution. Alternatively, the planar field generator consists of multiple circular coils which enables tracking over larger area compared to the triaxial FG. However, the generated magnetic field would be less unique (Figure 1-25).

Different methods have been proposed for localizing a magnetic sensor inside the magnetic field. To localize the magnetic sensor, its position and orientation should be defined. For example, if several sources are utilized the position can be computed by triangulation method. In order to estimate the orientation of the instrument, at least two sensors are required.

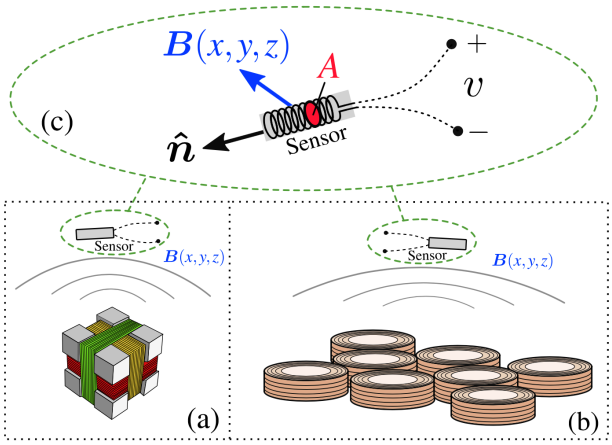

Figure 1-25. (a) A Triaxial field generator comprises of three orthogonal windings on a cube former. (b) A planar field generator comprises multiple circular coils. (c) The basic configuration of a magnetic sensor which shows the direction of magnetic flux density B [81].

1.6.3.2 Sources of error in EM tracking

The measurements made by electromagnetic tracking navigators typically generate systematic error and are affected by random noise and artifacts. Random noise is occasionally denoted as jitter and is generated during the measurement of a fixed EM tool over time. The other cause of random noise might be manufacturing inaccuracies or dynamic errors at a high frequency. Overall, electromagnetic tracking errors can be divided to static and dynamic errors. Static errors are generated as the EM tool remains in a fixed position and might be categorized as static distortion error and random noise. Dynamic errors are produced by the movement of the EM tool and are classified as dynamic distortion or sensor velocity error [82].

1.6.4 Optical Tracking

The most dominant tracking method in surgical navigation applications is optical tracking (OT). The location of objects is determined by measuring the light either transmitted or reflected by the object. In this section, we will explore the main components and general approaches of optical tracking, as well as its main benefits and limitations.

1.6.4.1 Main components and techniques of optical tracking system

An optical tracking system's main components [80]:

- Passive and active sensors (optical tools): passive sensors reflect the light emitted by the LEDs placed around each lens of the camera. Active

sensors emit light from attached LEDs and the light is captured by the optical camera.

- Optical camera: detects the energy emitted from the active markers or the energy reflected from the passive markers. The interfering ambient light is removed using an optical band-pass filter which is fixed in front of the camera lens.
- Control Unit: processes the received signal and computes the position and orientation of the markers.
- Workstation

A schematic of an optical tracking system with its main components is shown in Figure 1-26.

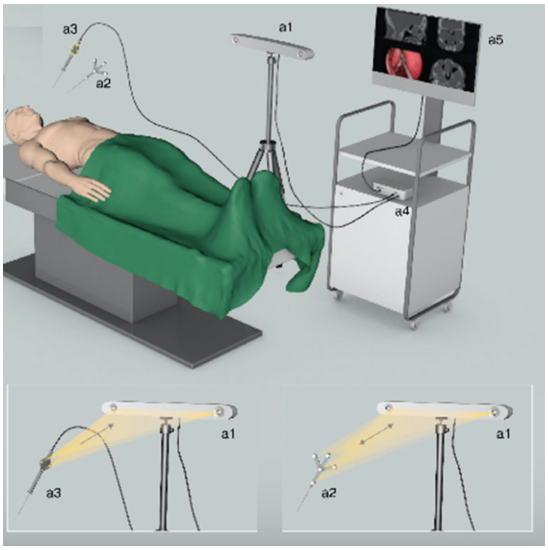

Figure 1-26. An optical tracking system and its main components including (a1) an optical camera, (a2) a passive optical tool, (a3) an active optical tool, (a4) a control unit, and (a5) a workstation [80].

Generally, optical tracking systems are one of these different structures [80]:

1. Inside-looking-out: The camera sensor is placed on the target and its movement is approximated with respect to some fixed references in the operating room.
2. Outside-looking-in: The optical camera fixed in the operating room tracks an optical pattern attached to the target. This method is favorable for detecting multiple objects in the operating room.

Optical tracking systems are classified based on the radio frequency signal utilized:

1. Infra-Red (IR) tracking system: comprises active and passive tracking systems. In an active tracking system, the IR LEDs which provide the signal source are rigidly fixed to the target object. These active sensors emit IR light which is detected and localized by two or three optical

cameras. The passive tracking system incorporates passive markers which can reflect the emitted light from IR LEDs placed on optical cameras. The active trackers require external wire running to the LED and passive trackers use wireless passive markers.

2. Videometric (visible light) tracking system: uses a chessboard pattern for calibrating stereoscopic cameras. The image sequences acquired from calibrated video cameras are employed to estimate the pose of the target. Due to interfering effect of environmental conditions such as thermal or mechanical deviation, the accuracy of the videometric tracking system is frequently lower than the IR tracking systems. However, the cost for this system is comparatively low and it is able to track multiple surgical instrument at the same time.
3. Laser tracking system: locates the position of an object using a laser tracker comprised of a laser beam and an array of photo sensors. The laser system is used less frequently than infrared and videometric methods.

In order to estimate the orientation and position of the surgical instrument using optical tracking, at least three noncollinear markers should be attached to the instrument. These three markers will define 6 degree of freedom (DoF) pose parameters including 3DoF position and 3DoF orientation. In addition, if the position and direction of the surgical tool tip must be computed and the orientation is not required, two markers would be sufficient (Figure 1-27). If only one marker is attached to the instrument, no information would be obtained regarding the orientation of the instrument.

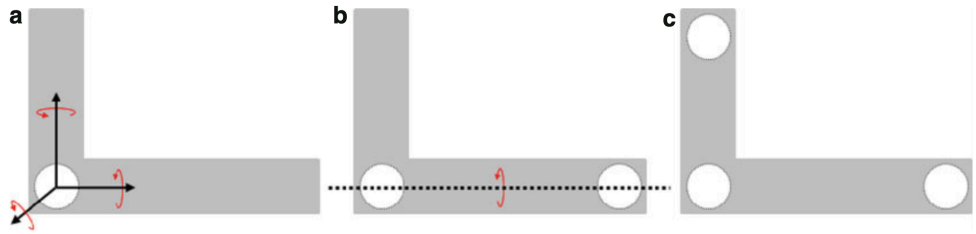

Figure 1-27. The effect of number of fiducial markers attached to a rigid tracker on identifying the orientation of the tracker: (a) one marker gives no information of the orientation (b) two markers do not provide the orientation value around the dotted line (c) three noncollinear markers provide the all orientation values needed for the tracking [12].

Different methods have been proposed for localizing the optical sensor in the visible sight of the camera. One conventional method would be triangulation, which is applied to the optical tracking system comprised of passive markers and

two IR cameras. A schematic of this method is shown in Figure 1-28. IR cameras measure the direction of the light reflected by the marker. The position is calculated using triangulation and the distance and direction of the light. One critical requirement that should be considered is the visibility of markers for the IR cameras. Recently, a sensor fusion approach has been proposed to solve the problem of limited field of view and occlusion [83].

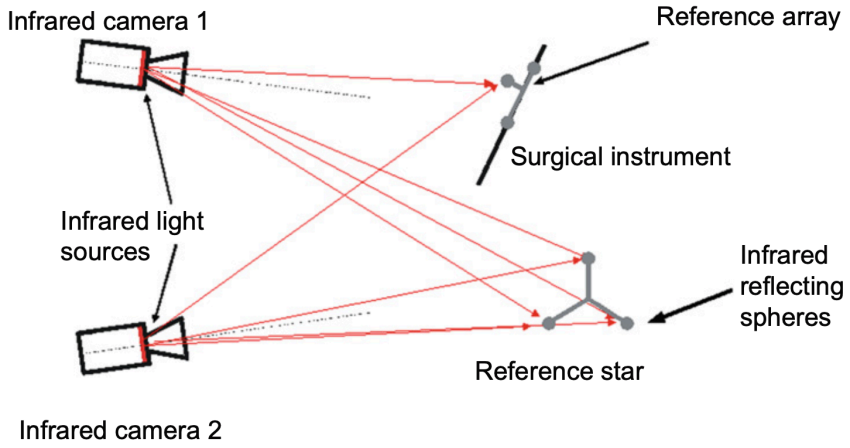

Figure 1-28. Triangulation is a typical method of optical tracking using two IR cameras [12]. This method would be useful for the passive markers where the direction of IR light reflected by the marker is measured by the IR camera. The position of the sensor is calculated using triangulation and the distance and direction of the light.

1.6.5 Using Inertial Measurement Unit for Tracking

Recently, Inertial Measurement Unit (IMU) is exploited for the tracking in surgical navigation systems. In fact, it provides a unique method of tracking motion, in which there is no dependency on external sources of information. In this thesis, two novel methods are proposed for the tracking in femoral head surgery based on IMU.

Inertial measurement is based on inertial sensors. Inertial sensors denote the combination of an accelerometer and a gyroscope. Tracking devices containing these sensors are commonly referred to as inertial measurement units (IMUs) [84]. Broadly, accelerometers measure specific forces or accelerations, while gyroscopes measure angular velocities [85]. These sensors are used to measure rotational and translational movements in three axes.

An accelerometer in IMU measures the external specific force acting on the body of the sensor. The external specific force on the earth consists of the sensor's acceleration and the earth's gravity. Gyroscope in IMU measures the angular velocity, i.e. the rate of change of the body of the sensor's orientation. There are different technologies used in gyroscopes and accelerometers e.g. mechanical and optical. Some sort of these sensors is based on microelectromechanical system

(MEMS) technology. These sensors are broadly used in recent days. MEMS based components are small, light, inexpensive, have low power consumption, short start-up times and their accuracy has significantly increased over the years [84].

Dead-reckoning is the concept behind the IMU sensors. The process of estimating the current state (position, orientation, velocity, ...) based on the knowledge of the previous pose, instantaneous velocity, course, and time duration is called dead (deduced) reckoning. Inertial tracking is applying the dead reckoning approach with the IMU sensors data. The inertial tracking system uses IMU output, which suffers from different types of noise and bias, to continuously update an estimation of a current state without any external reference. Therefore, such a system is subject to ever-increasing error since any arbitrarily small measurement error integrates over time which results in wrong estimation [86].

Gyrostabilized and strapdown are two types of Inertial measuring system [85]. Gyrostabilized systems are historically older and its sensors are mounted on the platform that is mechanically isolated and stabilized from moving object itself. It requires heavy mechanical setup. However, it offers high accuracy. In the strapdown system The IMU sensor has a solid attachment directly to the sensing object and experiences the same movements as the object. This approach leads to smaller, lighter and more durable system, and pays off with higher computation power to compute the desired physical quantities. So IMUs need basic on-board data processing to convert the raw sensor data to sensible specific forces or angular velocities.

1.6.6 Hybrid methods of Tracking

There are also ways to combine different tracking methods to integrate the information provided by the various techniques and increase the accuracy of tracking. For example, Ma et al. developed a hybrid EM and optical tracking method for distal intramedullary nailing (IMN) interlocking in a CAS system [87]. As shown in Figure 1-29, that proposed system consisted of optical tracking and an EM tracking device. The optical tracker is responsible for locating the electric drill, EM transmitter, and the IV overlay device using two optical trackers on each of them. EM sensor is calibrated for tracking distal holes of IMN in the pre-operative phase. The whole tracking procedure is performed by integrating the optical tracking of the IV overlay device and drill, and EM tracking of the IMN in the intra-operative phase. Kim et al. investigated more examples that combine marker-based and marker-less tracking methods [88].

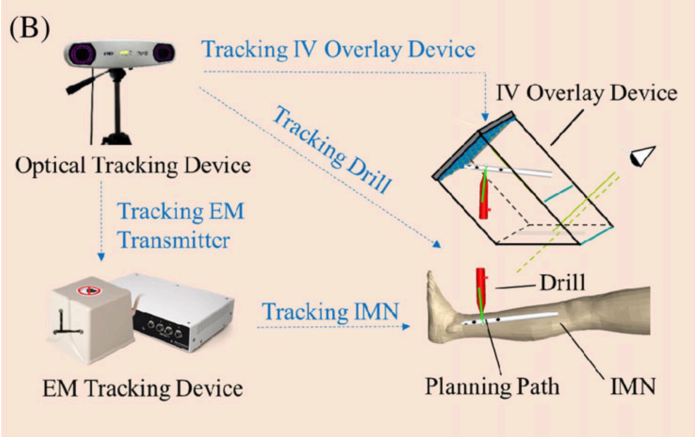

Figure 1-29. A hybrid tracking system for IMN interlocking which consists of an optical tracking and an electromagnetic tracking device [87].

1.6.7 Comparison of the Tracking Methods

As stated previously, electromagnetic and optical tracking are the principle tracking methods in CAS systems successfully integrated into commercial devices [80]. (Currently, mechanical and ultrasonic tracking are hardly used in available clinical applications.) Electromagnetic and optical methods are employed in various applications of surgical navigation. Each method has advantages and limitations, which are explored in this section.

Electromagnetic tracking methods enable accurate and fast tracking without the constraint of line-of-sight. Moreover, it can be employed for locating sensors that are not visible and exist inside the body. However, there are critical issues that should be addressed for EM tracking. Firstly, nearby metal, ferromagnetic sources, pacemakers, or other medical devices interfere with the magnetic field and destroy the performance of the system. Secondly, the EM tracking is not a robust method and covers the small workspace.

Optical tracking methods provides high accuracy, precision, and robustness under direct line-of-sight. Moreover, it is not affected by any metallic or conducting nearby objects. Despite those significant advantages, OT methods suffer from critical issues. Firstly, markers should be visible to the camera for passive optical tracking, which means that parts of the human body cannot be tracked. Secondly, surgical tool tracking is performed by locating the array of markers at the end of the instrument. Thus, the distance between the range of markers and tooltip is known before the intervention by calibration and should be fixed during the surgery. This distance has to be measured for the flexible catheters and endoscopes, which requires complicated and time-consuming image analysis. The complexity of these methods prevents tracking from being in real-time. Finally, any other source of infrared light might deteriorate the performance of optical tracking.

In a study by Sorriento et al., the behavior of two tracking methods was compared by several measures [80]. They concluded that both methods performed the same for the static measurement errors and latency, but Optical tracking has a significant advantage over EM tracking for dynamic measurement errors and existing disturbances.

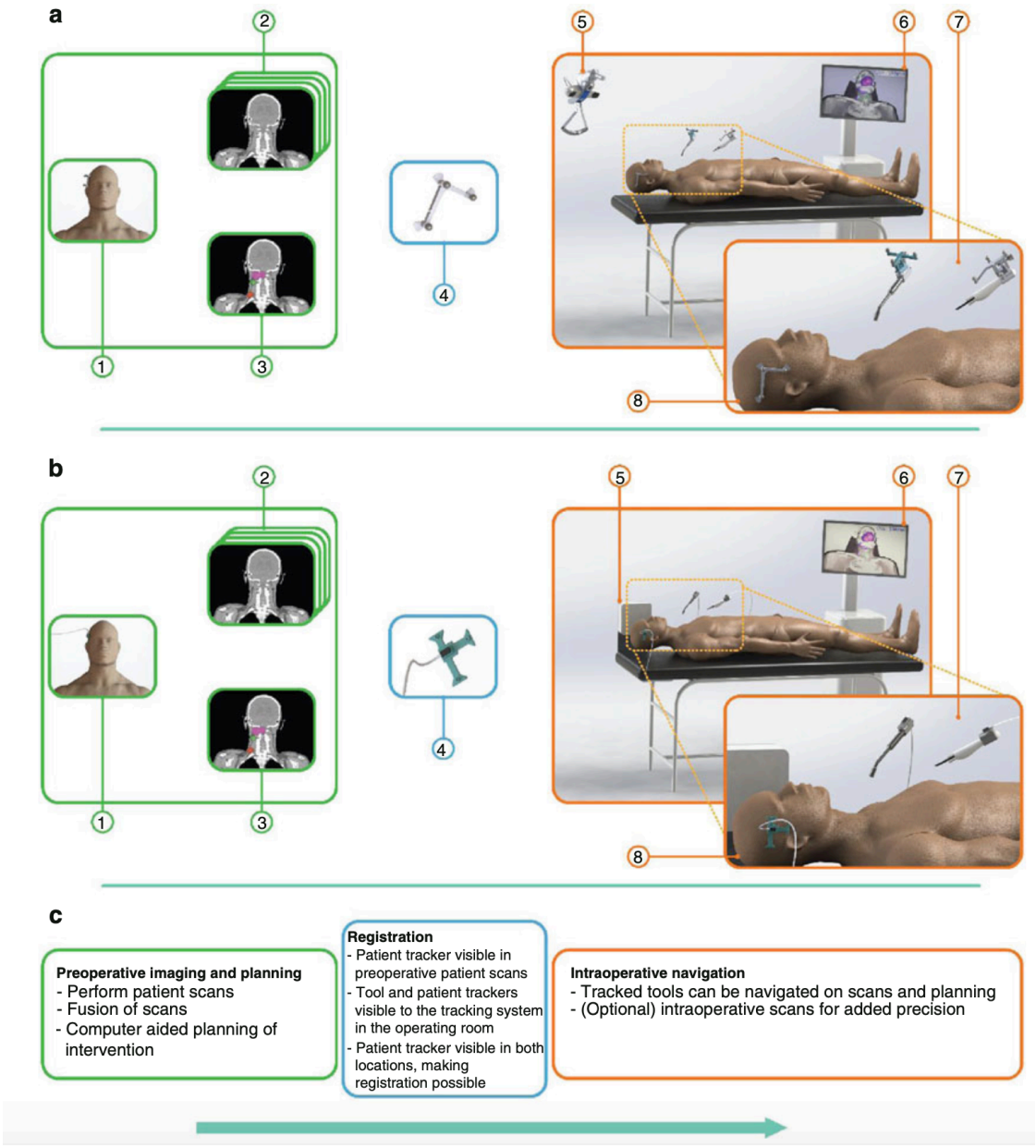

Figure 1-30. Comparison of optical and electromagnetic tracking methods in a typical surgical navigation system: (a) optical tracking, (b) electromagnetic tracking, (c) work steps required in pre-operative phase, registration, and intra-operative navigation. Steps 1 to 8 in each method are as follows: (1) patient with the tracker, (2) 3D pre-operative images, (3) pre-operative scanning, (4) tracker, (5) tracking system, (6) navigation display, (7) tracked tool, (8) patient with the tracker [12].

Figure 1-30 compares optical and electromagnetic tracking methods in pre-operative and intra-operative phases of the surgical navigation [12]. The position and orientation of the surgical instrument is determined by 8 steps in pre-operative planning and intra-operative navigation, and procedures are the same for two tracking methods.

Finally, optical tracking systems are mostly employed in the rigid body applications of CAS, such as neurosurgery and orthopedics. While EM tracking navigators are widely used in catheter placement, abdominal or percutaneous surgeries and endoscopic interventions, both optical and EM tracking systems have been used in several commercial surgical navigation devices. With the advancement of technology, the size and the weight of trackers has been reduced significantly and moved closer to the workspace. Consequently, the reference objects are more visible now and the line-of-sight challenge is addressed more efficiently [5].

(a)

(b)

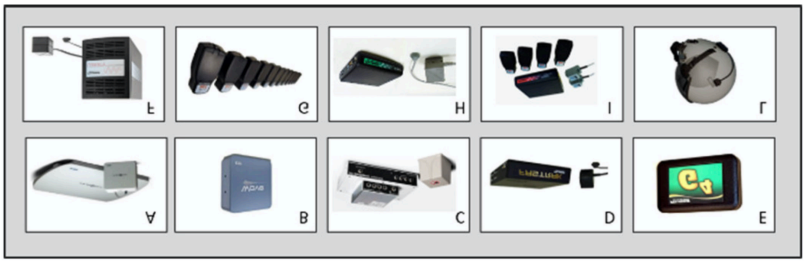

Figure 1-31. Example of (a) optical tracking and (b) electromagnetic tracking devices that exist in commercial surgical navigation systems [80].

1.7 Visualization Techniques

Visualization is an essential component of the surgical navigation system. The most important issue of the visualization in surgical navigation is to render the patient's anatomy related to the surgical instrument. An accurate visualization of the virtual instrument and surgical organ improves the surgeon's perception in intra-operative decision-making.

Generally, the visualization methods for CAS applications are categorized as visual representation, interaction, or simulation [5].

There are currently three categories for visualization medical data: planar visualization, surface rendering, and volume rendering [89]. In planar visualization, images are sampled and shown in slices with arbitrary orientation and position. The orthopedic surgeon usually prefers the standard axial, coronal, and sagittal views for planar visualization. Two other methods visualize the 3D representation of the surgical tissue. Surface rendering extracts the surface of the tissue from input images using predefined thresholds (iso-surfaces) or segmentation techniques Marching cubes is one prominent method of surface rendering. Volume rendering exploits the information of the whole volume and visualizes it by pre-defined opacity and color transfer functions. Ray casting and Maximum Intensity Projection (MIP) are two well-known techniques of the volume rendering.

1.8 Display Modes

In the previous section, we described the various approaches to visualization incorporated into CAS systems – essentially, the software needed in order to display the acquired images and virtual objects. Display modes are the hardware required for the presentation of that real and virtual information. Several studies have been conducted in this field especially for the AR-based CAS systems. These studies can be organized into these general classes [5]:

1. Optical see-through (OST) displays, in which virtual objects are projected onto view of reality. OST displays fall into two groups: the first group uses a mirror that maps the virtual objects onto a semi-transparent display. The second group exploits a semi-transparent view screen that allows the surgical team to see reality through it. One main group of prominent Head-Mounted Displays (HMD) belong to the first class of OST displays: Microsoft HoloLens is the most famous OST-HMD devices and performs better than the others in term of contrast perception, task load, and frame rate. There are some critical issues that should be addressed in OST displays, including weak depth perception. Microscope and endoscope augmentation can be considered as additional OST displays. Microscope augmentation overlays the virtual information with the microscope's

view. This class of display is mostly used in neurosurgery and gives us a good perception of the depth.

2. Video see-through (VST) display, in which the virtual objects and reality are captured by a camera and mixed electronically. One major problem with this integration is reduced image resolution and quality. However, there are some major benefits for the VST displays such as the better depth perception, perfect synchronization ability of the virtual and real information, and independence of the overlay from the viewer's position.
3. Projection-based augmented reality, in which virtual information is projected directly onto the patient using either video or laser projection. A serious challenge in this type of display is parallax error that is related to the visualization of information behind the tissue surface.
4. Augmented reality window in which a semi-transparent mirror is placed between the surgeon and the patient. The virtual information is generated with an autostereoscopic monitor using the technique of Integral Videography [90], [91].

Contributions and Summary

2.1 Contributions

The main focus of this thesis is one of the most widespread hip disorders called slipped capital femoral epiphysis (SCFE). SCFE is defined as "the posterior and inferior slippage of the proximal femoral epiphysis on the metaphysis (femoral neck), which occurs through the epiphyseal plate (growth plate)" [92]. It is a common precursor to hip pathology in adolescence and causes a deformity in the proximal femoral epiphysis. Untreated, this disorder is the leading contributor to 25% of deteriorating hip disease in adults requiring THA [93]. Figure 2-1 shows the anatomy of the hip including its main components, a radiography image of SCFE, and the method of its treatment. As demonstrated in this figure, the hip abnormality is treated by using a single cannulated screw to stabilize the proximal femur in-situ.

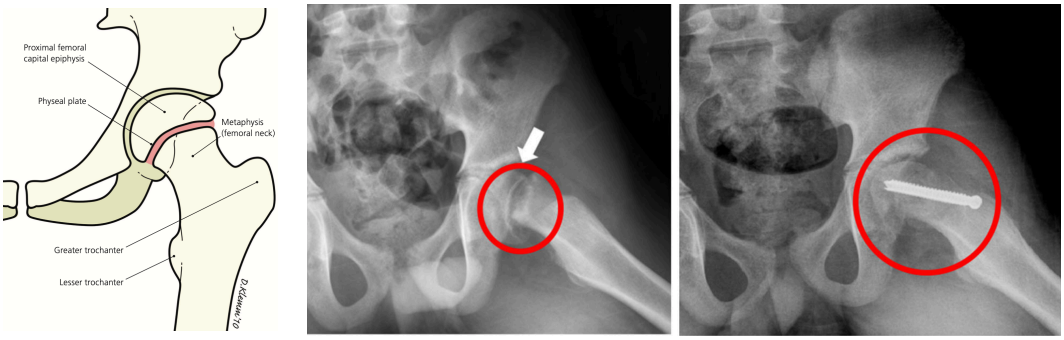

Figure 2-1. (Left) Anatomy of the hip [92], (Middle) Radiograph of a SCFE case (arrow), (Right) Fixation of the SCFE

The most crucial step to performing a successful SCFE surgery is to find the proper position and orientation of the implant, which is challenging because the intricate geometry of the proximal femur requires substantial radiation exposure to fully visualize. Computer-aided surgery alleviates these drawbacks by providing intra-operative navigation and path planning during the operation.

In this thesis, I compare three novel navigation guidance techniques utilizing robotic arm and Inertial Measurement Unit (IMU) devices to project the trajectory of the surgical tool and implant onto the pre-operative image planes:

1- In Method 1 we use an integrated software platform to guide the surgeon based on pre-operative CT images. This platform navigates the robot so that it aligns the drill orientation and tip position with the planned and intended trajectory. The proposed method increases the precision of screw placement and reduces the time of the SCFE procedure. The proposed

methodology is divided into steps including pre-operative planning, trajectory planning, and intra-operative robot positioning. In the first step, the four-quadrant view of the surgical anatomy is provided using pre-operative CT data. In the next step, the current position of the patient and the robot end-effector is measured. The transformation needed for the movement of robot from its current position to the planned position is computed for the trajectory planning. Next, the drill is guided along the planned path.

The drilling and screw placement tasks are performed using a phantom of the left femur bone with SCFE and the result of robotic-assisted surgery performed by an orthopedic surgeon is compared with the manual trials. To define the accuracy of the proposed method, several sources of error such as registration error, entry error, and target error are computed.

2- In Method 2 we used IMU-based navigation based on two orthogonal fluoroscopic images (A-P and Lateral). IMU is chosen because of its compact size, low cost, and accurate orientation representation. The coordinate registration is performed using two different approaches. The first one utilizes one image, one pivot point placed on the bone to identify an entry point, and a calibrated IMU placed within the image plane. The second one exploits two orthogonal x-ray images and four points including one pivot point and three fiducials. No additional calibration of the IMU is required in the second approach. The proposed techniques improve screw placement accuracy and reduce the number of required fluoroscopic X-ray images without changing the current workflow.

   After the path planning, the IMU orientation data is collected and logged until the surgeon has drilled to the target location. Once at the target location, the actual drill position is identified by acquiring a pair of confirmatory A-P and Lateral images. Post-operative validation is achieved by comparing the planned drill trajectory to the actual one. The phantom of left femur bone with SCFE is incorporated for method evaluation. The results are promising, both in overall radiation exposure reduction and improved accuracy to the conventional approach in a phantom study.

3- In Method 3 the navigation system was built based on two IMU devices. Together the IMUs provide the information needed for recovering the orthopedic tool trajectory, along with two orthogonal X-ray images in real-time. Based on this method, the surgeon has access to simultaneous visualization of the planned implant trajectory that is projected on both A-P and Lateral images, without requiring an external optical tracker. Moreover, efficient calibration of IMU devices significantly decreases the pre-operation setup time.

   Two 3D-printed fixtures are designed to house the IMU devices. One is rigidly mounted onto the drill base and the other is attached to the C-arm. The third fixture is attached to the patient table and synchronizes two

IMUs. The results also show 65% decrease in total error and 38% reduction in exposure time for both patient and the surgeon compared to the conventional manual approach.

All three methods superimposed the navigated path onto medical images. We also evaluate if these methods reduce the number of fluoroscopic images and radiation dose output calculations.

2.2 Paper 1: Improved Screw Placement for Slipped Capital Femoral Epiphysis (SCFE) Using Robotically-Assisted Drill Guidance

2.2.1 Summary

In this paper, we planned the surgical path using an integrated software platform that assists the surgeon in choosing the entry and target points efficiently. This method also increases the accuracy of screw placement procedure and decreases the overall duration of the surgery. The integrated software platform navigates the robot so that it aligns the drill orientation and tip position with the planned and intended trajectory. It then assists the surgeon in finding the target position while accounting for additional constraints along the planned trajectory.

The software also provides a quadrant view of the navigation and planning system, which the surgeon then uses to plan the trajectory. The axial, sagittal, coronal, and volumetric views (3D) are presented in the quadrant view. The surgeon can use the software to define the entry and target points of the orthopedic procedure.

With entry and target points defined, we used a robotic arm to orient the drill guide aligned with the orientation of the planned surgical trajectory. The software allows the surgeon to control the orientation and the position of the robot in real time. Also, the system can be reoriented in real time if there is any change in position and orientation of the patient, tracking system, or robotic arm. The optical tracking system feeds the current position and orientation of both the patient and the ends of the robotic arm into the navigation system module of the platform. The navigation system module then calculates the transformation matrix, recovering the new position and orientation of the robotic arm, and the new orientation aligns the robotic arm with the planned angle and trajectory. The navigation component of the surgical software then provides the registration between the pre-operative tracker coordinates and CT dataset. Then using a drill guide mounted to the robotic arm end-effector, we aligned the drill to the planned trajectory. The robotic arm stays in a docked state at the desired position and orientation, and the surgeon uses the drill to place the screw along the planned trajectory.

2.2.2 Contribution

The author of this thesis continued the implementation of the main idea, re-implemented the entire software and calibration methods, and executed five rounds of experiments to validate the methodology. In addition, the software design concept and evaluation of the entire system has been done by the author of this thesis. Co-authors helped in revising the paper and assisted in pre-trial work and main experiment.

2.2.3 Improved Screw Placement for Slipped Capital Femoral Epiphysis (SCFE) using Robotically-Assisted Drill Guidance

Bamshad Azizi Koutenaei, Ozgur Guler, Emmanuel Wilson,
Ramesh U. Thoranaghatte, Matthew Oetgen, Nassir Navab, Kevin Cleary

Improved Screw Placement for Slipped Capital Femoral Epiphysis (SCFE) Using Robotically-Assisted Drill Guidance

Bamshad Azizi Koutenaei[1,2], Ozgur Guler[1], Emmanuel Wilson[1], Ramesh U. Thoranaghatte[3], Matthew Oetgen[1], Nassir Navab[2,4], and Kevin Cleary[1]

[1] Children's National Medical Center, Washington D.C, United States
{bazizi,oguler,ewilson,moetgen,kcleary}@cnmc.org
[2] Chair for Computer Aided Medical Procedures (CAMP), TUM, Munich, Germany
{bazizi,nassir}@cs.tum.edu
[3] NeoMedz Sarl, Switzerland
rameshtu@yahoo.com
[4] Computer Aided Medical Procedures, Johns Hopkins University, USA

Abstract. Slipped Capital Femoral Epiphysis (SCFE) is a common hip displacement condition in adolescents. In the standard treatment, the surgeon uses intra-operative fluoroscopic imaging to plan the screw placement and the drill trajectory. The accuracy, duration, and efficacy of this procedure are highly dependent on surgeon skill. Longer procedure times result in higher radiation dose, to both patient and surgeon. A robotic system to guide the drill trajectory might help to reduce screw placement errors and procedure time by reducing the number of passes and confirmatory fluoroscopic images needed to verify accurate positioning of the drill guide along a planned trajectory. Therefore, with the long-term goals of improving screw placement accuracy, reducing procedure time and intra-operative radiation dose, our group is developing an image-guided robotic surgical system to assist a surgeon with pre-operative path planning and intra-operative drill guide placement.

Keywords: Slipped Capital Femoral Epiphysis (SCFE), Robotically-assisted orthopedic surgery, Computer-aided intervention.

1 Introduction

Slipped capital femoral epiphysis (SCFE) is a common hip disorder in early adolescence that results in displacement of the proximal femoral epiphysis into a posterior and inferior position in relation to the proximal femoral metaphysis. Symptoms of SCFE include groin or knee pain, decreased hip range of motion, and a limp. Due to the risk of permanent injury to the hip joint with continued displacement, SCFE is considered an orthopedic emergency. Surgical treatment is aimed at stabilization of the proximal femoral epiphysis to prevent further displacement, and traditionally has been done by placing one or two screws from the proximal femoral metaphysis across

P. Golland et al. (Eds.): MICCAI 2014, Part I, LNCS 8673, pp. 488–495, 2014.
© Springer International Publishing Switzerland 2014

the physis into the femoral head (shown in fig. 1). The SCFE procedure is done in a minimally invasive manner using X-ray fluoroscopic imaging for visualization. Minimally invasive surgical techniques are advantageous to patients, as they are less disruptive to the soft tissues and often lead to faster functional patient recovery. Despite this benefit, the lack of direct field visualization while operating, as opposed to open surgery, makes these techniques much more technically challenging and requires the surgeon to have an extensive three-dimensional understanding of anatomy to perform the procedure safely. Minimally invasive techniques in orthopedic surgery are often aided by X-ray fluoroscopic imaging. However, concerns exist regarding radiation dose when using fluoroscopy, particularly in pediatrics.

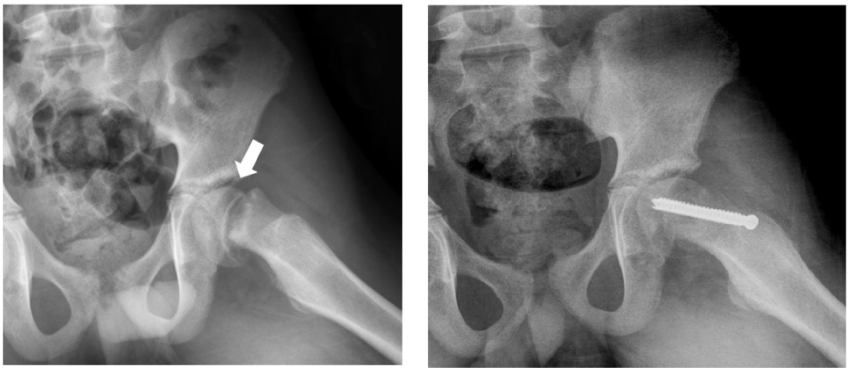

Fig. 1. (Left) Presenting radiograph of a child with slipped capital femoral epiphysis. The proximal epiphysis is displaced posteriorly on the femoral neck (arrow). (Right) Hip radiograph showing fixation of the slipped capital femoral epiphysis with a single screw into the hip.

In the current treatment of SCFE, the surgeon uses intra-operative fluoroscopic imaging to guide the placement of the screw guide pin, confirm the drill trajectory, and direct the final screw placement. Optimal placement of the screw requires precision, with the best position being perpendicular to the physis and deep and central in the femoral head. Improper screw placement, either off center or poorly angled in relation to the physis, leads to the possibility of significant complications from the implant including hip joint penetration, chondrolysis, femoral head vascular injury, proximal femoral avascular necrosis, and poor patient outcomes. The accuracy, duration, and efficacy of this procedure are dependent on surgeon skill and experience. Longer procedures involve higher radiation dose, to both the patient and surgeon.

Other researchers have investigated navigation techniques for orthopedic procedures. For distal locking of intramedullary implants, Suhm et al. showed that radiation exposure time could be decreased from 108 seconds to 7 seconds by using a computer aided surgery navigation system. While procedure time was increased slightly by the use of the navigation system, radiation dose was decreased significantly [1]. In another study of distal locking by Rohilla et al., the average number of fluoroscopy images used for the complete procedure was 48.27 [2], which results in significant radiation exposure. To improve visualization during minimally invasive procedures

and reduce radiation exposure, many researchers have proposed augmented reality systems such as video see-through binocular systems [3], half-mirror display devices [4], systems that directly project images onto the patient's body [5], and single laser-beam pointers [6]. However, these systems have some other challenges such as complexity in surgical tool alignment in proper position and orientation.

In many orthopedic surgeries, navigating the surgical tool to the desired target position is crucial. In addition to image-guided navigation techniques, other methods have been investigated, either to augment the available visual information or to provide additional guidance to a conventional surgical approach. An infrared system was used to track the surgical tool position and provide depth guidance during drilling [7]. Simpler mechanical frames, in the form of a physical stopper, depth guide and depth guidance rings have been implemented to constrain the drill depth. Alternatively, a combination of image-guided and robot-assisted navigation would be a reliable method to provide all required information to perform an intervention in the most efficient and precise way. In regards to the placement of implants to treat SCFE, a navigated robotic system could help reduce both screw placement errors and procedure time by allowing more precise screw placement and decreasing the number of fluoroscopic images needed to accurately position the drill guide along the planned trajectory. The goal of this study was to improve screw placement accuracy, and reduce procedure time and intra-operative radiation dose, by developing an image-guided robotic surgical system to assist the orthopedic surgeon with pre-operative path planning and intra-operative drill guide placement.

2 Methodology

A conventional SCFE procedure relies on fluoroscopy to provide the visual feedback needed by the surgeon to accurately place the fixation screw. This exposes the surgeon to significant radiation exposure over their operating lifetime. In addition, the precision of screw placement is highly dependent on the surgeon's skill and ability to visualize the 3D trajectory of the screw from 2D X-ray images. A few millimeters of screw misplacement could potentially lead to major complications. It requires an experienced surgeon to determine the proper position and orientation of the screw and mentally transform the patient space to image space. All these reasons lead us to develop our robotic assist system for the SCFE procedure. The major contribution of this paper is developing and demonstrating an integrated platform for surgeons that assists in path planning by choosing the entry and target point easier and faster. In addition, we aim to increase the precision of screw placement and decrease the time of the SCFE procedure by navigating the robot to align the drill tip position and drill path along a planned trajectory. When the drill guide is at the planned target location, it provides a rigid and constrained trajectory for the drill to advance.

Pre-operative Planning: The surgical workstation uses preoperative CT data to provide a four-quadrant view of the surgical anatomy. The workstation was created using the open source software package the image-guided surgical toolkit (IGSTK)[8]. This

four-quadrant view consists of axial, sagittal, coronal and 3D rendered volumetric views, which can be used by the surgeon to define skin entry and final target points for screw placement (as shown in fig. 2).

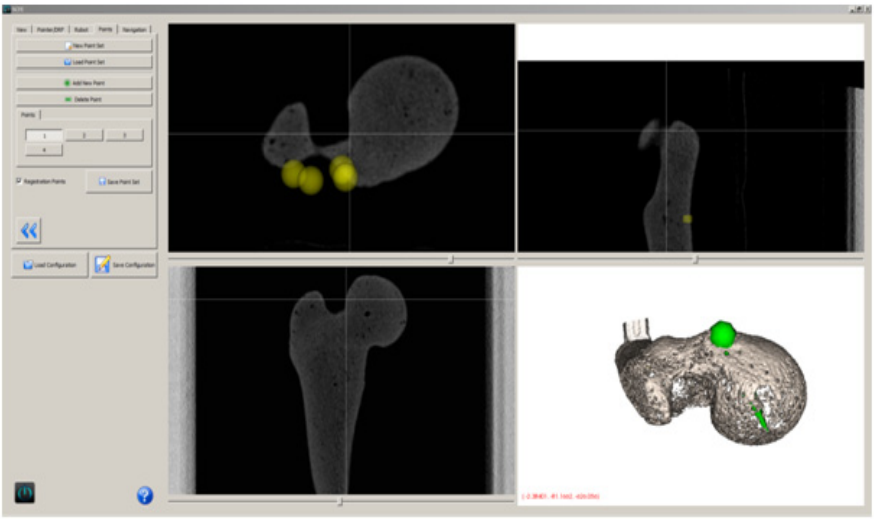

Fig. 2. Surgical navigation workstation showing axial, sagittal, coronal, and 3D views

Trajectory Planning and Calculation of Robot Transformation: The robotic arm used to position the drill guide is a 7 DOF KUKA Light Weight Robot (LWR) robot[1]. The KUKA Fast Research Interface (FRI) API is used to establish a communication between workstation PC and KUKA robot. The application and FRI communication run in parallel using multi-threading. FRI can transfer 20 packets per second which allows the system to update the current position and orientation of the robot in real-time. This update rate means any position change of patient, tracking system, or KUKA base will be compensated quickly via FRI. The surgical navigation component measures the current position of the patient and the robot end-effector and calculates the transformation needed to move the robot from its current position to the planned position. The transformation is then sent to the robot via FRI. A Polaris™ optical tracking system[2] is used to track the locations of the bone phantom and KUKA end-effector and provides a means of computing the transformations between patient and robotic workspace, shown in fig. 3 Two unique rigid body markers, one mounted to the KUKA drill guide tool and one mounted to the bone phantom, are used to track their locations in tracker camera coordinates. The surgical navigation component provides registration between the pre-operative CT dataset and tracker coordinates. This is done using paired-point registration [9] of identifiable phantom surface

[1] KUKA Robotics GMBH, Germany.
[2] Northern Digital Inc., Waterloo, Canada.

features. The transformation from CT to camera coordinates is then used to transform the skin entry and target points (selected by the surgeon within the surgical planning application) to robot coordinate space. Since the drill guide is aligned precisely to the X-axis of the KUKA, our application finds the angles between the X-axis of KUKA and the line crossing transformed entry and target point by using (1) where "a" is KUKA x-axis and "b" is desired trajectory.

$$\cos\theta = \frac{\bar{a}.\bar{b}}{|a|\times|b|} \tag{1}$$

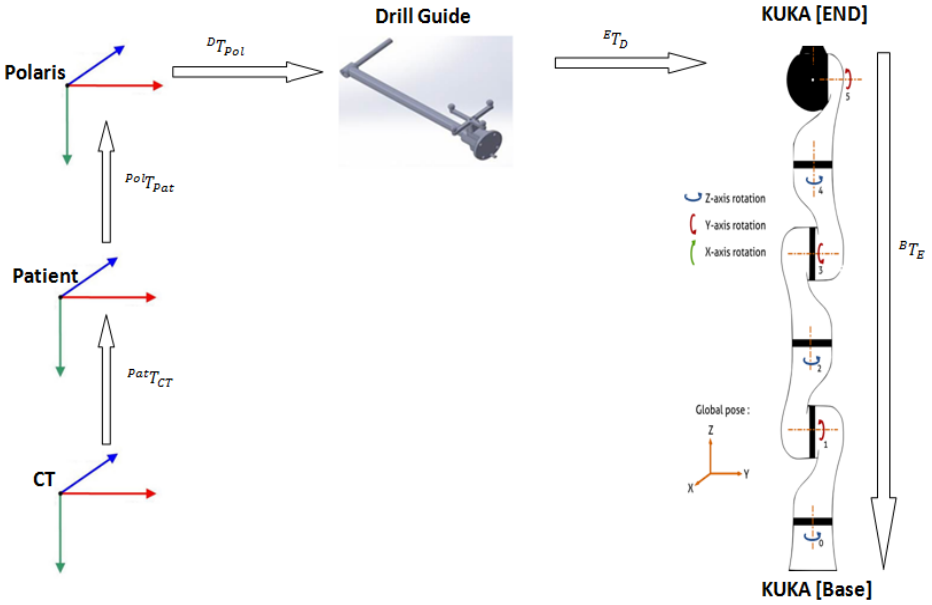

Fig. 3. Chain of transformation from patient coordinate system to KUKA[3] coordinate system

Intra-operative Robot Positioning: A drill guide was designed and fabricated through rapid prototyping[4] to affix to the KUKA end-effector, and securely align the drill along a planned trajectory. The drill guide was designed with a long offset to give the surgeon room to manipulate the drill through the guide. The desired robot end-effector path is converted to joint space using inverse kinematics and communicated to the KUKA controller via FRI. Once the drill guide has reached the commanded position, the KUKA thread inside the application software updates the KUKA coordinates 20 times in one second and calculates the average position and orientation. This helps to reduce the effects of noise in tracker measurements. The

[3] KUKA from `http://www.openrobots.org/morse/doc/latest/user/actuators/kuka_lwr.html`

[4] Objet Connex500, Stratasys Ltd., USA.

robotic arm then maintains its position in a docked state and the surgeon can use the drill to create the pilot hole for screw placement. Several safety concerns have been addressed in this project. First, a virtual region in the KUKA controller has been set in addition to the internal safety features of the KUKA robot. Therefore, the KUKA robot will be turned off if it goes outside of this region. Second, there is a physical stop in the drill guide and a safety offset in the application to prevent the surgeon from drilling beyond a pre-specified depth.

Once the integrated software application was developed, we conducted preliminary tests to assess the contribution of errors from the different system components within the transformation chain. The first proof of concept test conducted in the lab used a CT dataset of a Lego model in the KUKA coordinate system and moved the robot to several predefined points in different orientations. After the lab test, we completed a study in the operating room to position all required devices for image-guided robotic system without any interference with other existing tools and devices. We used 10 pre-scanned sawbones in the operating room test and the surgeon selected entry and target points for screw placement on our interventional workstation. Then we navigated the KUKA to the proper position and the surgeon drilled the wire into the sawbones models.

3 Results

After the initial experiment described above, the overall procedural workflow was tested again and validated in a laboratory environment to get more precise results. First, we redesigned the drill guide to make it stiffer and position the optical tracking frame closer to the tip to minimize offset error. Second, we ran the KUKA robot iteratively to filter the tracking system noise by averaging. The KUKA can receive 20 message packets including new accessible positions and orientations in each second. After system accuracy optimization, additional tests were then conducted in the operating room. Left femur bone models with slipped capital epiphysis deformity were used to perform the drilling and screw placement tasks, as shown in fig. 4. The results from 10 robotic assisted trials performed by an orthopedic surgeon showed sufficient accuracy in comparison to 10 manual trials as detailed below. Of primary note is that all the procedures were done very quickly in these phantom studies, with average times of 4:49 (minutes:seconds). Secondarily, the accuracy results show an overall error that is sufficient for the clinical application [10]. The results are shown in Tables 1- 3.

Table 1. Average time of each step in robotic assisted SCFE surgery phantom experiment (minutes:seconds)

	Planning	Registration	Navigation	Drilling	Total
Average of 10	2:35	0:33	0:43	0:58	4:49

Table 2. Accuracy results (all results in mm). Average of Entry Error and Target error calculated based on distance of desired points and drilled points. Total Error is average of sum of robotic system error and surgeon path planning error for target points.

	Registration Error	Entry Error	Target Error	Total Error
Average of 10	0.588	1.95	2.36	7.04

Table 3. 10 manual trial result conducted by same surgeon. Total Error is measured just for target points based on distance of desired points and drilled points.

	Time	# of fluoroscopy images	Total Error (mm)
Average of 10	2:46	20.4	7.6

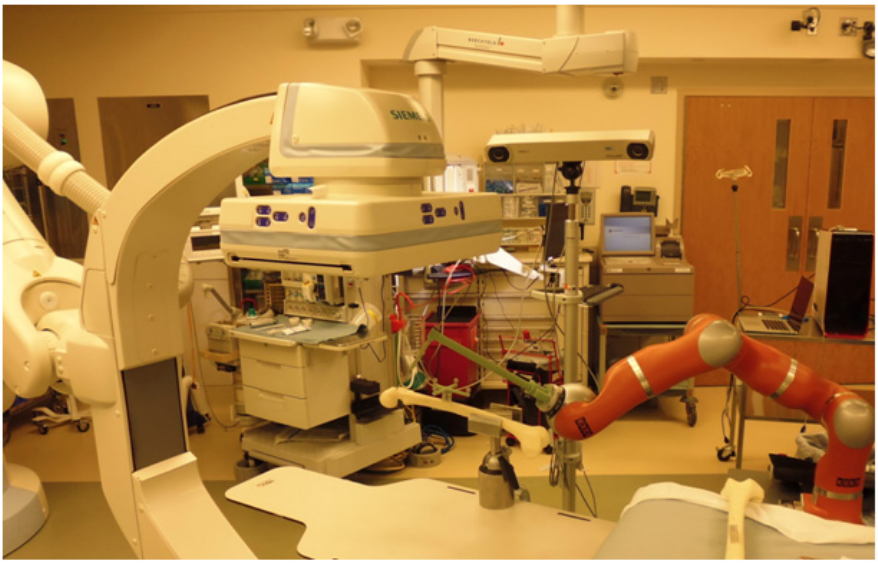

Fig. 4. Phantom study in interventional suite. It demonstrates orange KUKA robotic arm, 3D printed drill guide mounted to the KUKA, bone model and Polaris tracking system.

4 Conclusion and Future Work

Slipped capital femoral epiphysis is a relatively common orthopedic procedure where the accurate placement of the fixation screw is critical to the success of the operation. This paper introduces the system concept and overall architecture for robotically-assisted SCFE procedures. We also present our initial results using phantom models in the operating room. The long term goal is to pursue a clinical trial to determine if this approach could lead to an improved SCFE procedure for patients. For this purpose we also need to improve the workstation and obtain clinical approvals for the system.

Acknowledgment. This research was partially supported by an internal grant from the Sheikh Zayed Institute for Pediatric Surgical Innovation at Children's National Medical Center, which is funded by the government of Abu Dhabi. Partial support was also provided by a Board of Visitor's Grant from Children's and by NIH grant R01CA172244. We would also like to acknowledge the assistance of Radiology Technologists Moaaz Ali and William Powell.

References

1. Suhm, N., Messmer, P., Zuna, I., Jacob, L.A., Regazzoni, P.: Fluoroscopic guidance versus surgical navigation for distal locking of intramedullary implants. a prospective, controlled clinical study. Injury 35(6), 567–574 (2004)
2. Rohilla, R., Singh, R., Magu, N., Devgan, A., Siwach, R., Sangwan, S.: Simultaneous use of cannulated reamer and schanz screw for closed intramedullary femoral nailing. ISRN Surg. (2011) (published online)
3. Fuchs, H., State, A., Pisano, E.D., Garrett, W.F., Hirota, G., Livingston, M., Whitton, M.C., Pizer, S.M.: Towards Performing Ultrasound-Guided Needle Biopsies from within a Head-Mounted Display. In: Höhne, K.H., Kikinis, R. (eds.) VBC 1996. LNCS, vol. 1131, pp. 591–600. Springer, Heidelberg (1996)
4. Liao, H., Ishihara, H., Tran, H.H., Masamune, K., Sakuma, I., Dohi, T.: Fusion of Laser Guidance and 3-D Autostereoscopic Image Overlay for Precision-Guided Surgery. In: Dohi, T., Sakuma, I., Liao, H. (eds.) MIAR 2008. LNCS, vol. 5128, pp. 367–376. Springer, Heidelberg (2008)
5. Volonte, F., Pugin, F., Bucher, P., Sugimoto, M., Ratib, O., Morel, P.: Augmented Reality and Image Overlary Navigation with OsiriX in Laparoscopic and Robotic Surgery: Not Only a Matter of Fashion. J. Hepatobiliary Pancreat. Sci. 18, 506–509 (2011)
6. Marmurek, J., Wedlake, C., Pardasani, U., Eagleson, R., Peters, T.: Image-Guided Laser Projection for Port Placement in Minimally Invasive Surgery. Stud. Health Technol. Inform. 119, 367–372 (2006)
7. Gavaghan, K., Oliveira-Santos, T., Peterhans, M., Reyes, M., Kim, H., Anderegg, S., Weber, S.: Evaluation of a portable image overlay projector for the visualization of surgical navigation data: phantom studies. Int. J. Comp. Assis. Radio. Surg. 7, 547–556 (2012)
8. Enquobahrie, A., Cheng, P., Gary, K., Ibanez, L., Gobbi, D., Lindseth, F., Yaniv, Z., Aylward, S., Jomier, J., Cleary, K.: The image-guided surgery toolkit IGSTK: An open source C++ software toolkit. Journal of Digital Imaging 20(suppl. 1), 21–33 (2007)
9. Arun, K.S., Huang, T.S., Blostein, S.D.: Least-squares fitting of two 3-D point sets. IEEE Transactions on Pattern Analysis and Machine Intelligence 9(5), 698–700 (1987)
10. Pring, E.M., Adamczyk, M., Hosalkar, H.S., Bastrom, T.P., Wallace, C.D., Newton, P.O.: In situ screw fixation of slipped capital femoral epiphysis with a novel approach: a double-cohort controlled study. Journal of Children's Orthopaedics 4(3), 239–244 (2010)

2.3 Paper 2: Inertial Measurement Unit for Radiation-Free Navigated Screw Placement in Slipped Capital Femoral Epiphysis Surgery

2.3.1 Summary

In this paper, we used two different methods for intra-operative navigation with an Inertial Measurement Unit (IMU).

Method (A): this method uses two fluoroscopic images, an entry point identifier on the bone, and an IMU device which is calibrated with the orthogonal image planes. Specifically, the surgeon marks the entry point by drilling a small pilot hole on the bone surface and two orthogonal fluoroscopic images are collected. Once calibration and registration are completed, the surgical software projects the updated orientation of surgical tools onto both orthogonal fluoroscopic images in real time.

Method (B): this method uses four correspondent points on two orthogonal fluoroscopic images (three fiducial points and one pivot point to perform coordinate registration). The surgeon first identifies a pivot point on the bone surface and drills a pilot hole to mark the entry point using a passive arm; leaving the drill tip fixed so that it touches the pilot hole. Then two orthogonal fluoroscopic images are collected, capturing the drill tip and three fiducial points on both images. Then the surgeon selects those four points in corresponding order in orthogonal fluoroscopic images and the surgical software assigns the optimal pivot point and center of the spheres semi-automatically. With all four points on those image planes, the application can calculate the 3D position of all fiducial points and the pivot point. The application then calculates the transformation matrix between image coordinates and world coordinates.

Once surgical planning is completed, the surgical software collects IMU orientation in real time while the surgeon is drilling toward the target point. The actual drill position is then identified by acquiring a pair of confirmatory A-P and Lateral images. By comparing the planned drill trajectory to actual drill position and orientation we can perform the post-operative validation.

2.3.2 Contribution

The author of this thesis initiated the main idea and executed 3 rounds of experiments to validate the methodology. In addition, the software design and evaluation of the entire system has been done by the author of this thesis. Co-authors helped in implementation of Method (B) along with revising the paper and assisting in pre-trial work and the main experiment.

2.3.3 Inertial Measurement Unit for Radiation-Free Navigated Screw Placement in Slipped Capital Femoral Epiphysis Surgery

Bamshad Azizi Koutenaei, Ozgur Guler, Emmanuel Wilson, Matthew Oetgen,
Patrick Grimm, Nassir Navab, and Kevin Cleary

Inertial Measurement Unit for Radiation-Free Navigated Screw Placement in Slipped Capital Femoral Epiphysis Surgery

Bamshad Azizi Koutenaei[1,2], Ozgur Guler[1], Emmanuel Wilson[1], Matthew Oetgen[1], Patrick Grimm[1], Nassir Navab[2,3], and Kevin Cleary[1]

[1] Children's National Medical Center, Washington D.C, United States
{bazizi,oguler,ewilson,moetgen,pgrimm,kcleary}@cnmc.org
[2] Chair for Computer Aided Medical Procedures (CAMP), TUM, Munich, Germany
[3] Computer Aided Medical Procedures (CAMP), Johns Hopkins University, USA
nassir@cs.tum.edu

Abstract. Slipped Capital Femoral Epiphysis (SCFE) is a common pathologic hip condition in adolescents. In the standard treatment, a surgeon relies on multiple intra-operative fluoroscopic X-ray images to plan the screw placement and to guide a drill along the intended trajectory. More complex cases could require more images, and thereby, higher radiation dose to both patient and surgeon. We introduce a novel technique using an Inertial Measurement Unit (IMU) for recovering and visualizing the orthopedic tool trajectory in two orthogonal X-ray images in real-time. The proposed technique improves screw placement accuracy and reduces the number of required fluoroscopic X-ray images without changing the current workflow. We present results from a phantom study using 20 bones to perform drilling and screw placement tasks. While dramatically reducing the number of required fluoroscopic images from 20 to 4, the results also show improvement in accuracy compared to the manual SCFE approach.

Keywords: Slipped Capital Femoral Epiphysis (SCFE), Computer-assisted Orthopedic Surgery, Computer-aided Intervention, Inertial Measurement Unit.

1 Introduction

Computer-assisted surgery (CAS) has been used in various clinical procedures. Surgical planning methods for image guidance fall within two broad categories: volumetric image-based navigation (primarily, CT and MRI) and intraoperative fluoroscopic navigation [1]. Both methods could be used in passive and active CAS systems [2]. CAS systems have found increased use particularly in orthopedic surgery, where surgeon interaction is largely with rigid anatomy that is immobilized with relative efficacy. In many orthopedic procedures, the surgeon relies heavily on intra-operative fluoroscopic images; from planning implant trajectory, to guiding intra-operative positioning, and finally, to confirming implant position at completion. Antirotator proximal femoral nailing and intramedullary nailing of femur fracture are examples of

© Springer International Publishing Switzerland 2015
N. Navab et al. (Eds.): MICCAI 2015, Part I, LNCS 9349, pp. 355–362, 2015.
DOI: 10.1007/978-3-319-24553-9_44

orthopedic procedures that broadly follow this approach with regards to image acquisition. The pre-operative fluoroscopic images are crucial in planning the procedure, and post-operative images are needed to validate procedural accuracy. The number of additional images acquired during the procedure to orient and reposition a tool depend on surgeon skill and experience, and leads to increased radiation dose and procedure times. For instance, the average number of fluoroscopy images used for distal locking was 48.27 that causes significant radiation exposure [3]. Therefore many augmented reality systems proposed to reduce radiation exposure during the surgery for instance: half-mirror display devices [4], single laser-beam pointers [5], video see-through binocular systems [6] visualization based on IMU [7], systems that directly project images onto the patient's body [8], and other radiation-free drill guidance for orthopedic surgery [9][10][11][12].

Therefore we introduce a system in this paper that could reduce radiation dose, while improving implant accuracy with applicability in many orthopedic procedures. As a case study we chose slipped capital femoral epiphysis (SCFE) surgery.

SCFE is a common hip disorder that causes displacement of the proximal femoral epiphysis. Traditional surgical treatment requires placing screws from the proximal femoral metaphysis into the femoral head for stabilization of the proximal femoral epiphysis (Fig. 1). In the conventional approach to SCFE, the surgeon uses intra-operative fluoroscopic imaging as visualization aid to guide the screw placement and confirm the drill trajectory.

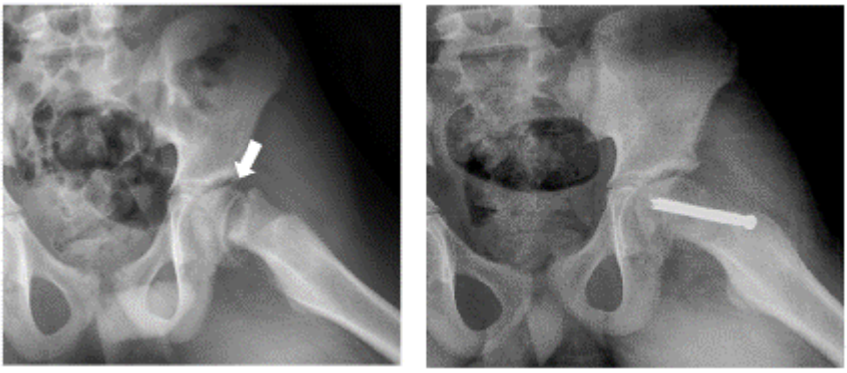

Fig. 1. (Left) radiograph of a SCFE case (arrow). (Right) fixation of the SCFE

In regards to the placement of implants to treat SCFE, a navigation system based on inertial measurement unit (IMU) could help reduce both radiation dose and procedure time. Therefore we implemented a system that superimposes IMU information onto two orthogonal fluoroscopic images.

2 Methodology

A conventional SCFE procedure uses intra-operative fluoroscopic images for visualization to accurately place the screw. This causes significant radiation exposure for

both surgeon and patient. A typical work-flow involves the surgeon extrapolating a tool entry point based on target site and optimal tool orientation using fluoroscopic images. Once an optimal tool trajectory is evaluated, additional X-ray images are acquired to confirm that the tool is being inserted along this planned path. On average, about 20 x-ray images are acquired to deduce the best orientation and guide the tool during the procedure. The question we asked is: "What new information of clinical utility are these additional x-ray images providing?" Once a surgeon has mapped out the procedural workflow using pre-operative planning images, these additional images serve no clinical utility beyond confirming tool orientation. Our approach was to use a relatively inexpensive hardware device to augment this information in lieu of x-ray image. We were able to register and super-impose the real-time tool trajectory on two pre-operative orthogonal x-ray images. This results in improving screw placement and greatly decreased radiation exposure.

We chose an Inertial Measurement Unit (IMU) because of its compact size, low cost, and accurate orientation representation. The IMU used for this system is an X-IMU (x-io Technologies, Bristol, UK). The device consists of a 3-axis gyroscope, 3-axis accelerometer, and a 3-axis magnetometer. It sends combined data from the various sensors encapsulated in each data packet. Data transfer is done over Bluetooth LowEnergy (BLE) wireless protocol to our application running on a laptop at a rate of 512 packets per second. The laptop application uses a sensor fusion algorithm [13] to calculate the current orientation. We designed a 3D-printed fixture which mounts to the drill base and houses the IMU device. This provides a fixed, known relation between the drill bit and IMU. We used an Epiphan DVI2USB3.0 frame-grabber (Epiphany Systems Inc., Palo Alto, CA) to frame-grab the x-ray images from the Siemens Zeego system. To facilitate a more ergonomic surgeon experience, we streamed the laptop visualization to a Samsung tablet placed next to the surgeon.

In this paper, we introduce two different methods to assist the surgeon. In method (A) we use one image, one pivot point placed on the bone to identify an entry point, and a calibrated IMU placed within the image plane. In method (B) we use two orthogonal x-ray images and four points (1 pivot point and three fiducials for coordinate registration). No additional calibration of the IMU is required in the latter approach.

Pre-operative Set-up: In method (A), we used a 3D-printed calibration fixture to align the IMU to the patient table coordinate, shown in Fig 2a. During the procedure, we used a second 3D-printed fixture to affix the IMU to the drill, shown in Figure 2b. The IMU calibration fixture orients the IMU XY-plane with the A-P fluoroscopic image plane, and IMU YZ-plane with the lateral fluoroscopic plane. The patient table position and Zeego robot coordinates are inherently calibrated. Therefore, by orienting the IMU coordinate frame with respect to the patient table, we have a calibration between fluoroscopic image plane and the IMU coordinates. For method (B), the registration between IMU and fluoroscopic image coordinates is done based on selection of four corresponding points in each pair of orthogonal x-ray images. The four points are comprised of the drill tip and three 8mm diameter metal sphere fiducials, shown in Fig 2c.

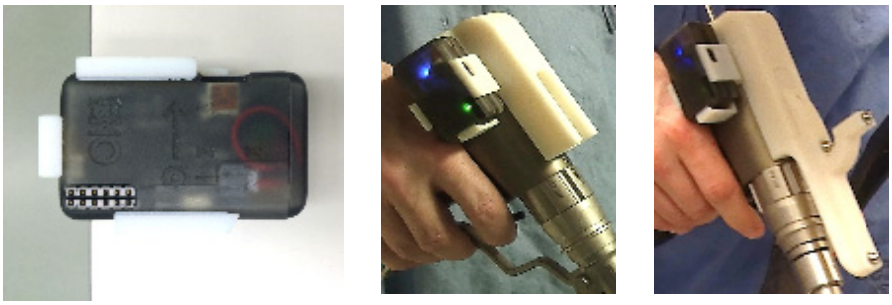

(a) **(b)** **(c)**

Fig. 2. (a) Calibration fixture (b) Drill fixture (c) Fiducial spheres for coordinate registration

Intra-Operative Planning: Here we explain the two methods employed to register the drill coordinates to image space in real-time.

Method (A): The surgeon identifies an entry point by drilling a small divot at the bone surface. Two orthogonal x-rays images are acquired (in A-P and Lateral orientations). As mentioned before, in this method navigation can be based off one image alone. However, image augmentation and navigation was done using both the A-P and Lateral images, as this approach is clinically most relevant. After loading those images in our application, we define the drill tip as a pivot point. We use seed based region growing segmentation to choose the best possible pivot point in a semi-automatic manner. Subsequently, the IMU is placed within the calibration fixture and placed at the edge of the patient table. The calibration fixture was designed such that it orients the IMU coordinates in a known configuration with respect to image coordinates. Based on our setting, the IMU X-Y plane maps to the A-P image plane and the IMU Y-Z frame maps to the lateral image (Error < 0.6 mm). Afterward, our method projects the updated orientation to two orthogonal images. These two projections are calculated by the following chain of transformations, and shown in Figure 3.

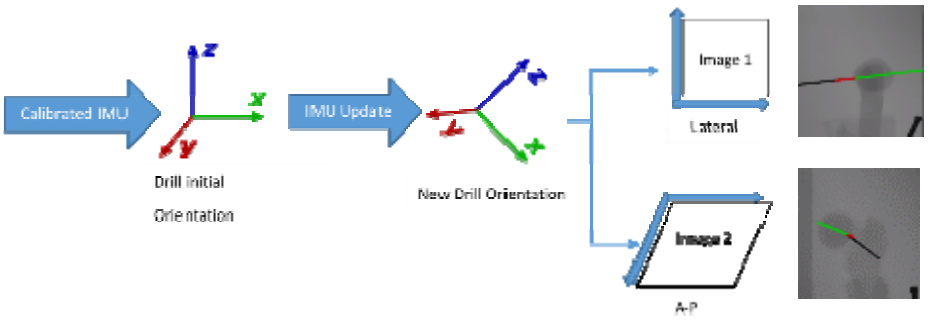

Fig. 3. Flow chart of method (A) transformation chain

T is a 4x4 transformation matrix, P is a projection matrix, and Tr is a translation matrix. (IMU = device, WRD = World defined by IMU, IMG = C-arm)

$$^{Pivot}Tr_{XY} * {}^{XY}P_{IMG} * {}^{IMG}T_{WRD} * {}^{WRD}T_{IMU} \quad (1)$$

$$^{Pivot}Tr_{YZ} * {}^{YZ}P_{IMG} * {}^{IMG}T_{WRD} * {}^{WRD}T_{IMU} \quad (2)$$

Method (B): The surgeon defines the entry point and drills into the bone surface to create an identifying divot point. The drill is fixed besides the table using a passive arm such that the drill tip is within the divot. Two orthogonal x-ray images (AP and Lateral) that visualize the drill tip and the three fiducials are acquired. After loading the images in our application, the three fiducials and drill tip are identified in commensurate order in both AP and Lateral images. We used a seed based region growing segmentation to choose the best possible pivot point and also center of the spheres in a semi-automatic manner. The application calculates the 3D position of those fiducial points by combining selected point positions in the two images (we obtain x and y coordinates from AP, and z coordinate from the Lateral image). With this we calculate the transformation between world coordinates to image coordinates. Since the drill bit is aligned precisely to the X-axis of the IMU, our application projects the x-axis of the IMU in the AP and Lateral images (Error < 0.8 mm). These two projections are calculated by the following chain of transformation, shown in Figure 4.

T is a 4x4 transformation matrix, P is a projection matrix, and Tr is a translation matrix. (IMU = device, WRD = World defined by IMU, IMG = C-arm)

$$^{Pivot}Tr_{XY} * {}^{XY}P_{IMG} * {}^{IMG}T_{Drill} * {}^{Drill}T_{IMUi} * {}^{IMUi}T_{WRD} * {}^{WRD}T_{IMUup} \quad (3)$$

$$^{Pivot}Tr_{YZ} * {}^{YZ}P_{IMG} * {}^{IMG}T_{Drill} * {}^{Drill}T_{IMUi} * {}^{IMUi}T_{WRD} * {}^{WRD}T_{IMUup} \quad (4)$$

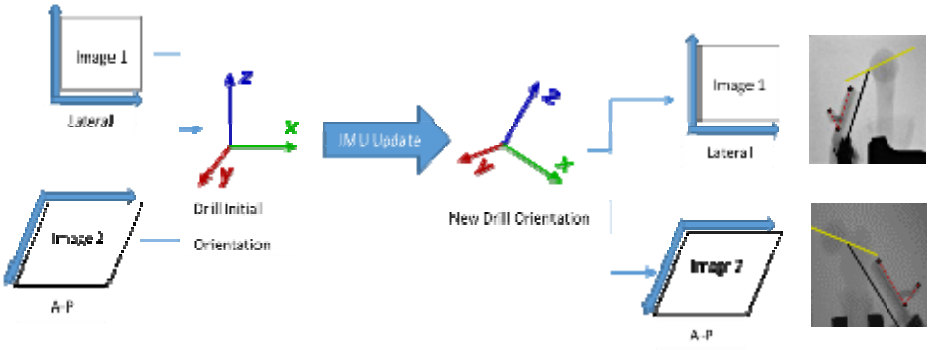

Fig. 4. Flow chart of method (B) transformation chain

Post-Operative Verification: Once the surgeon plans a path, the application collects and logs IMU orientation data until the surgeon has drilled to the target location. Once at the target location, a pair of confirmatory AP and Lateral images are acquired to correctly identify actual drill position. Post-operative validation is achieved by comparing the planned drill trajectory to actual, as shown in Fig 5.

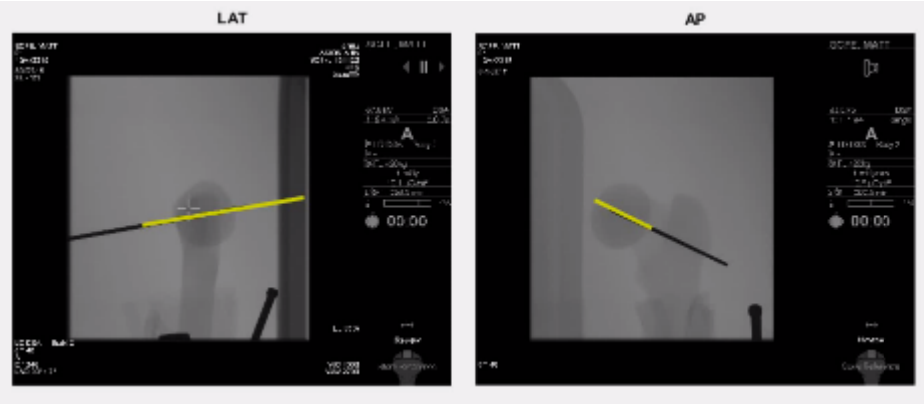

Fig. 5. Post x-ray evaluation in Lateral and A-P (yellow line is the trajectory before drilling)

3 Results

We started the study by assessing the accuracy of the x-IMU device using a Polaris optical tracker (Northern Digital Inc., Waterloo, Canada). In addition, the internal report of X-IMU shows the IMU device and algorithm we used is highly accurate[1]. The first proof-of-concept test in the lab used two orthogonal images with a standard smartphone camera to assess the efficacy of this approach. These tests confirmed the validity of our concept. Following lab tests, we completed a study in the operating room, including image acquisition from the Siemens Zeego C-arm system.

Left femur bone models with slipped capital epiphysis deformity (Model # 1161, Sawbones Worldwide, Vashon Island, WA) were used to perform the drilling and screw placement tasks, shown in Figure 6. 10 manual procedures were performed by the experienced surgeon, which served as baseline assessment of the procedural accuracy and completion time. Subsequently, 30 assisted trials were performed by the experienced orthopedic surgeon, and another 10 assisted trials performed by an orthopedic resident with no experience in SCFE surgery. For each trial, the total procedure time and number of fluoroscopic images acquired were logged, and the final placement accuracy computed from confirmatory orthogonal images acquired at the end of each trial. Average procedure time for the manual trials was 2:46 (mm:ss). Average procedure time was 1:51 (mm:ss) for the assisted trials for the experienced surgeon and 4:31 (mm:ss) for the non-experienced surgeon. The longer procedure time for the assisted trials for the non-experienced surgeon can be in part attributed to considerations given to learning curve and set-up time. The accuracy results show clear improvement with the assisted trials. Pending a study on a larger number of data samples, this shows sufficient accuracy in comparison to the conventional [14] and robotic-assisted approach [15]. The results are shown in Table 1.

[1] http://www.x-io.co.uk/res/doc/madgwick_internal_report.pdf

Table 1. 10 manual and 40 navigated trials conducted by experienced and non-experienced surgeon. Total error is measured for target points based on distance of desired and drilled points (Statistical Significance: $p < 0.05$, Registration Error: Err < 0.8 mm).

	Skill in SCFE	Total time	# of images	Total error
10 Manual	Experienced	2:46	20.4	7.6 mm
30 Assisted	Experienced	1:51	4	3.59 mm
10 Assisted	Non-Experienced	4:31	4	6.35 mm

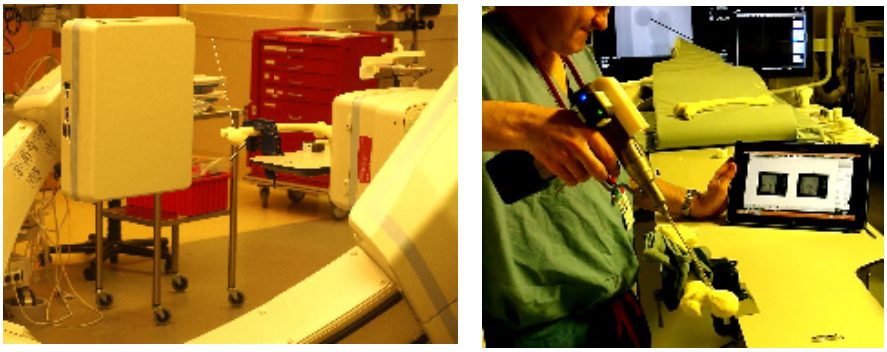

(a) **(b)**

Fig. 6. Phantom study in interventional suite. (a) Setup for lateral exposure (b) Surgeon using the visualization for planning optimal tool path

4 Conclusion and Future Work

Slipped capital femoral epiphysis is a relatively common orthopedic procedure in children where the accurate placement of the fixation screw often requires 20 x-ray images or a CT dataset in a conventional approach. This paper introduces a simple, cost-effective system to assist surgeons in intra-operative path planning in a real-time manner based on an IMU device. With this device setup, and reliance on only two orthogonal x-ray images, we were able to streamline the SCFE procedure. In addition, these techniques could be extended to many other orthopedic procedures that follow a similar clinical workflow. This preliminary study shows promising results, both in overall radiation exposure reduction and improved accuracy to the conventional approach in a phantom study. In future, the system could be complemented by using a head mounted display and more sophisticated navigation and visualization tools. Our long term goal is to pursue a clinical trial to determine if this approach could lead to a more accessible SCFE workflow and improved clinical outcome for patients.

References

1. Sugano, N.: Computer-assisted orthopedic surgery. Journal of Orthopaedic Science 8(3), 442–448 (2003)
2. Musahl, V., Plakseychuk, A., Fu, F.H.: Current opinion on computer-aided surgical navigation and robotics: role in the treatment of sports-related injuries. Sports Med. 32(13), 809–818 (2002)
3. Rohilla, R., Singh, R., Magu, N., Devgan, A., Siwach, R., Sangwan, S.: Simultaneous use of cannulated reamer and schanz screw for closed intramedullary femoral nailing. ISRN Surg. (2011) (published online)
4. Liao, H., Ishihara, H., Tran, H.H., Masamune, K., Sakuma, I., Dohi, T.: Fusion of Laser Guidance and 3-D Autostereoscopic Image Overlay for Precision-Guided Surgery. In: Dohi, T., Sakuma, I., Liao, H. (eds.) MIAR 2008. LNCS, vol. 5128, pp. 367–376. Springer, Heidelberg (2008)
5. Marmurek, J., Wedlake, C., Pardasani, U., Eagleson, R., Peters, T.: Image-Guided Laser Projection for Port Placement in Minimally Invasive Surgery. Stud. Health Technol. Inform. 119, 367–372 (2006)
6. Fuchs, H., State, A., Pisano, E.D., Garrett, W.F., Hirota, G., Livingston, M., Whitton, M.C., Pizer, S.: Towards Performing Ultrasound-Guided Needle Biopsies from within a Head-Mounted Display. In: Höhne, K.H., Kikinis, R. (eds.) VBC 1996. LNCS, vol. 1131, pp. 591–600. Springer, Heidelberg (1996)
7. Walti, J., Jost, G.F., Cattin, P.C.: A New Cost-Effective Approach to Pedicular Screw Placement. In: Linte, C.A. (ed.) AE-CAI 2014. LNCS, vol. 8678, pp. 90–97. Springer, Heidelberg (2014)
8. Volonte, F., Pugin, F., Bucher, P., Sugimoto, M., Ratib, O., Morel, P.: Augmented Reality and Image Overlary Navigation with OsiriX in Laparoscopic and Robotic Surgery: Not Only a Matter of Fashion. J. Hepatobiliary Pancreat Sci. 18, 506–509 (2011)
9. Diotte, B., Fallavollita, P., Wang, L., Weidert, S., Thaller, P.-H., Euler, E., Navab, N.: Radiation-free drill guidance in interlocking of intramedullary nails. In: Ayache, N., Delingette, H., Golland, P., Mori, K. (eds.) MICCAI 2012, Part I. LNCS, vol. 7510, pp. 18–25. Springer, Heidelberg (2012)
10. Hoffmann, M., et al.: Next generation distal locking for intramedullary nails using an electromagnetic X-ray-radiation-free real-time navigation system. Journal of Trauma and Acute Care Surgery 73, Jg., Nr. 1, 243–248 (2012)
11. Stathopoulos, I., et al.: Radiation-free distal locking of intramedullary nails: Evaluation of a new electromagnetic computer-assisted guidance system. Injury, 44. Jg., Nr. 6, 872–875 (2013)
12. Arlettaz, Y., et al.: Distal locking of femoral nails: evaluation of a new radiation independent targeting system. Journal of Orthopaedic Trauma 26. Jg., Nr. 11, S. 633–637 (2012)
13. Madgwick, S.O.H., Harrison, A.J.L., Vaidyanathan, R.: Estimation of IMU and MARG orientation using a gradient descent algorithm. In: 2011 IEEE International Conference Rehabilitation Robotics (ICORR), pp. 1–7 (2011), doi:10.1109/ICORR.2011.5975346
14. Pring, E.M., Adamczyk, M., Hosalkar, H.S., Bastrom, T.P., Wallace, C.D., Newton, P.O.: In situ screw fixation of slipped capital femoral epiphysis with a novel approach: a double-cohort controlled study. Journal of Children's Orthopaedics 4(3), 239–244 (2010)
15. Azizi Koutenaei, B., Guler, O., Wilson, E., et al.: Improved Screw Placement for Slipped Capital Femoral Epiphysis (SCFE) using Robotically-Assisted Drill Guidance. In: International Conference on Medical Image Computing and Computer-Assisted Intervention, vol. 17(01), pp. 488–495 (2014)

2.4 Paper 3: Radiation-free Methods for Navigated Screw Placement in Slipped Capital Femoral Epiphysis Surgery

2.4.1 Summary

In this paper, we discuss three novel navigation guidance methods that use either robotic arms, or a single- or dual-Inertial Measurement Unit (IMU) device configuration to project the trajectory of the surgical tool and implant onto the pre-operative image planes. We demonstrate that these methods reduce the number of fluoroscopic images (and thereby, radiation dose) while improving SCFE procedure accuracy. We then demonstrate how the portability and efficient calibration of the dual IMU method significantly decreases the pre-operation setup time in comparison with existing navigation methods. The advantage of using two IMU devices versus other radiation-free navigation methods is the quick and repeatable calibration method for attachable devices. The first two methods have been explained in previous summaries.

The dual IMU method acquires two sample X-ray images of two fixed drill bits with a constant length and known angle, and the orientation of these two lines in the C-arm coordinate system is used to form a full 3D orientation representation. The surgeon drills a small pilot hole at the bone surface to identify the entry point, then two fluoroscopic images are acquired. These two images can be acquired at any angle because the two IMU devices provide the orientation of both the C-arm and the surgical tool, so the orientation of the image plane does not affect the calculation or accuracy of the method. The surgeon then defines the drill tip as a pivot point, which provides the translation matrix that will be used later in the transformation chain. The application picks the most precise pivot point in a semi-automatic manner. Post-operative placement confirmation is achieved by comparing the provided projection of the drill trajectory and the actual placed implant.

2.4.2 Contribution

The author of this thesis initiated the main idea and executed 10 total rounds of experiments to validate all three methodologies. In addition, the software design and evaluation of the entire system has been done by the author of this thesis. Co-authors helped revise the paper and assisted in pre-trial work and the main experiment.

2.4.3 Radiation-free methods for navigated screw placement in slipped capital femoral epiphysis surgery

Bamshad Azizi Koutenaei, Javad Fotouhi, Farshid Alambeigi, Emmanuel Wilson, Ozgur Guler, Mathew Oetgen, Kevin Cleary, Nassir Navab

International Journal of Computer Assisted Radiology and Surgery (2019) 14:2199–2210
https://doi.org/10.1007/s11548-019-02026-9

ORIGINAL ARTICLE

Radiation-free methods for navigated screw placement in slipped capital femoral epiphysis surgery

Bamshad Azizi Koutenaei[1,2] · Javad Fotouhi[3] · Farshid Alambeigi[3] · Emmanuel Wilson[4] · Ozgur Guler[4] · Mathew Oetgen[2] · Kevin Cleary[2] · Nassir Navab[1,3]

Received: 15 December 2018 / Accepted: 3 July 2019 / Published online: 18 July 2019
© CARS 2019

Abstract

Purpose For orthopedic procedures, surgeons utilize intra-operative medical images such as fluoroscopy to plan screw placement and accurately position the guide wire with the intended trajectory. The number of fluoroscopic images needed depends on the complexity of the case and skill of the surgeon. Since more fluoroscopic images lead to more exposure and higher radiation dose for both surgeon and patient, a solution that decreases the number of fluoroscopic images would be an improvement in clinical care.

Methods This article describes and compares three different novel navigation methods and techniques for screw placement using an attachable Inertial Measurement Unit device or a robotic arm. These methods provide projection and visualization of the surgical tool trajectory during the slipped capital femoral epiphysis procedure.

Results These techniques resulted in faster and more efficient preoperative calibration and set up times compared to other intra-operative navigation systems in our phantom study. We conducted an experiment using 120 model bones to measure the accuracy of the methods.

Conclusion As conclusion, these approaches have the potential to improve accuracy of surgical tool navigation and decrease the number of required X-ray images without any change in the clinical workflow. The results also show 65% decrease in total error compared to the conventional manual approach.

Keywords Slipped capital femoral epiphysis (SCFE) · Computer-assisted orthopedic surgery · Computer-aided intervention · Inertial measurement unit

Introduction and related work

Currently, many clinical procedures employ computer-assisted surgery (CAS) methods to improve the performance and precision of the entire surgical process including pre-planning, execution and postoperative verification. Orthopedic surgery is a good candidate for CAS, since most of the surgical interaction is on immobilized rigid anatomy. Many orthopedic procedures depend heavily on preoperative and intra-operative fluoroscopic images. Fluoroscopic images are used to plan implant trajectory, guide intra-operative navigation, and to postoperatively confirm implant position and orientation. As examples, intramedullary nailing of femur fracture and anti-rotator proximal femoral nailing follow this approach. In all these procedures, the surgeon's skill and experience is the main factor in limiting the number of images needed to perform the procedure accurately. Additional fluoroscopic images will result in increased radiation dose for

Kevin Cleary and Nassir Navab contributed equally to the project organization and execution and should be co-last authors.

Electronic supplementary material The online version of this article (https://doi.org/10.1007/s11548-019-02026-9) contains supplementary material, which is available to authorized users.

✉ Bamshad Azizi Koutenaei
bamshad@mytum.de

1 Chair for Computer Aided Medical Procedures and Augmented Reality, Department of Informatics, Technical University of Munich (TUM), Munich, Germany

2 Sheikh Zayed Institute for Pediatric Surgical Innovation, Children's National Health System, Washington, DC, USA

3 Laboratory for Computational Sensing and Robotics, Johns Hopkins University, Baltimore, MD, USA

4 E-Kare Inc, Fairfax, VA, USA

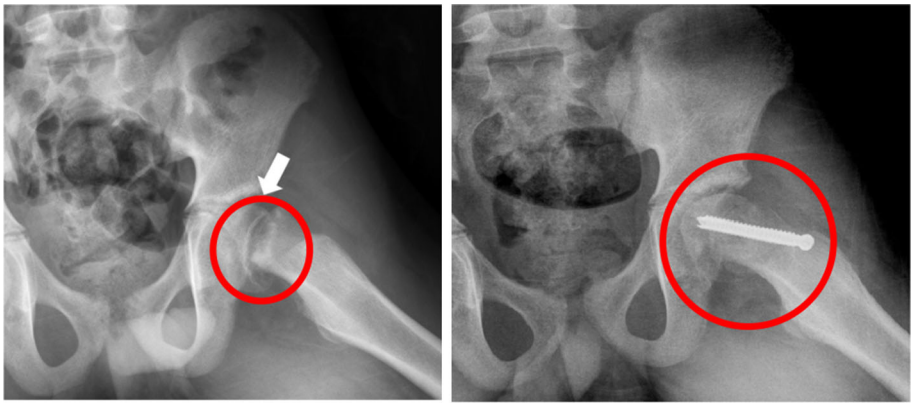

Fig. 1 (Left) Radiograph of a SCFE case (arrow). (Right) Fixation of the SCFE

the patient and surgeon and an increase in procedure time. For example, for the distal locking procedure, 48.27 fluoroscopy images are needed on average which results in high radiation exposure [1]. Therefore, many CAS or augmented reality methods have been investigated to decrease the number of fluoroscopic images during the surgery. These methods include the following categories: half-mirror displays [2], single and dual laser-beam pointers [3], camera-augmented mobile C-arm (CAMC) [4] IMU-based visualization method [5], systems that superimpose images onto the patient's body directly [6], and other guidance tools for radiation-free navigation for orthopedic surgery [7–10].

In this paper, we focus on slipped capital femoral epiphysis (SCFE), a common precursor to hip pathology in adolescence. This condition causes a deformity in the proximal femoral epiphysis. It is postulated that this condition is the reason for 25% of degenerative hip disease in adults requiring total hip arthroplasty [11, 12]. The typical treatment for this hip deformity is placing a single cannulated screw to stabilize the proximal femur in an in situ fashion (Fig. 1). It is well accepted that this screw should be positioned as closely as possible to the center of the epiphysis and perpendicular to the physis in both the coronal and sagittal planes to avoid iatrogenic injury to the hip from joint penetration of the surgical implant [13]. This ideal implant position results in optimal biomechanical fixation and promotes earlier physeal closure and deformity stabilization [13, 14]. Conversely, flawed implant position within the proximal femur can cause delayed physeal closure and lead to deformity progression [15, 16]. Therefore, proper implant positioning and orientation is the most important step of this surgical procedure.

Some methods have been introduced to improve imaging, such as using a second fluoroscopic C-arm for acquiring concurrent A–P and lateral images, thus allowing the surgeon to navigate the implant insertion in both images at once. This technique has improved the accuracy in comparison with the conventional single C-arm approach [17]. However, this dual C-arm approach is rarely used in clinical practice because it is more expensive and resource-intensive. Augmented navigation and guidance approaches can potentially reduce the reliance on intra-operative fluoroscopic imaging.

In this paper, we discuss three novel navigation guidance techniques utilizing robotic arm and Inertial Measurement Unit (IMU) devices to project the trajectory of the surgical tool and implant onto the preoperative image planes. We apply these techniques using robotic arms, a single IMU, and dual IMU configurations as described in "Methodology" section. In "Results" section, we evaluate if these methods reduce the number of fluoroscopic images and radiation dose output calculation. We then finish with discussion in "Discussion and Conclusions and future work" sections; we give conclusions and suggestions for future work.

Methodology

In this paper, we provide and compare three different CAS methods, which use a hardware device (IMU or robotic arm) to provide the orientation of the surgical tool instead of the intra-operative medical images. We begin with a description of the robotic method [18] and follow that by describing two other methods which are based on IMU devices.

Method 1: Robotic arm

In this method, we use an integrated software platform developed by our team [18]. The integrated software platform navigates the robot so that it aligns the drill orientation and tip position with the planned and intended trajectory. Also, the software platform may assist the surgeon in finding the target position.

Preoperative planning, setup and calibration

A preoperative CT is used by the surgical software for trajectory planning. The software assists the surgeon in planning the trajectory by providing a quadrant view of the navigation and planning system. An open source library called the

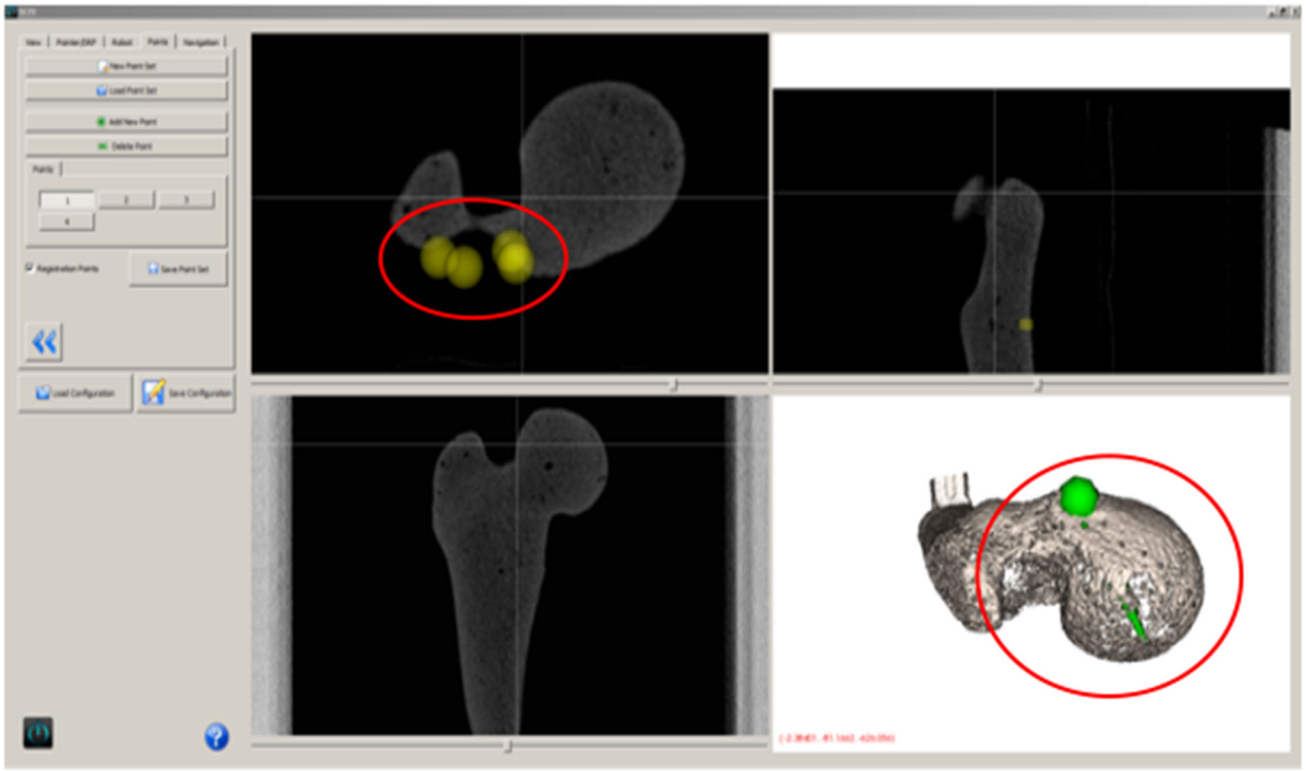

Fig. 2 Integrated surgical navigation software showing quadrant views

image-guided surgical toolkit (IGSTK) [19] was used to build the integrated platform. The axial, sagittal, coronal and volumetric views (3-D) are presented in the quadrant view. The surgeon can use the software to define the entry and target points of the orthopedic procedure as shown in Fig. 2.

Trajectory planning and calculation of robot transformation

In Method 1, we use a robotic arm to align the drill guide with the orientation of the planned surgical trajectory. The robotic arm is a seven degree of freedom (DoF) KUKA Light Weight Robot (LWR).[1] The KUKA C2 lr controller consists of a robot PC, with power unit, safety logic communicating with the surgical workstation PC via FRI. The robot PC operates Windows OS that performs sequence control, path planning, monitoring, as well as interface to host computers, other controllers or networks. We communicate to the robot PC via FRI at a rate not exceeding 20 Hz. The robot PC consists of a motherboard with interfaces, processor, memory, HDD, the robot controller (MFC3) card, network and safety interfaces and batteries. In a generalized manner, KUKA can be replaced with any generic robot. Therefore, we refer to it as robotic arm throughout this paper.

The navigation system module of the platform receives the current position and orientation of both the patient and the end of the robotic arm from a Polaris optical tracking system.[2] The system then calculates the transformation matrix recovering the new position and orientation of the robotic arm. This new orientation aligns the robotic arm with the planned angle and trajectory, shown in Fig. 3. Two unique markers on a rigid body, one mounted to the bone phantom and one mounted to the drill guide tool, are used to track the position and orientation of the patient and robot in optical tracker coordinates. The navigation component of the surgical software then provides the registration between the preoperative tracker coordinates and CT dataset. The registration is performed by using paired-point registration [20] of identifiable features on the phantom surface. To transform the entry point and target point to the robotic arm coordinate system, we used the transformation matrix from CT coordinates to camera coordinates. The drill guide is aligned with the x-axis of the robotic arm since it is rigidly mounted this way. Therefore, the software can calculate the angle between the X-axis of the robotic arm and the line crossing the transformed entry point and target point by using Eq. (1) where "a" is the x-axis of robotic arm and "b" is the planned tra-

[1] KUKA Robotics GMBH, Germany.

[2] Northern Digital Inc., Waterloo, Canada.

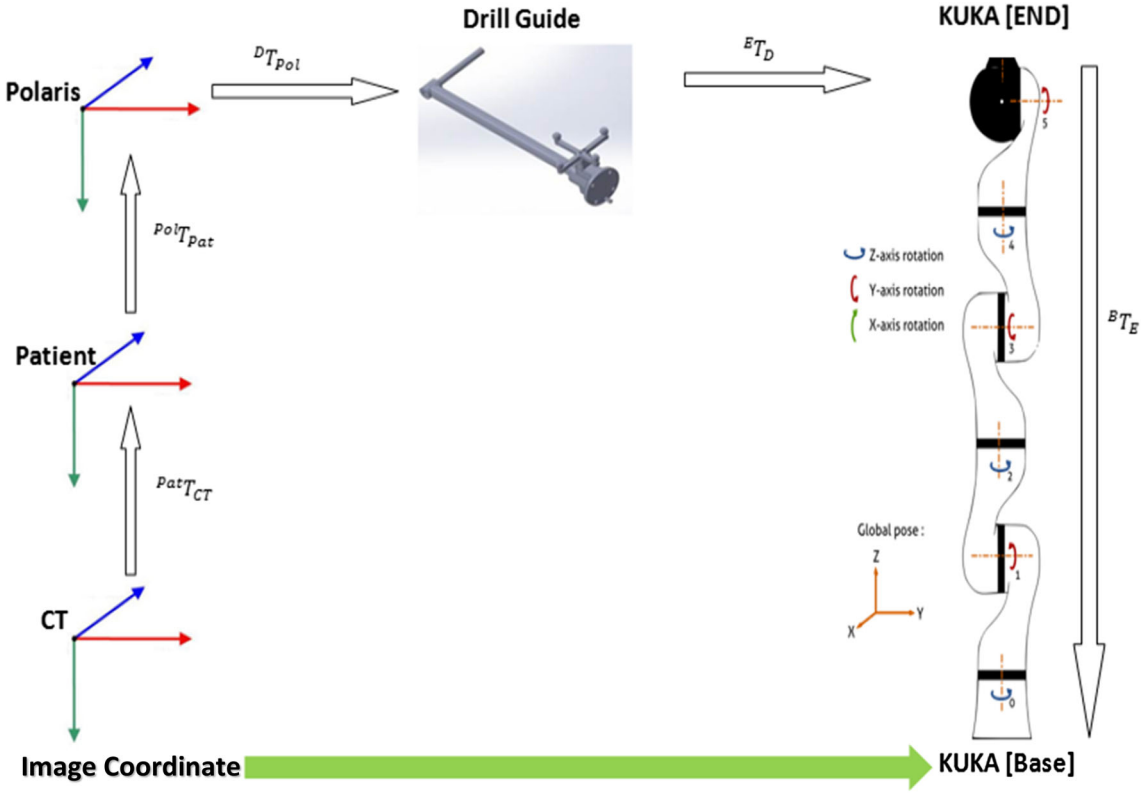

Fig. 3 Transformation chain from image coordinate system to KUKA (KUKA from http://www.openrobots.org/morse/doc/latest/user/actuators/kuka_lwr.html) (robotic arm) coordinate system

jectory. Then, the new orientation and position will be sent to the robot via FRI.

$$\cos\theta = \frac{\bar{a}.\bar{b}}{|a| \times |b|} \tag{1}$$

As a result, we can use Eq. (2) to calculate the rigid transformation matrix from image coordinate system to robotic arm coordinate system. Using this transformation matrix and Eq. (3), we can transform any given point or line from the image coordinate system to the robotic arm coordinate system.

$$^{B}T_{\mathrm{CT}} = {}^{B}\mathrm{Tr}_{E} * {}^{E}T_{D} * {}^{D}T_{\mathrm{Pol}} * {}^{\mathrm{Pol}}T_{\mathrm{Pat}} * {}^{\mathrm{Pat}}T_{\mathrm{CT}} \tag{2}$$

$$P_{B} = {}^{B}T_{\mathrm{CT}} * P_{\mathrm{CT}} \tag{3}$$

where T is a rigid transformation matrix, P is a 3D point, and Tr is a translation matrix. (CT = Medical Image, Pat = Patient Table, Pol = Optical Tracker, D = Drill Guide, E = Robot End-effector, B = Robot Base).

Intra-operative planning/positioning and drilling

In Method 1, we use a drill guide which was designed and built through rapid prototyping. It is mounted to the robotic arm end-effector to align the drill to the planned trajectory. With a long offset, the drill guide was designed to provide the surgeon enough room to manipulate the drill through the guide. The desired robot end-effector orientation and position is converted to joint coordinate space using inverse kinematics. The information of the new position and orientation is transferred to the robotic arm controller via FRI. The robotic arm control module in the integrated software platform updates the robotic arm coordinates in real time, once the drill guide has reached the desired position and orientation. This helps to decrease the effective error in position and orientation that occurs from noise in tracking measurements. The robotic arm then stays in a docked state at the desired position and orientation. The surgeon uses the drill to place the screw along the planned trajectory.

Method 2: Single IMU

In this method, an Inertial Measurement Unit (IMU) is used. The IMU used in this method is an X-IMU.[3] It provides orientation data via three-axis gyroscope, three-axis accelerometer, and three-axis magnetometer sensors. The surgical software communicates with the IMU device via

[3] X-IO Technologies, Bristol, UK.

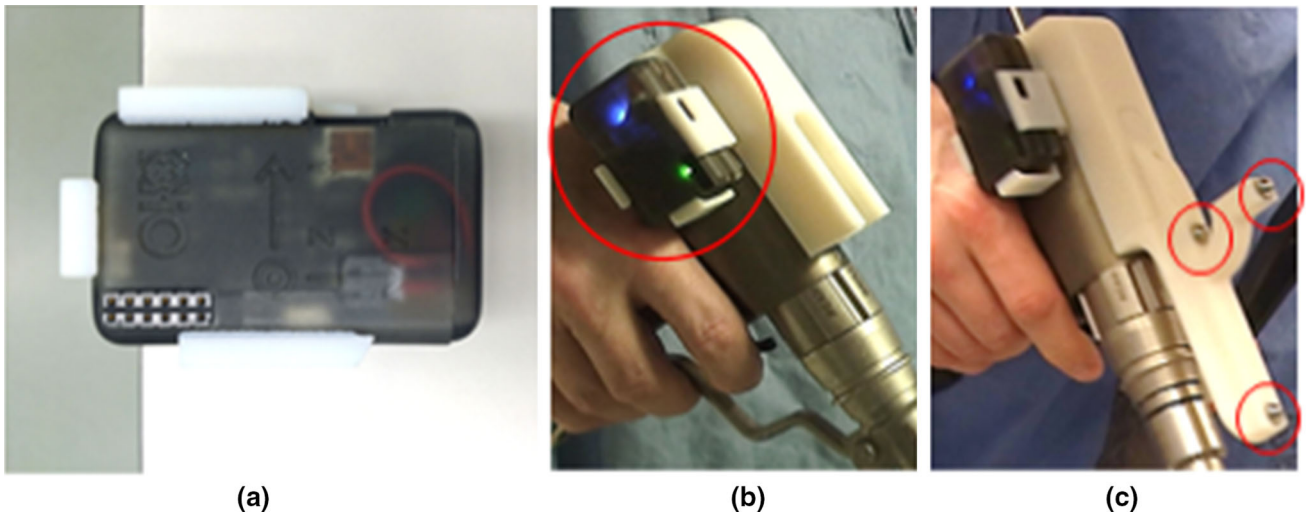

Fig. 4 **a** Calibration fixture, **b** drill fixture, **c** fiducial spheres for coordinate registration

Bluetooth low energy (BLE) wireless protocol. The surgical software calculates the device orientation by using a sensor fusion algorithm [21]. To mount the IMU device to the drill, we designed and fabricated a 3D-printed fixture (Fig. 4a). This way, we can calculate the orientation of the drill bit by using IMU orientation in real time. An Epiphan DVI2USB3.0 frame-grabber[4] is used to collect X-ray images from the Siemens Zeego X-ray robot. To provide a better user interface for surgeons, we wirelessly stream the surgical software visualization to a tablet device that was placed on the patient table next to the surgeon.

For this method, we use two different techniques to perform the intra-operative navigation [22]. Method 2A uses two fluoroscopic images, entry point identifier on the bone, and an IMU device which is calibrated with the orthogonal image planes. Method 2B uses four correspondent points on two orthogonal fluoroscopic images (three fiducial points and one pivot point to perform coordinate registration.

Preoperative planning, setup and calibration

Method 2A: We align the IMU to the patient table coordinate by using a 3D-printed calibration fixture, shown in Fig. 4a. We also attach the IMU to the drill base by using a second 3D-printed fixture, as shown in Fig. 4b. The IMU calibration fixture aligns the IMU YZ-plane with the lateral fluoroscopic image plane and the IMU XY-plane with the A–P fluoroscopic image plane. Also, we assume that the Zeego robot and the patient table orientations are inherently calibrated. Therefore, a transformation matrix between fluoroscopic image plane and IMU device orientation can be achieved by calibrating the IMU coordinate frame with respect to the patient table.

Method 2B: The surgeon selects four corresponding points in each pair of orthogonal X-ray images that provide enough data to perform registration between IMU and fluoroscopic image coordinates. Three of those four points are 8-mm diameter metal sphere fiducials attached to the drill bit; the fourth point is the drill tip, as shown in Fig. 4c. IMU calibration is not required for method 2B.

Intra-operative planning/positioning and drilling

In the following, we describe two single IMU techniques which can be used to superimpose the drill trajectory on orthogonal image planes in real time.

Method 2A: In this method, the surgeon marks the entry point by drilling a small pilot hole on the bone surface. Then, two orthogonal (one A–P and one Lateral) fluoroscopic images are collected. In this method, the registration and navigation are done using A–P and lateral images, even though it is possible to use only one X-ray image. After the images are provided to the surgical software, the surgeon defines the pivot point by drilling a pilot hole. To choose the optimal pivot point, we use a region-growing segmentation algorithm (seed-based) in a semiautomatic manner. The IMU device is affixed to the patient table by a 3D-printed calibration fixture. The fixture is placed in a known orientation with respect to the image plane coordinates. The IMU Y–Z frame maps to the lateral image and the IMU X–Y plane aligns with the A–P image. Once calibration and registration are completed, the surgical software projects the updated orientation of surgical

[4] Epiphany Systems Inc., Palo Alto, CA.

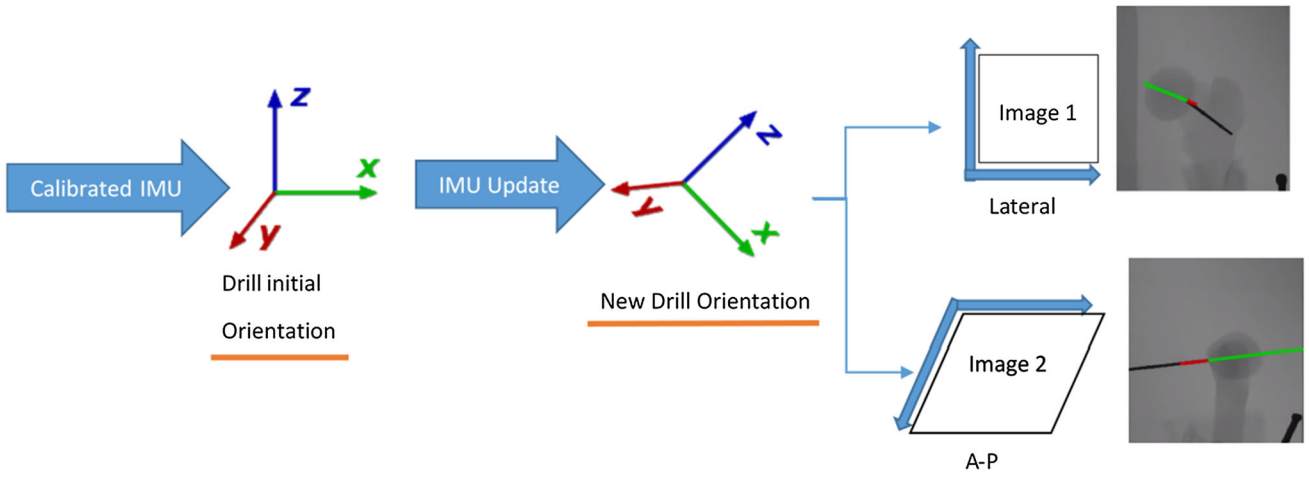

Fig. 5 Flowchart of method (A) transformation chain

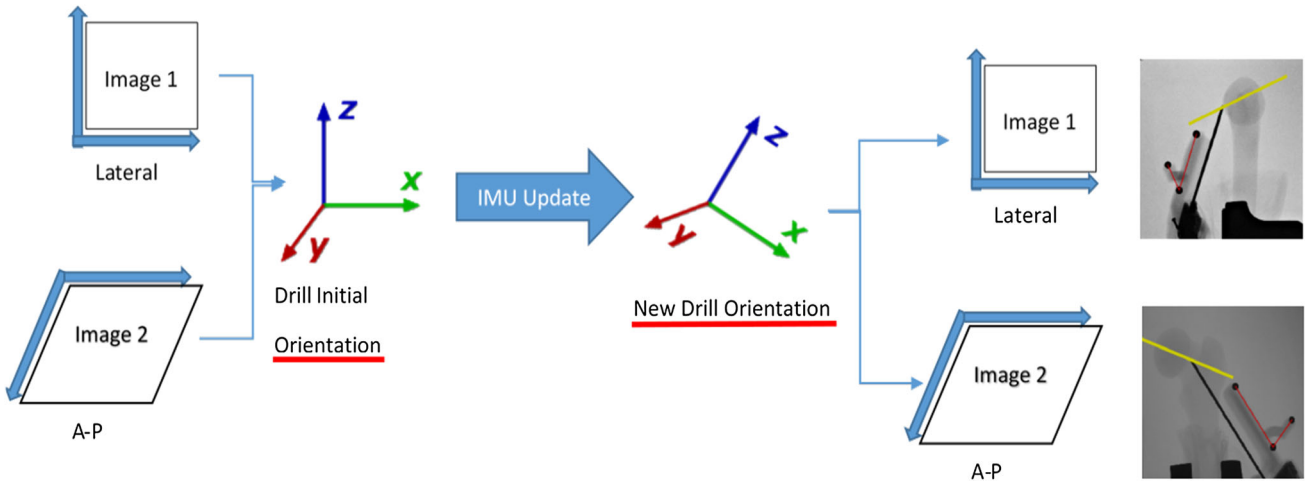

Fig. 6 Flowchart of method (B) transformation chain

tools onto both orthogonal fluoroscopic images in real time by the following transformation chain and as shown in Fig. 5.

$$^{\text{Pos in } XY}T_{\text{IMU}} = {}^{\text{Pivot}}\text{Tr}_{XY} * {}^{XY}P_{\text{IMG}} * {}^{\text{IMG}}T_{\text{WRD}} * {}^{\text{WRD}}T_{\text{IMU}} \quad (4)$$

$$^{\text{Pos in } YZ}T_{\text{IMU}} = {}^{\text{Pivot}}\text{Tr}_{YZ} * {}^{YZ}P_{\text{IMG}} * {}^{\text{IMG}}T_{\text{WRD}} * {}^{\text{WRD}}T_{\text{IMU}} \quad (5)$$

T is a transformation matrix, P is a projection matrix, and Tr is a translation matrix. (IMU = device, WRD = World defined by IMU, IMG = C-arm).

Method 2B: In this method, the surgeon identifies a pivot point on the bone surface and drills a pilot hole to mark the entry point using a passive arm, the drill tip should be fixed so that it touches the pilot hole. Then, two orthogonal fluoroscopic images (one A–P and one Lateral) are collected, making certain to capture the drill tip and three fiducial points on both images. Then, the surgeon selects those four points in commensurate order in orthogonal fluoroscopic images and the surgical software uses a seed-based, region-growing segmentation algorithm to assign the optimal pivot point and center of the spheres semiautomatically. With all four points on those image planes, the application can calculate the 3D position of all fiducial points and the pivot point (x and y coordinates are picked from A–P image plane, and z coordinate is picked from the lateral image plane). Then, the application calculates the transformation matrix between image coordinates and world coordinates. Now, our application can project the x-axis of the IMU in the A–P and lateral image planes (Drill bit is aligned precisely to the x-axis of the IMU). Both projections to A–P and lateral image planes are calculated by the following transformation chains and shown in Fig. 6.

$$^{\text{Pos in } XY}T_{\text{IMU}} = {}^{\text{Pivot}}\text{Tr}_{XY} * {}^{XY}P_{\text{IMG}} * {}^{\text{IMG}}T_{\text{Drill}} * {}^{\text{Drill}}T_{\text{IMU}i} * {}^{\text{IMU}i}T_{\text{WRD}} * {}^{\text{WRD}}T_{\text{IMUup}} \quad (6)$$

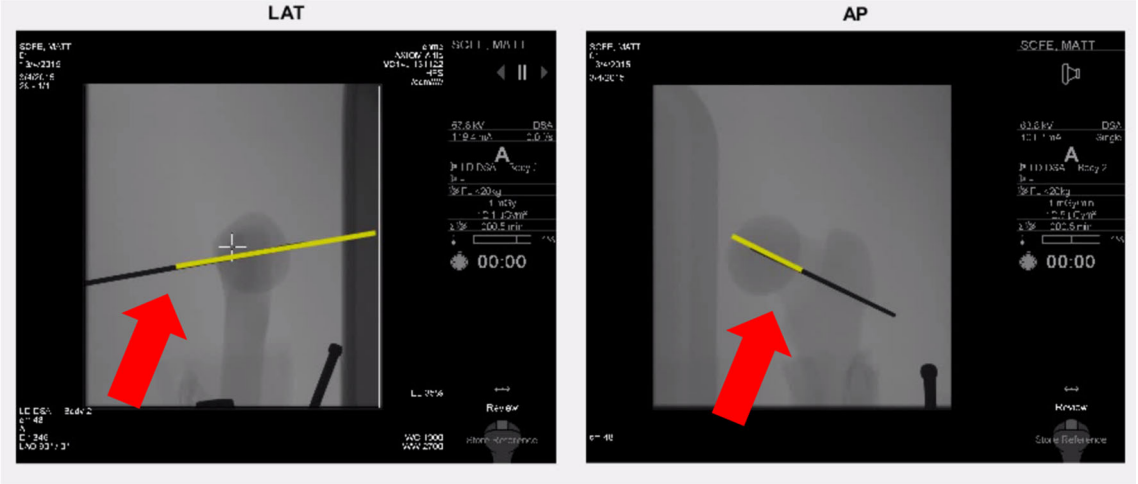

Fig. 7 Post-X-ray evaluation in lateral and A–P (yellow line represents trajectory before drilling)

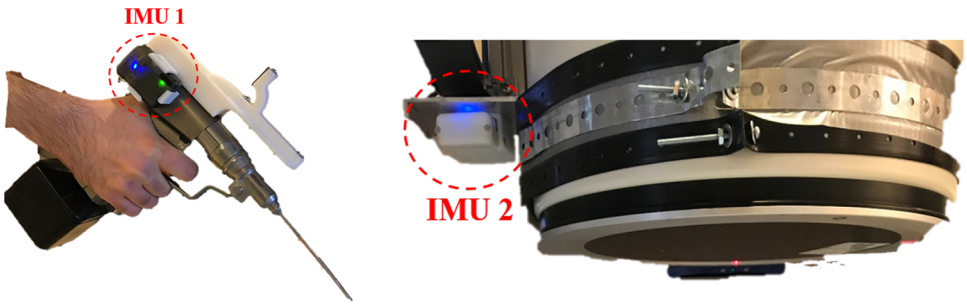

Fig. 8 Left: Drill fixture, right: C-arm fixture

$$^{\text{Pos in } YZ}T_{\text{IMU}} = {}^{\text{Pivot}}\text{Tr}_{YZ} * {}^{YZ}P_{\text{IMG}} * {}^{\text{IMG}}T_{\text{Drill}} * {}^{\text{Drill}}T_{\text{IMU}i} * {}^{\text{IMU}i}T_{WRD} * {}^{\text{WRD}}T_{\text{IMUup}} \quad (7)$$

T is transformation matrix, P is a projection matrix, and Tr is a translation matrix. (IMU = device, WRD = World defined by IMU, IMG = C-arm).

Postoperative placement confirmation

After surgical planning is done, the surgical software collects IMU orientation in real time while the surgeon is drilling toward the target point. Then, we identify the actual drill position by acquiring a pair of confirmatory AP and lateral images. By comparing the planned drill trajectory to actual drill position and orientation, we can perform the postoperative validation, as shown in Fig. 7.

Method 3: Dual IMU

Preoperative planning, setup and calibration

Since both IMU devices are portable and attachable, we designed and used three 3D-printed fixtures. The first fixture is rigidly mounted on to the drill base and houses the first IMU device. This provides a fixed, known relation between the drill bit and the IMU orientation. The second fixture is attached to the C-arm and houses the second IMU device. This provides a fixed, known relation between the image plane and the IMU (Fig. 8). A third fixture is attached to the patient table; this fixture only serves as a mechanism to synchronize the two IMUs and is otherwise uninvolved. This third fixture will be used as a starting point for both IMU devices to connect two separated transformation chains and provides the surgical tool trajectory in the image planes. As long as both IMU devices share the same reference starting position and orientation before being placed on the drill or C-arm, our method will be able to maintain the relationship of the surgical tool and image planes.

Critical to the calibration step is relating the second IMU (IMU2, attached to the C-arm) and the C-arm coordinate system (T:IMU2 ≥ C-arm). We acquire two sample X-ray images (from different angles) of two fixed drill bit (straight-line shape) with a constant length and known angle (non-orthogonal). The image should be taken from an angle that produces the 2D line of each drill bit. This provides the orientation of these two lines (drill bits) in the C-arm coordinate system (L1 and L2). The cross-product of L1 and L2

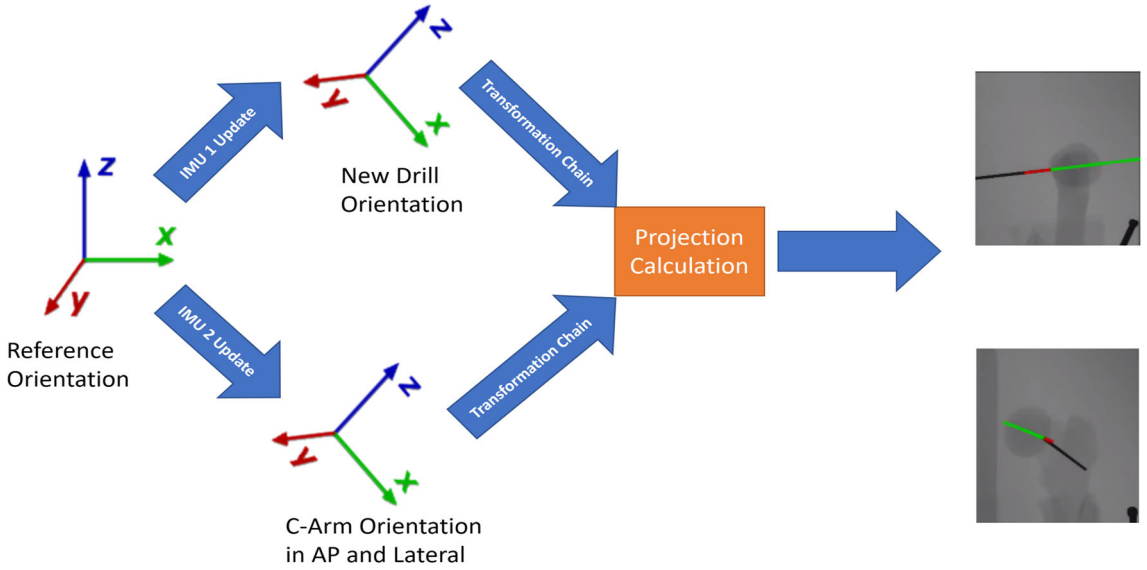

Fig. 9 Flow of transformation chain and projection calculation for dual IMU approach

provides L3, which is orthogonal to L1. The cross-product of L1 and L3 provides L4 that is orthogonal to both L1 and L3. These three lines form a full 3D orientation representation called $R1 = [\mathrm{N(L1)\ N(L3)\ N(L4)}]$, where N is the normalization function. Next, we attach the drill (calibrated with IMU1) to both drill bits to find the orientation of drill bits with respect to the World (WRD) coordinate system, which is defined by reference orientation of IMU. Then, we can form the full 3D orientation representation (called $R2$) in the WRD coordinate system. Therefore, the full transformation chain is:

$$R1 = {}^{\text{C-arm}}T_{\text{IMU2}} * {}^{\text{IMU2}}T_{\text{WRD}} * R2 \tag{8}$$

where T is a 3×3 matrix. We can then calculate the transformation matrix between the IMU2 and C-arm (T:IMU2 $\geq$ C-arm) using the following equation:

$${}^{\text{C-arm}}T_{\text{IMU2}} = R1 * (R2)^{-1} * \left({}^{\text{IMU2}}T_{\text{WRD}}\right)^{-1} \tag{9}$$

Intra-operative planning/positioning and drilling

The surgeon drills a small pilot hole at the bone surface to identify the entry point. Two fluoroscopic images are then acquired. Then, the surgeon defines the drill tip as a pivot point. This pivot point provides the translation matrix that will be used later in the transformation chain. The application uses seed-based, region-growing segmentation to pick the most precise pivot point in a semiautomatic manner. Based on the calibration and setup of those three fixtures, the drill trajectory is now known with respect to image coordinates. Afterward, our method projects the updated orientation to both A–P and lateral images (Fig. 9). These two projections are calculated by the following chain of transformations (Tr is a translation matrix):

$${}^{\text{Pivot}}\text{Tr}_{\text{Image}} * {}^{\text{Image}}T_{\text{C-arm}} * {}^{\text{C-arm}}T_{\text{IMU2}} * {}^{\text{IMU2}}T_{\text{WRD}} * {}^{\text{WRD}}T_{\text{IMU1}} \tag{10}$$

Postoperative placement confirmation

After the surgeon has successfully placed the implant, postoperative A–P and lateral images are acquired to compare the actual implant position and the projected line. Since the application collects and logs the latest orientation data of the drill and the C-arm in both A–P and lateral positions, it can project the same line on top of the postoperative images. As shown in Fig. 10, postoperative placement confirmation is achieved by comparing the provided projection of the drill trajectory and actual placed implant.

Results

In this section, we compare the results of manual trials and our three novel navigation guidance techniques. In all the experiments, left femur bone models[5] with slipped capital epiphysis deformity were used, and 20–40 assisted trials were performed. For each trial, the total experiment time and number of intra-operative fluoroscopic images were measured, and the accuracy of the procedure was calculated by con-

[5] Model # 1161, Sawbones Worldwide, Vashon Island, WA.

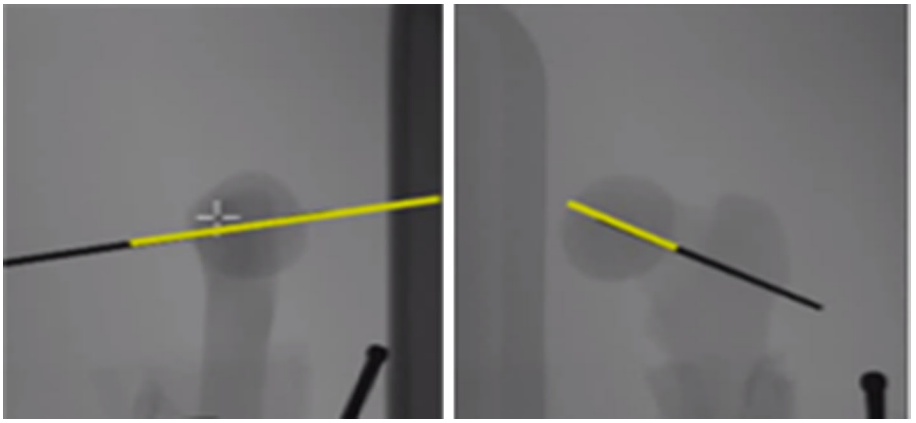

Fig. 10 Postoperative lateral and A–P images

Table 1 Twenty manual trials conducted by experienced surgeon

	Total time	# of images	Mean of total error (mm)	SD	Max error
20 Manual	2:37	23.8	7.44	2.23	10.21

Total error is measured just for target points based on distance between desired and drilled points

firmatory postoperative images. To establish a baseline for comparison, we also asked an experienced surgeon to perform 20 manual procedures. We logged the number of X-ray images and total procedure time for each, acquired confirmatory orthogonal images, and computed final placement accuracy.

In Method 1, we used Siemens' Zeego X-ray robot and KUKA as the robotic arm. For IMU-based Methods 2 and 3, first the accuracy of the IMU devices was assessed using a Polaris optical tracker. The result confirmed the internal report of X-IO Technologies that shows the accuracy of the IMU device and algorithm used. Afterward, the main study was concluded in the operating room using two IMU devices to track both surgical tool and the C-arm.

Manual trial

Twenty traditional manual trials without any software assistance were performed to provide a baseline comparison to each method. The results are shown in Table 1.

Method 1: Robotic arm

Figure 11 shows the experiment setup with KUKA and Zeego C-Arm. The comparison between 20 manual trials and 40 assisted trials conducted by an orthopedic surgeon showed total error decreased by 7%. All the procedures were completed with an average time of 3:57 (minutes/seconds). (Since the rapid prototyping is not always dimensionally accurate, we recalibrated the system each time to minimize this error.) Results confirm that the robotic method provides sufficient accuracy for the clinical application [23] as shown in Table 2.

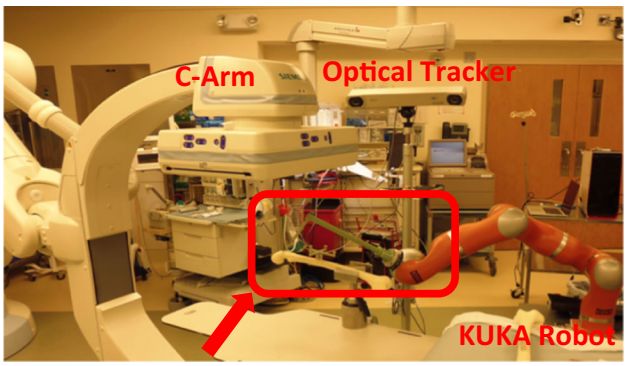

Fig. 11 Robotic-based assisted trial setup in OR. It shows a configuration of KUKA robotic arm, 3D-printed drill guide mounted to the KUKA, bone model and Polaris tracking system

Method 2: Single IMU

Figure 12 shows the experiment setup. In this experiment, an orthopedic surgeon performed 40 assisted trials by single IMU method. The result confirms that total error decreased by 39%. (We reset the IMU device after each procedure to avoid any possible drift error.) This suggests there is a higher level of accuracy with IMU-based navigation compared to the conventional SCFE procedure [23] and robotic arm-based navigation method [18], as shown in Table 3.

Method 3: Dual IMU

The experiment setup is shown in Fig. 13. Twenty assisted trials were done using two IMU devices. Average procedure

Table 2 Forty navigated trial results conducted by experienced and non-experienced surgeons

	Navigation time	Total time	# of images	Mean of total error (mm)	SD	Max error
40 Assisted	0:38	3:48	4	6.97	0.53	7.26

Total error is measured only for target positions based on distance between the drilled and desired points (statistical significance: $p < 0.05$, registration error: Err < 0.7 mm)

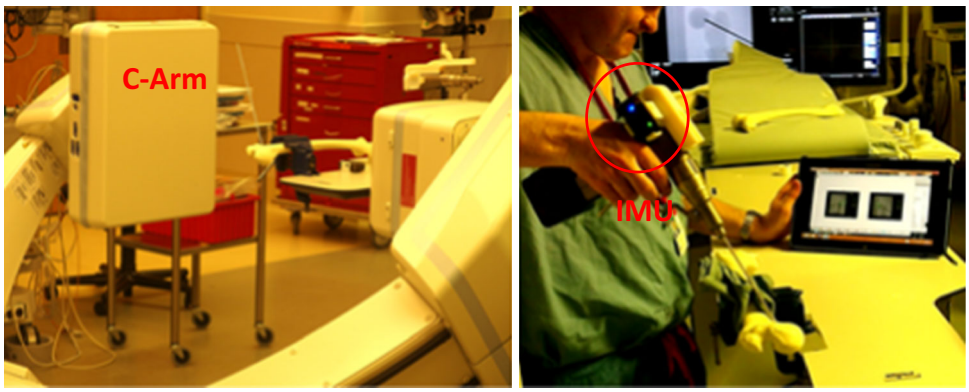

Fig. 12 Setup of assisted trial method based on single IMU approach in OR. **a** Setup for lateral exposure, **b** Surgeon using the visualization for planning optimal tool path

Table 3 An experienced orthopedic surgeon conducted 20 manual and 40 navigated trial

	Navigation time	Total time	# of images	Total error (mm)	SD	Max error
40 Assisted	0:33	2:07	4	4.59	0.25	5.21

Total error is calculated based on distance between planned and drilled points (Reg Err < 0.5 mm, Stat Sig: $p < 0.05$)

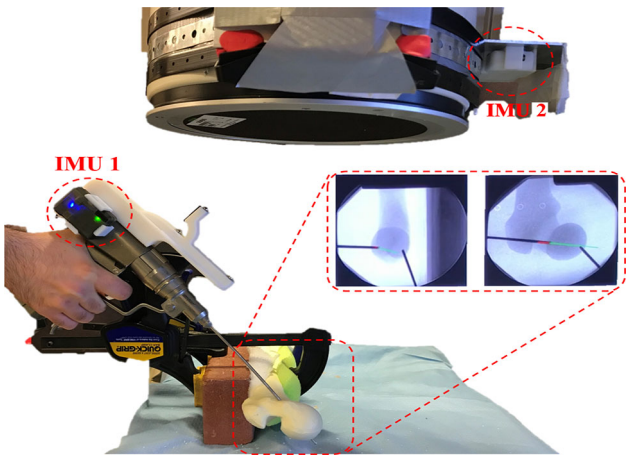

Fig. 13 Planning optimal path based on data received from IMU devices

time for assisted trials was 1:43 (minutes/seconds), and average total error was 2.67 mm. The results show significant improvement in accuracy with the assisted trials since the total error decreased by 65%, as shown in Table 4.

Results from all three methods show improvement in screw placement and reduction in radiation exposure in phantom studies.

Further, in comparison with existing navigation methods, the portability and efficient calibration of the IMU-based navigation methods significantly decreases the pre-operation setup time.

Discussion

Currently, intra-operative medical images are used in the conventional SCFE procedure to aid in screw placement. This can lead to high radiation exposure for all parties involved in the surgery including both patient and surgeon. Conventionally, surgeons use fluoroscopic images to extrapolate an entry point for the surgical tool based on optimal tool orientation and target point. Then, additional fluoroscopic images are acquired to confirm the position and orientation of the surgical tool. During the SCFE procedure, an average of 20 images is acquired to confirm the orientation and alignment of the tool with the planned trajectory and navigate the surgical tool. The question is: "What is the clinical value of these additional fluoroscopic images?" The answer is that these additional fluoroscopic images are only useful as postoperative confirmation and they do not provide valuable clinical information during the planning or navigation phases of the procedure.

In this paper, we introduced three different methods: Method 1 using a robotic arm and Methods 2 and 3 utilizing IMU device for navigation system. In Method 1, we

Table 4 Twenty navigated trials conducted by medical experts

	Navigation time	Total time	# of images	Mean of total error (mm)	SD	Max error
20 Assisted trials	0:31	1:43	4	2.67	0.22	3.09

Total error is measured for target points based on distance of desired and drilled points (statistical significance: $p < 0.04$, registration error: Err < 0.3 mm)

introduced a platform that assists the surgeon in planning the surgical path by choosing the entry point and the target point in a faster and easier way. Additionally, this method increases the screw placement procedure accuracy and decreases the overall time of the surgery. For the robotic method, the main error source was propagation of optical tracking system error into the entire transformation chain.

In Methods 2 and 3, we chose an IMU because it provides accurate orientation information with the benefits of compact size and low cost. For IMU-based methods, the main error source was the error of calibration process and IMU drift which we were able to minimize it by recalibrating the devices after each trial.

The main difference between the robotic method and the IMU-based methods is the real-time navigation. In the robotic method, the surgeon uses a preoperative CT dataset to choose entry and target point, and then the robot aligns the drill guide to desired trajectory and entry point position. In the IMU-based method, the surgeon can see the projection of the drill in real time on the X-ray image while drilling for screw placement.

Of the three methods explored, the dual IMU-based method (Method 3) performed best. Comparing to Method 1, this method significantly decreased radiation exposure to all parties involved by using only two medical images and in addition it provided real-time guidance to the surgeon. Comparing the single IMU (Method 2) and dual IMU (Method 3), the results suggest that the dual IMU method is more accurate since utilizing two IMU devices to track both the drill and the C-arm provides a more precise transformation matrix between the X-ray image and the surgical tool. Although the IMU-based navigation methods are more accurate and cost effective, the robotic arm-based method is inherently capable of tracking and providing navigation with more geometrical information such as tool position.

IMU-based methods were designed in a manner to assist SCFE procedures relying only on tool orientation. Therefore, they require only two X-ray images without any external optical tracker to track the position of surgical tools. A challenge in IMU-based navigation methods is the drift of IMU devices. Even though we used a sensor fusion algorithm to compensate for errors of each sensor (Gyroscope, Accelerometer and Magnetometer), we still recommend recalibrating the IMU sensors after performing each single experiment. The orientation of the image plane does not affect the calculation or accuracy of the IMU-based methods. In addition, navigation can be done relying on one image alone. However, in this study, we incorporated two orthogonal images and augmented the planned trajectory using both A–P and lateral images, as these approaches are more relevant to the traditional clinical workflow.

For Method 3, these two images can be acquired at any angle because the two IMU devices provide the orientation of both the C-arm and the surgical tool. However, it is usually preferable for these two images to be in A–P and lateral orientations to provide the best possible medical detail to the surgeon.

Conclusions and future work

The conventional SCFE procedure can result in substantial radiation exposure to the patient and surgeon to achieve accurate placement of the fixation screw. In this paper, we introduced three novel methods for intra-operative navigation and real-time path planning which can minimize the radiation dose. In the first method, we used a robotic arm to guide the surgeon based on preoperative CT images. In the second and third methods, we used IMU-based navigation based on two orthogonal fluoroscopic images (A–P and Lateral). All three methods superimposed the navigated path onto medical images. The phantom study results showed that these three different novel navigation methods and techniques for navigated screw placement can reduce overall radiation exposure while improving accuracy of implant placement without leading to prolonged operative time or necessitating conventional workflow adaptations.

In the future, a head-mounted display could be used to provide visual feedback to surgeons in a real-time manner. Our long-term goal is to conduct a clinical trial to determine the efficacy of this augmented approach for human patients. Our aim is to improve clinical outcomes for patients by improving accuracy in image-guided screw placement interventions.

Additionally, these three navigation methods can be used in other orthopedic procedures with relevant clinical workflow to reduce overall radiation exposure.

Funding This research was internally funded by the Sheikh Zayed Institute for Pediatric Surgical Innovation at Children's National Health System.

Compliance with ethical standards

Conflict of interest The authors declare that they have no conflict of interest.

Ethical standards All procedures performed in studies involving human participants were in accordance with the ethical standards of the institutional and/or national research committee and with the 1964 Helsinki declaration and its later amendments or comparable ethical standards.

References

1. Rohilla R, Singh R, Magu N, Devgan A, Siwach R, Sangwan S (2011) Simultaneous use of cannulated reamer and schanz screw for closed intramedullary femoral nailing. ISRN Surg (published online)
2. Liao H, Ishihara H, Tran HH, Masamune K, Sakuma I, Dohi T (2008) Fusion of laser guidance and 3-D autostereoscopic image overlay for precision-guided surgery. Lect Notes Comput Sci 5128:367–376
3. Marmurek J, Wedlake C, Pardasani U, Eagleson R, Peters T (2006) Image-guided laser projection for port placement in minimally invasive surgery. Stud Health Technol Inform 119:367–372
4. Navab N, Heining SM, Traub J (2010) Camera augmented mobile C-arm (CAMC): calibration, accuracy study, and clinical applications. IEEE Trans Med Imaging 29(7):1412–1423
5. Walti J, Jost GF, Cattin PC (2014) A new cost-effective approach to pedicular screw placement. Augment Environ Comput Assist Interv Lect Notes Comput Sci 8678(2014):90–97
6. Volonte F, Pugin F, Bucher P, Sugimoto M, Ratib O, Morel P (2011) Augmented reality and image overlary navigation with OsiriX in laparoscopic and robotic surgery: not only a matter of fashion. J Hepatobiliary Pancreat Sci 18:506–509
7. Diotte B, Fallavollita P, Wang L, Weidert S, Thaller P, Euler E, Navab N (2012) Radiation-free drill guidance in interlocking of intramedullary nails. In: Medical image computing and computer-assisted intervention. Springer, Berlin, pp 18–25
8. Hoffmann M, Schröder M, Lehmann W, Kammal M, Rueger JM, Herrman RueckerA (2012) Next generation distal locking for intramedullary nails using an electromagnetic X-ray-radiation-free real-time navigation system. J Trauma Acute Care Surg 73(1):243–248
9. Stathopoulos I, Karampinas P, Evangelopoulos DS, Lampropoulou-Adamidou K, Vlamis J (2013) Radiation-free distal locking of intramedullary nails: evaluation of a new electromagnetic computer-assisted guidance system. Injury 44(6):872–875
10. Arlettaz Y, Dominguez A, Farron A, Ehlinger M, Moor BK (2012) Distal locking of femoral nails: evaluation of a new radiation-independent targeting system. J Orthop Trauma 26(11):633–637
11. Murgier J, Espie A, Bayle-Iniguez X, Cavaignac E, Chiron P (2013) Frequency of radio-graphic signs of slipped capital femoral epiphysiolysis sequelae in hip arthroplasty candidates for coxarthrosis. Orthop Traumatol Surg Res 99(7):791–797
12. Ulucay C, Ozler T, Guven M, Akman B, Kocadal AO, Altintas F (2013) Etiology of coxarthrosis in patients with total hip replacement. Acta Orthop Traumatol Turc 47(5):330–333
13. Morrissy RT (1990) Slipped capital femoral epiphysis technique of percutaneous in situ fixa-tion. J Pediatr Orthop 10(3):347–350
14. Nguyen D, Morrissy RT (1990) Slipped capital femoral epiphysis: rationale for the technique of percutaneous in situ fixation. J Pediatr Orthop 10(3):341–346
15. Ward WT, Stefko J, Wood KB, Stanitski CL (1992) Fixation with a single screw for slipped capital femoral epiphysis. J Bone Joint Surg Am 74(6):799–809
16. Carney BT, Birnbaum P, Minter C (2003) Slip progression after in situ single screw fixation for stable slipped capital femoral epiphysis. J Pediatr Orthop 23(5):584–589
17. Westberry DE, Davids JR, Cross A, Tanner SL, Blackhurst DW (2008) Simultaneous biplanar fluoroscopy for the surgical treatment of slipped capital femoral epiphysis. J Pediatr Orthop 28(1):43–48
18. Koutenaei BA, Guler O, Wilson E, Thoranaghatte RU, Oetgen M, Navab N, Cleary K (2014) Improved screw placement for slipped capital femoral epiphysis (SCFE) using robotically-assisted drill guidance. In: International conference on medical image computing and computer-assisted intervention, vol 17, no. 01, pp 488–495
19. Enquobahrie A, Cheng P, Gary K, Ibanez L, Gobbi D, Lindseth F, Yaniv Z, Aylward S, Jomier J, Cleary K (2007) The image-guided surgery toolkit IGSTK: an open source C ++ software toolkit. J Digit Imaging 20(1):21–33
20. Arun KS, Huang TS, Blostein SD (1987) Least-squares fitting of two 3-D point sets. IEEE Trans Pattern Anal Mach Intell 9(5):698–700
21. Madgwick SOH, Harrison AJL, Vaidyanathan R (2011) Estimation of IMU and MARG orientation using a gradient descent algorithm. In: 2011 IEEE international conference on rehabilitation robotics (ICORR), pp 1–7. https://doi.org/10.1109/icorr.2011.5975346
22. Koutenaei BA, Guler O, Wilson E, Oetgen M, Grimm P, Navab N, Cleary K (2015) Inertial measurement unit for radiation-free navigated screw placement in slipped capital femoral epiphysis surgery. In: International conference on medical image computing and computer-assisted intervention. Springer, Cham, pp 355–362
23. Pring EM, Adamczyk M, Hosalkar HS, Bastrom TP, Wallace CD, Newton PO (2010) In situ screw fixation of slipped capital femoral epiphysis with a novel approach: a double-cohort controlled study. J Child Orthop 4(3):239–244

Publisher's Note Springer Nature remains neutral with regard to jurisdictional claims in published maps and institutional affiliations.

Conclusion and Future Works

In this thesis, a novel CAS system for SCFE surgery has been developed. The general concept of CAS and its applications and main components were introduced in chapter 1. Also Tracking methods were described in detail as the main component of a surgical navigation system. Then concepts and main differences of tracking, registration, and calibration were described.. Electromagnetic and optical tracking, the two most prominent tracking methods, were investigated in detail, and their main benefits and drawbacks were described. Lastly, the other components of the CAS system, including visualization and display methods, were described.

Currently, intra-operative medical images are used in the conventional SCFE procedure to aid in screw placement. This can lead to high radiation exposure for all parties involved in the surgery including both patient and surgeon. Conventionally, surgeons use fluoroscopic images to extrapolate an entry point for the surgical tool based on optimal tool orientation and target point. Then, additional fluoroscopic images are acquired to confirm the position and orientation of the surgical tool. During the SCFE procedure, an average of 20 images is acquired to confirm the orientation and alignment of the tool with the planned trajectory and navigate the surgical tool. The question is: “What is the clinical value of these additional fluoroscopic images?” The answer is that these additional fluoroscopic images are only useful as post-operative confirmation and they do not provide valuable clinical information during the planning or navigation phases of the procedure.

In this thesis, I introduced three novel methods for intra-operative navigation and real-time path planning which can minimize the radiation dose:

- Method 1 using a robotic arm,
- Method 2 using a single IMU device for navigation,
- Method 3 using dual IMU devices for navigation.

In Method 1 we introduced a platform that assists the surgeon in planning the surgical path by choosing the entry point and the target point in a faster and easier way than the conventional approach.This method increases the accuracy of the screw placement procedure and decreases the overall time of the surgery. For the robotic method, the main error source was propagation of optical tracking system error into the entire transformation chain.

In Methods 2 and 3 we chose an IMU because it provides accurate orientation information with the benefits of compact size and low cost. For the IMU-based

methods, the main error sources were the error in the calibration process and IMU drift, which we were able to minimize by recalibrating the devices after each trial.

The main difference between the robotic method and the IMU-based methods is the real-time navigation. In the robotic method, the surgeon uses a pre-operative CT dataset to choose entry and target points, and then the robot aligns the drill guide to the desired trajectory and entry point position. In the IMU-based methods, the surgeon can see the projection of the drill in real time on the X-ray image while drilling for screw placement.

Of the three methods explored, the dual IMU-based method (Method 3) performed best. Compared to Method 1, this method significantly decreased radiation exposure to all parties involved by using only two medical images, while also providing real-time guidance to the surgeon. Comparing the single IMU (Method 2) and dual IMU (Method 3) approaches, these results suggest that the dual IMU method is more accurate since utilizing two IMU devices to track both the drill and the C-arm provides a more precise transformation matrix between the X-ray image and the surgical tool. Although the IMU-based navigation methods (Methods 2 and 3) are more accurate and cost effective, the robotic arm-based method (Method 1) is inherently capable of tracking and providing navigation with more geometrical information such as tool position.

IMU-based methods were designed in a manner to assist SCFE procedures relying only on tool orientation. Therefore, they require only two X-ray images without any external optical tracker to track the position of surgical tools. A challenge in IMU-based navigation methods is the drift of IMU devices. Even though we used a sensor fusion algorithm to compensate for errors of each sensor (Gyroscope, Accelerometer, and Magnetometer), we still recommend recalibrating the IMU sensors after performing each single experiment. The orientation of the image plane does not affect the calculation or accuracy of the IMU-based methods. In addition, navigation can be done relying on one image alone. However, in this thesis we incorporated two orthogonal images and augmented the planned trajectory using both A-P and lateral images, as these approaches are more relevant to the traditional clinical workflow. For Method 3, these two images can be acquired at any angle because the two IMU devices provide the orientation of both the C-arm and the surgical tool. However, it is usually preferable for these two images to be in A-P and lateral orientations to provide the best possible medical detail to the surgeon.

In phantom studies, Method 3 improved the accuracy of the screw placement procedure by 65% and decreased the procedure and the exposure time for both patient and the surgeon by 38%. This method introduces more efficient setup and calibration compared to other radiation-free navigation methods: it can be set up in less than 60 seconds and does not exhibit any line of sight issues.

The long-term goal is to pursue a clinical trial to determine if this approach could lead to an improved SCFE procedure for patients. For this purpose, we also need to improve the workstation and obtain clinical approvals for the system. Our aims

are to improve clinical outcomes for patients and improve the accuracy in image-guided screw placement interventions.

There are also some points that could be improved in future studies. For instance, real bones have significant variation on deformity type. We used the sawbones model that comes with a uniform model with no overlying soft tissue. Therefore, we need to conduct additional trials to confirm the accuracy and precision of this novel navigation technique in a wider variety of shapes and models. Additionally, in the next round of trials we plan to make the surgeons blinded to the model, to make sure the studies are as close as possible to the real clinical procedures.

In the future, a head-mounted display could be used to provide visual feedback to surgeons in a real-time manner. The proposed idea is to conduct a clinical trial to determine the efficacy of this augmented approach for human patients. Our aim is to improve clinical outcomes for patients by improving accuracy in image-guided screw placement interventions. Additionally, these three navigation methods can be used in other orthopedic procedures with relevant clinical work-flow to reduce overall radiation exposure.

References

[1] "The Cambridge English Dictionary." [Online]. Available: https://dictionary.cambridge.org/dictionary/english/surgery.

[2] C. J. Fan *et al.*, "Minimally invasive versus open surgery in the Medicare population: a comparison of post-operative and economic outcomes," *Surg. Endosc.*, vol. 32, no. 9, pp. 3874–3880, 2018.

[3] S. Payandeh, *Visual Tracking in Conventional Minimally Invasive Surgery*. Chapman and Hall/CRC, 2016.

[4] J. F. Oliveira, H. Capote, J. B. Pagador, and J. L. Moyano, "PERSPECTIVES ON COMPUTER ASSISTED SURGERY."

[5] B. Preim and C. P. Botha, *Visual computing for medicine: theory, algorithms, and applications*. Newnes, 2013.

[6] U. Mezger, C. Jendrewski, and M. Bartels, "Navigation in surgery," *Langenbeck's Arch. Surg.*, vol. 398, no. 4, pp. 501–514, 2013.

[7] S. Sukegawa, T. Kanno, and Y. Furuki, "Application of computer-assisted navigation systems in oral and maxillofacial surgery," *Jpn. Dent. Sci. Rev.*, vol. 54, no. 3, pp. 139–149, 2018.

[8] V. Vitiello, K.-W. Kwok, and G.-Z. Yang, "Introduction to robot-assisted minimally invasive surgery (MIS)," in *Medical Robotics*, Elsevier, 2012, pp. 1-P1.

[9] B. S. Peters, P. R. Armijo, C. Krause, S. A. Choudhury, and D. Oleynikov, "Review of emerging surgical robotic technology," *Surg. Endosc.*, vol. 32, no. 4, pp. 1636–1655, 2018.

[10] G. Figueras-Benítez, L. Urbano, A. Acero, M. Huerta, and M. Castro, "Surgical navigation systems: A technological overview," 2014.

[11] C. H. Ewurum, Y. Guo, S. Pagnha, Z. Feng, and X. Luo, "Surgical Navigation in Orthopedics: Workflow and System Review," in *Intelligent Orthopaedics*, Springer, 2018, pp. 47–63.

[12] P. Waelkens, M. N. van Oosterom, N. S. van den Berg, N. Navab, and F. W. B. van Leeuwen, "Surgical navigation: an overview of the state-of-the-art clinical applications," in *Radioguided Surgery*, Springer, 2016, pp. 57–73.

[13] M. Tanzer and A. M. Makhdom, "Preoperative planning in primary total knee arthroplasty," *JAAOS-Journal Am. Acad. Orthop. Surg.*, vol. 24, no. 4, pp. 220–230, 2016.

[14] R. Bucholz and L. McDurmont, "The history, current status, and future of the stealthstation treatment guidance system," in *Textbook of Stereotactic and Functional Neurosurgery*, 2009.

[15] D. E. Azagury *et al.*, “Image-guided surgery,” *Curr. Probl. Surg.*, vol. 52, no. 12, pp. 476–520, 2015.

[16] P. Mascagni *et al.*, “New intraoperative imaging technologies: Innovating the surgeon’s eye toward surgical precision,” *J. Surg. Oncol.*, vol. 118, no. 2, pp. 265–282, 2018.

[17] T. M. Peters, C. A. Linte, Z. Yaniv, and J. Williams, *Mixed and Augmented Reality in Medicine*. CRC Press, 2018.

[18] T. Peters and K. Cleary, *Image-guided interventions: technology and applications*. Springer Science & Business Media, 2008.

[19] R. Tang *et al.*, “Augmented reality technology for preoperative planning and intraoperative navigation during hepatobiliary surgery: a review of current methods,” *Hepatobiliary Pancreat. Dis. Int.*, vol. 17, no. 2, pp. 101–112, 2018.

[20] B. AG, “No Title.” [Online]. Available: https://www.brainlab.org/get-educated/spine/understand-image-guided-surgery-for-spine-disorder/what-is-image-guided-surgery-for-spine/.

[21] J. Sutherland *et al.*, “Applying modern virtual and augmented reality technologies to medical images and models,” *J. Digit. Imaging*, vol. 32, no. 1, pp. 38–53, 2019.

[22] L. Chen, T. W. Day, W. Tang, and N. W. John, “Recent developments and future challenges in medical mixed reality,” in *2017 IEEE International Symposium on Mixed and Augmented Reality (ISMAR)*, 2017, pp. 123–135.

[23] P. Milgram and F. Kishino, “A taxonomy of mixed reality visual displays,” *IEICE Trans. Inf. Syst.*, vol. 77, no. 12, pp. 1321–1329, 1994.

[24] D. Schmalstieg and T. Hollerer, *Augmented Reality: Principles and Practice*. Pearson Education, 2016.

[25] T. Sielhorst, M. Feuerstein, and N. Navab, “Advanced medical displays: A literature review of augmented reality,” *J. Disp. Technol.*, vol. 4, no. 4, pp. 451–467, 2008.

[26] S. Bernhardt, S. A. Nicolau, L. Soler, and C. Doignon, “The status of augmented reality in laparoscopic surgery as of 2016,” *Med. Image Anal.*, vol. 37, pp. 66–90, 2017.

[27] H.-B. Kwon, Y.-S. Park, and J.-S. Han, “Augmented reality in dentistry: a current perspective,” *Acta Odontol. Scand.*, vol. 76, no. 7, pp. 497–503, 2018.

[28] G. J. C. van Baar, T. Forouzanfar, N. P. T. J. Liberton, H. A. H. Winters, and F. K. J. Leusink, “Accuracy of computer-assisted surgery in mandibular reconstruction: A systematic review,” *Oral Oncol.*, vol. 84, pp.

52–60, 2018.

[29] H.-H. Lin and L.-J. Lo, “Three-dimensional computer-assisted surgical simulation and intraoperative navigation in orthognathic surgery: a literature review,” *J. Formos. Med. Assoc.*, vol. 114, no. 4, pp. 300–307, 2015.

[30] X. Chen, L. Xu, Y. Sun, and C. Politis, “A review of computer-aided oral and maxillofacial surgery: planning, simulation and navigation,” *Expert Rev. Med. Devices*, vol. 13, no. 11, pp. 1043–1051, 2016.

[31] I. N. Ltd., “Image Guided Implantology.” 2019, [Online]. Available: https://image-navigation.com/igi/.

[32] L. R. Sayadi *et al.*, “The New Frontier: A Review of Augmented Reality and Virtual Reality in Plastic Surgery,” *Aesthetic Surg. J.*

[33] Y. Kim, H. Kim, and Y. O. Kim, “Virtual reality and augmented reality in plastic surgery: a review,” *Arch. Plast. Surg.*, vol. 44, no. 3, p. 179, 2017.

[34] D. W. Roberts, J. W. Strohbehn, J. F. Hatch, W. Murray, and H. Kettenberger, “A frameless stereotaxic integration of computerized tomographic imaging and the operating microscope,” *J. Neurosurg.*, vol. 65, no. 4, pp. 545–549, 1986.

[35] W. O. C. López, P. A. Navarro, and S. Crispin, “Intraoperative clinical application of augmented reality in neurosurgery: A systematic review,” *Clin. Neurol. Neurosurg.*, 2018.

[36] A. Meola, F. Cutolo, M. Carbone, F. Cagnazzo, M. Ferrari, and V. Ferrari, “Augmented reality in neurosurgery: a systematic review,” *Neurosurg. Rev.*, vol. 40, no. 4, pp. 537–548, 2017.

[37] M. N. van Oosterom, H. G. van der Poel, N. Navab, C. J. H. van de Velde, and F. W. B. van Leeuwen, “Computer-assisted surgery: virtual-and augmented-reality displays for navigation during urological interventions,” *Curr. Opin. Urol.*, vol. 28, no. 2, pp. 205–213, 2018.

[38] M. Joshipura, C. Mock, and R. A. Gosselin, “Global Burden of Musculoskeletal Conditions,” in *Global Orthopedics*, Springer, 2020, pp. 9–11.

[39] R. H. Taylor *et al.*, “An image-directed robotic system for precise orthopaedic surgery,” *IEEE Trans. Robot. Autom.*, vol. 10, no. 3, pp. 261–275, 1994.

[40] F. Picard, A. H. Deakin, P. E. Riches, K. Deep, and J. Baines, “Computer assisted orthopaedic surgery: Past, present and future,” *Med. Eng. Phys.*, vol. 72, pp. 55–65, 2019.

[41] J. P. Van der List, H. Chawla, and A. D. Pearle, “Robotic-assisted knee arthroplasty: an overview,” *Am J Orthop*, vol. 45, no. 4, p. 202, 2016.

[42] L. Chenin, J. Peltier, and M. Lefranc, “Minimally invasive transforaminal lumbar interbody fusion with the ROSA TM Spine robot and intraoperative flat-panel CT guidance,” *Acta Neurochir. (Wien).*, vol. 158, no. 6, pp. 1125–1128, 2016.

[43] J. H. Lonner, J. R. Smith, F. Picard, B. Hamlin, P. J. Rowe, and P. E. Riches, “High degree of accuracy of a novel image-free handheld robot for unicondylar knee arthroplasty in a cadaveric study,” *Clin. Orthop. Relat. Res.*, vol. 473, no. 1, pp. 206–212, 2015.

[44] L. Joskowicz and E. J. Hazan, “Computer-Aided Orthopedic Surgery: Incremental Shift or Paradigm Change?,” in *Intelligent Orthopaedics*, Springer, 2018, pp. 21–30.

[45] Y. Yukawa, “Pedicle Screw Fixation in Cervical Spine,” in *Cervical Spine Surgery: Standard and Advanced Techniques*, Springer, 2019, pp. 449–454.

[46] L. P. Nolte, H. Visarius, E. Arm, F. Langlotz, O. Schwarzenbach, and L. Zamorano, “Computer-aided fixation of spinal implants,” *J. Image Guid. Surg.*, vol. 1, no. 2, pp. 88–93, 1995.

[47] A. Manbachi, R. S. C. Cobbold, and H. J. Ginsberg, “Guided pedicle screw insertion: techniques and training,” *Spine J.*, vol. 14, no. 1, pp. 165–179, 2014.

[48] N. Sugano, *Computer Assisted Orthopaedic Surgery for Hip and Knee: Current State of the Art in Clinical Application and Basic Research*. Springer, 2018.

[49] S. Kurtz, K. Ong, E. Lau, F. Mowat, and M. Halpern, “Projections of primary and revision hip and knee arthroplasty in the United States from 2005 to 2030,” *Jbjs*, vol. 89, no. 4, pp. 780–785, 2007.

[50] C. W. Jones and S. A. Jerabek, “Current role of computer navigation in total knee arthroplasty,” *J. Arthroplasty*, vol. 33, no. 7, pp. 1989–1993, 2018.

[51] L. Bai, J. Yang, X. Chen, Y. Sun, and X. Li, “Medical robotics in bone fracture reduction surgery: A review,” *Sensors*, vol. 19, no. 16, p. 3593, 2019.

[52] R. J. Lilly, D. M. Koueiter, K. C. Graner, G. P. Nowinski, J. Sadowski, and K. D. Grant, “Computer-assisted navigation for intramedullary nail fixation of intertrochanteric femur fractures: A randomized, controlled trial,” *Injury*, vol. 49, no. 2, pp. 345–350, 2018.

[53] H. Liu, E. Auvinet, J. Giles, and F. R. y Baena, “Augmented reality based navigation for computer assisted hip resurfacing: a proof of concept study,” *Ann. Biomed. Eng.*, vol. 46, no. 10, pp. 1595–1605, 2018.

[54] R. Mosheiff and A. Khoury, “Innovations in Fracture Reduction

Computer-Assisted Surgery," in *Fracture Reduction and Fixation Techniques*, Springer, 2018, pp. 43–49.

[55] B. Carl, M. Bopp, B. Saß, B. Voellger, and C. Nimsky, "Implementation of augmented reality support in spine surgery," *Eur. Spine J.*, vol. 28, no. 7, pp. 1697–1711, 2019.

[56] L. Joskowicz and E. J. Hazan, "Computer aided orthopaedic surgery: incremental shift or paradigm change?" Elsevier, 2016.

[57] I. Hacihaliloglu, "3D ultrasound for orthopedic interventions," in *Intelligent Orthopaedics*, Springer, 2018, pp. 113–129.

[58] M. Mitschke and N. Navab, "Recovering the X-ray projection geometry for three-dimensional tomographic reconstruction with additional sensors: Attached camera versus external navigation system," *Med. Image Anal.*, vol. 7, no. 1, pp. 65–78, 2003.

[59] N. Navab, S.-M. Heining, and J. Traub, "Camera augmented mobile C-arm (CAMC): calibration, accuracy study, and clinical applications," *IEEE Trans. Med. Imaging*, vol. 29, no. 7, pp. 1412–1423, 2009.

[60] R. H. Taylor, "Computer-integrated interventional medicine: A 30 year perspective," in *Handbook of Medical Image Computing and Computer Assisted Intervention*, Elsevier, 2020, pp. 599–624.

[61] I. S. Alam *et al.*, "Emerging intraoperative imaging modalities to improve surgical precision," *Mol. Imaging Biol.*, vol. 20, no. 5, pp. 705–715, 2018.

[62] J. H. Bong, H. Song, Y. Oh, N. Park, H. Kim, and S. Park, "Endoscopic navigation system with extended field of view using augmented reality technology," *Int. J. Med. Robot. Comput. Assist. Surg.*, vol. 14, no. 2, p. e1886, 2018.

[63] J. F. Hughes, A. Van Dam, J. D. Foley, M. McGuire, S. K. Feiner, and D. F. Sklar, *Computer graphics: principles and practice*. Pearson Education, 2014.

[64] J. Lee, K. Mekuria, T. Son, W. S. Jeong, J. W. Choi, and Y. Kim, "A Novel Noninvasive Patient-Specific Navigation Method for Orbital Reconstructive Surgery: A Phantom Study Using Patient Data," *Plast. Reconstr. Surg.*, vol. 143, no. 3, pp. 602e-612e, 2019.

[65] D. Rueckert and J. A. Schnabel, "Medical image registration," in *Biomedical image processing*, Springer, 2010, pp. 131–154.

[66] F. Alam, S. U. Rahman, S. Ullah, and K. Gulati, "Medical image registration in image guided surgery: Issues, challenges and research opportunities," *Biocybern. Biomed. Eng.*, vol. 38, no. 1, pp. 71–89, 2018.

[67] G. A. Gimeneza, L. Lopeza, P. P. Cespedesa, J. Limaa, and D. P. Pinto-Roaa, "3D Medical Image Registration using Mutual Information and

Scatter Search."

[68] M. Modat, "Efficient dense non-rigid registration using the free-form deformation framework." UCL (University College London), 2012.

[69] G. Song, J. Han, Y. Zhao, Z. Wang, and H. Du, "A review on medical image registration as an optimization problem," *Curr. Med. Imaging*, vol. 13, no. 3, pp. 274–283, 2017.

[70] S. Murlidaran, "A mixed reality framework for surgical navigation: approach and preliminary results," 2019.

[71] D. Zhi, "Towards estimating fiducial localization error of point-based registration in image-guided neurosurgery," *Biomed. Mater. Eng.*, vol. 26, no. s1, pp. S943–S949, 2015.

[72] Z. Min, H. Ren, and M. Q.-H. Meng, "Statistical model of total target registration error in image-guided surgery," *IEEE Trans. Autom. Sci. Eng.*, vol. 17, no. 1, pp. 151–165, 2019.

[73] R. F. Labadie, O. Majdani, and J. M. Fitzpatrick, "Image-guided technique in neurotology," *Otolaryngol. Clin. North Am.*, vol. 40, no. 3, pp. 611–624, 2007.

[74] H. Kato, "Inside ARToolKit," 2007.

[75] J. Fotouhi *et al.*, "Co-localized augmented human and X-ray observers in collaborative surgical ecosystem," *Int. J. Comput. Assist. Radiol. Surg.*, pp. 1–11, 2019.

[76] E. M. Carrillo, "Advanced tracking and image registration techniques for intraoperative radiation therapy," Universidad Carlos III de Madrid, 2017.

[77] V. Horsley and R. H. Clarke, "The structure and functions of the cerebellum examined by a new method.," *Brain*, vol. 31, no. 1, pp. 45–124, 1908.

[78] Z. Fan, G. Chen, J. Wang, and H. Liao, "Spatial position measurement system for surgical navigation using 3-D image marker-based tracking tools with compact volume," *IEEE Trans. Biomed. Eng.*, vol. 65, no. 2, pp. 378–389, 2017.

[79] A. M. Franz, T. Haidegger, W. Birkfellner, K. Cleary, T. M. Peters, and L. Maier-Hein, "Electromagnetic tracking in medicine—a review of technology, validation, and applications," *IEEE Trans. Med. Imaging*, vol. 33, no. 8, pp. 1702–1725, 2014.

[80] A. Sorriento *et al.*, "Optical and electromagnetic tracking systems for biomedical applications: a critical review on potentialities and limitations," *IEEE Rev. Biomed. Eng.*, vol. 13, pp. 212–232, 2019.

[81] H. A. Jaeger and P. Cantillon-Murphy, "Electromagnetic tracking using modular, tiled field generators," *IEEE Trans. Instrum. Meas.*, vol. 68, no.

12, pp. 4845–4852, 2019.

[82] J. Much, “Error classification and propagation for electromagnetic tracking,” *Master’s thesis, Tech. Univ. Munich, München, Ger.*, 2008.

[83] J. Wang, S. Song, H. Ren, C. M. Lim, and M. Q.-H. Meng, “Surgical Instrument Tracking By Multiple Monocular Modules and a Sensor Fusion Approach,” *IEEE Trans. Autom. Sci. Eng.*, no. 99, pp. 1–11, 2018.

[84] M. Kok, J. D. Hol, and T. B. Schön, “Using inertial sensors for position and orientation estimation,” *arXiv Prepr. arXiv1704.06053*, 2017.

[85] N. El-Sheimy and A. Youssef, “Inertial sensors technologies for navigation applications: state of the art and future trends,” *Satell. Navig.*, vol. 1, no. 1, p. 2, 2020.

[86] D. Česenek, “Inertial measurement unit modeling,” 2019.

[87] L. Ma *et al.*, “Three-dimensional augmented reality surgical navigation with hybrid optical and electromagnetic tracking for distal intramedullary nail interlocking,” *Int. J. Med. Robot. Comput. Assist. Surg.*, vol. 14, no. 4, p. e1909, 2018.

[88] K. Kim, M. Billinghurst, G. Bruder, H. B.-L. Duh, and G. F. Welch, “Revisiting trends in augmented reality research: A review of the 2nd decade of ISMAR (2008–2017),” *IEEE Trans. Vis. Comput. Graph.*, vol. 24, no. 11, pp. 2947–2962, 2018.

[89] G. Wang, L. Li, S. Xing, and H. Ding, “Intelligent HMI in Orthopedic Navigation,” in *Intelligent Orthopaedics*, Springer, 2018, pp. 207–224.

[90] H. Liao, N. Hata, S. Nakajima, M. Iwahara, I. Sakuma, and T. Dohi, “Surgical navigation by autostereoscopic image overlay of integral videography,” *IEEE Trans. Inf. Technol. Biomed.*, vol. 8, no. 2, pp. 114–121, 2004.

[91] H. Liao, T. Inomata, I. Sakuma, and T. Dohi, “3-D augmented reality for MRI-guided surgery using integral videography autostereoscopic image overlay,” *IEEE Trans. Biomed. Eng.*, vol. 57, no. 6, pp. 1476–1486, 2010.

[92] D. Peck, “Slipped capital femoral epiphysis: diagnosis and management,” *Am. Fam. Physician*, vol. 82, no. 3, pp. 258–262, 2010.

[93] J. Murgier, A. Espié, X. Bayle-Iniguez, E. Cavaignac, and P. Chiron, “Frequency of radiographic signs of slipped capital femoral epiphysiolysis sequelae in hip arthroplasty candidates for coxarthrosis,” *Orthop. Traumatol. Surg. Res.*, vol. 99, no. 7, pp. 791–797, 2013.

[94] B. A. Koutenaei *et al.*, “Improved screw placement for slipped capital femoral epiphysis (SCFE) using robotically-assisted drill guidance,” in *International Conference on Medical Image Computing and Computer-Assisted Intervention*, 2014, pp. 488–495.

[95] B. A. Koutenaei *et al.*, “Inertial Measurement Unit for Radiation-Free Navigated Screw Placement in Slipped Capital Femoral Epiphysis Surgery,” in *International Conference on Medical Image Computing and Computer-Assisted Intervention*, 2015, pp. 355–362.

[96] S. Andress *et al.*, “on-the-fly augmented reality for orthopaedic surgery using a multi-modal fiducial,” in *Medical Imaging 2018: Image-Guided Procedures, Robotic Interventions, and Modeling*, 2018, vol. 10576, p. 105760H.

[97] Y. Nakajima *et al.*, “Surgical tool alignment guidance by drawing two cross-sectional laser-beam planes,” *IEEE Trans. Biomed. Eng.*, vol. 60, no. 6, pp. 1467–1476, 2012.

[98] X. Zhang, G. Chen, and H. Liao, “High-quality see-through surgical guidance system using enhanced 3-D autostereoscopic augmented reality,” *IEEE Trans. Biomed. Eng.*, vol. 64, no. 8, pp. 1815–1825, 2016.

[99] C. Ma, G. Chen, X. Zhang, G. Ning, and H. Liao, “Moving-tolerant Augmented Reality Surgical Navigation System using Autostereoscopic 3D Image Overlay,” *IEEE J. Biomed. Heal. informatics*, 2018.

[100] R. Wang, M. Zhang, X. Meng, Z. Geng, and F.-Y. Wang, “3-D Tracking for Augmented Reality Using Combined Region and Dense Cues in Endoscopic Surgery,” *IEEE J. Biomed. Heal. informatics*, vol. 22, no. 5, pp. 1540–1551, 2017.

[101] L. Qian *et al.*, “Comparison of optical see-through head-mounted displays for surgical interventions with object-anchored 2D-display,” *Int. J. Comput. Assist. Radiol. Surg.*, vol. 12, no. 6, pp. 901–910, 2017.

[102] J. Magaraggia *et al.*, “A portable intra-operative framework applied to distal radius fracture surgery,” in *International Conference on Medical Image Computing and Computer-Assisted Intervention*, 2015, pp. 323–330.

[103] J. T. Liang *et al.*, “A fluorolaser navigation system to guide linear surgical tool insertion,” *Int. J. Comput. Assist. Radiol. Surg.*, vol. 7, no. 6, pp. 931–939, 2012.

[104] J. Walti, G. F. Jost, and P. C. Cattin, “A new cost-effective approach to pedicular screw placement,” in *Workshop on Augmented Environments for Computer-Assisted Interventions*, 2014, pp. 90–97.

[105] H. Liao, H. Ishihara, H. H. Tran, K. Masamune, I. Sakuma, and T. Dohi, “Precision-guided surgical navigation system using laser guidance and 3D autostereoscopic image overlay,” *Comput. Med. Imaging Graph.*, vol. 34, no. 1, pp. 46–54, 2010.

[106] Q. Lin, K. Cai, R. Yang, H. Chen, Z. Wang, and J. Zhou, “Development and validation of a near-infrared optical system for tracking surgical

instruments," *J. Med. Syst.*, vol. 40, no. 4, p. 107, 2016.

[107] B. He *et al.*, "A novel navigation system to guide metallic foreign body extraction," *Int. J. Comput. Assist. Radiol. Surg.*, vol. 11, no. 11, pp. 2105–2110, 2016.

[108] X. Chen *et al.*, "Development of a surgical navigation system based on augmented reality using an optical see-through head-mounted display," *J. Biomed. Inform.*, vol. 55, pp. 124–131, 2015.

[109] C. Zeng, W. Xing, Z. Wu, H. Huang, and W. Huang, "A combination of three-dimensional printing and computer-assisted virtual surgical procedure for preoperative planning of acetabular fracture reduction," *Injury*, vol. 47, no. 10, pp. 2223–2227, 2016.

[110] G. F. Jost, J. Walti, L. Mariani, S. Schaeren, and P. Cattin, "Inertial Measurement Unit–Assisted Implantation of Thoracic, Lumbar, and Sacral Pedicle Screws Improves Precision of a Freehand Technique," *World Neurosurg.*, vol. 103, pp. 11–18, 2017.

[111] I. Kovler *et al.*, "Haptic computer-assisted patient-specific preoperative planning for orthopedic fractures surgery," *Int. J. Comput. Assist. Radiol. Surg.*, vol. 10, no. 10, pp. 1535–1546, 2015.

[112] T. Doke, J. T. Liang, S. Onogi, and Y. Nakajima, "Fluoroscopy-based laser guidance system for linear surgical tool insertion depth control," *Int. J. Comput. Assist. Radiol. Surg.*, vol. 10, no. 3, pp. 275–283, 2015.

[113] H. Takai *et al.*, "Accuracy analysis of computer-assisted surgery for femoral trochanteric fracture using a fluoroscopic navigation system: Stryker ADAPT® system," *Injury*, vol. 49, no. 6, pp. 1149–1154, 2018.

[114] S. Pflugi *et al.*, "A cost-effective surgical navigation solution for periacetabular osteotomy (PAO) surgery," *Int. J. Comput. Assist. Radiol. Surg.*, vol. 11, no. 2, pp. 271–280, 2016.

[115] S. Pflugi *et al.*, "Augmented marker tracking for peri-acetabular osteotomy surgery," *Int. J. Comput. Assist. Radiol. Surg.*, vol. 13, no. 2, pp. 291–304, 2018.

[116] H. Wang, F. Wang, A. P. Y. Leong, L. Xu, X. Chen, and Q. Wang, "Precision insertion of percutaneous sacroiliac screws using a novel augmented reality-based navigation system: a pilot study," *Int. Orthop.*, vol. 40, no. 9, pp. 1941–1947, 2016.

[117] H. Ogawa, S. Hasegawa, S. Tsukada, and M. Matsubara, "A pilot study of augmented reality technology applied to the acetabular cup placement during total hip arthroplasty," *J. Arthroplasty*, vol. 33, no. 6, pp. 1833–1837, 2018.

[118] J. Herzog, R. Wendlandt, S. Hillbricht, R. Burgkart, and A.-P. Schulz, "Optimising the tip-apex-distance in trochanteric femoral fracture fixation

using the ADAPT-navigated technique, a longitudinal matched cohort study," *Injury*, 2019.

[119] G. F. Jost, J. Walti, L. Mariani, S. Schaeren, and P. Cattin, "Inertial Measurement Unit-Assisted Implantation of Pedicle Screws in Combination With an Intraoperative 3-Dimensional/2-Dimensional Visualization of the Spine," *Oper. Neurosurg.*, vol. 16, no. 3, pp. 326–334, 2018.

[120] Y. Jiang, H.-R. Wang, P.-F. Wang, and S.-G. Xu, "The Surgical Approach Visualization and Navigation (SAVN) System reduces radiation dosage and surgical trauma due to accurate intraoperative guidance," *Injury*, 2019.

[121] J. Ahn, H. Choi, J. Hong, and J. Hong, "Tracking Accuracy of a Stereo Camera-Based Augmented Reality Navigation System for Orthognathic Surgery," *J. Oral Maxillofac. Surg.*, 2019.

[122] J. Magaraggia *et al.*, "Design and evaluation of a portable intra-operative unified-planning-and-guidance framework applied to distal radius fracture surgery," *Int. J. Comput. Assist. Radiol. Surg.*, vol. 12, no. 1, pp. 77–90, 2017.

[123] S. Y. Vetter *et al.*, "Virtual guidance versus virtual implant planning system in the treatment of distal radius fractures," *Int. J. Med. Robot. Comput. Assist. Surg.*, vol. 14, no. 5, p. e1945, 2018.

[124] N. Mahmoud *et al.*, "On-patient see-through augmented reality based on visual SLAM," *Int. J. Comput. Assist. Radiol. Surg.*, vol. 12, no. 1, pp. 1–11, 2017.

[125] F. Liebmann *et al.*, "Pedicle screw navigation using surface digitization on the Microsoft HoloLens," *Int. J. Comput. Assist. Radiol. Surg.*, pp. 1–9, 2019.

[126] J. Wu *et al.*, "Novel laser positioning navigation to aid puncture during percutaneous nephrolithotomy: a preliminary report," *World J. Urol.*, vol. 37, no. 6, pp. 1189–1196, 2019.

[127] B. Carl, M. Bopp, B. Voellger, B. Saß, and C. Nimsky, "Augmented Reality in Transsphenoidal Surgery," *World Neurosurg.*, 2019.

[128] B. Carl, M. Bopp, B. Saß, and C. Nimsky, "Microscope-Based Augmented Reality in Degenerative Spine Surgery: Initial Experience," *World Neurosurg.*, 2019.

[129] J. T. Gibby, S. A. Swenson, S. Cvetko, R. Rao, and R. Javan, "Head-mounted display augmented reality to guide pedicle screw placement utilizing computed tomography," *Int. J. Comput. Assist. Radiol. Surg.*, vol. 14, no. 3, pp. 525–535, 2019.

[130] A. Elmi-Terander *et al.*, "Pedicle Screw Placement Using Augmented Reality Surgical Navigation with Intraoperative 3D Imaging: A First In-

Human Prospective Cohort Study," *Spine (Phila. Pa. 1976).*, vol. 44, no. 7, pp. 517–525, 2019.

[131] A. Amarillo, J. Oñativia, and E. Sanchez, "RoboTracker: Collaborative robotic assistant device with electromechanical patient tracking for spinal surgery," in *2018 IEEE/RSJ International Conference on Intelligent Robots and Systems (IROS)*, 2018, pp. 1312–1317.

Appendix A: Abstracts of Publications not discussed in the dissertation

A novel surgical navigation technology for placement of implants in slipped capital femoral epiphysis

Matthew E. Oetgen, Jody Litrenta, Bamshad Azizi Koutenaei, Kevin R. Cleary

Abstract

Background:

Fixation with a single screw is the recommended treatment for slipped capital femoral epiphysis (SCFE). Achieving optimal implant positioning can be difficult owing to the complex geometry of the proximal femur in SCFE. We assessed a novel navigation technology incorporating an inertial measurement unit to facilitate implant placement in an SCFE model.

Methods:

Guidewires were placed into 30 SCFE models, using a navigation system that displayed the surgeon's projected implant trajectory simultaneously in multiple planes. The accuracy and the precision of the system were assessed as was the time to perform the procedure.

Results:

Implants were placed an average of 5.3 mm from the femoral head center, with a system precision of 0.94 mm. The actual trajectory of the implant deviated from the planned trajectory by an average of $4.9° \pm 2.2°$. The total average procedure time was 97 seconds.

Conclusion:

The use of computer-based navigation in a SCFE model demonstrated good accuracy and precision in terms of both implant trajectory and placement in the center of the femoral head.

Robotic natural orifice transluminal endoscopic surgery (R-NOTES): Literature review and prototype system

Bamshad Azizi Koutenaei, Emmanuel Wilson, Reza Monfaredi, Craig Peters, Gernot Kronreif, Kevin Cleary

Abstract

In minimally invasive surgery methods such as laparoscopic surgery, surgical instruments are introduced through small incisions to minimize patient trauma and recovery times. To reduce the number of incisions, new techniques such as natural orifice transluminal endoscopic surgery (NOTES) have been proposed. Compared to laparoscopic surgery, the NOTES approach, which requires new technology and improved instruments, presents some unique challenges. Robotic NOTES (R-NOTES) could be an enabling technology for these procedures. In this paper, we first review relevant work in R-NOTES. We then present our work and the system architecture for an R-NOTES prototype system incorporating wireless command and control. The system was tested twice in swine animal studies.

Integrated and teleoperated system for wireless Robotic Natural Orifice Transluminal Endoscopic Surgery (R-NOTES)

Bamshad Azizi Koutenaei, R. Kojcev, Emmanuel Wilson, K. A. Gary, Nassir Navab, Kevin Cleary

Abstract

In minimally invasive surgery methods such as laparoscopic surgery, surgical instruments are introduced through small incisions to reduce patient trauma and shorten the recovery time. To reduce the number of incisions, new techniques such as single port surgery and Natural Orifice Transluminal Endoscopic Surgery (NOTES) have been proposed. In this work, the system architecture for a novel Robotic NOTES (R-NOTES) concept is described. As a step towards implementation, a small circular printed circuit board for motor control and wireless communication based on the ZigBee protocol was developed. This board was incorporated in a three Degree Of Freedom (DOF) robotic module called the MicroBot. An embedded application based on ZigBee was developed to control each DOF of the MicroBot. The prototype system was tested in a swine animal study.

Robot-assisted ultrasound imaging:

Overview and development of a parallel telerobotic system

Reza Monfaredi, Emmanuel Wilson, Bamshad Azizi koutenaei, Brendan Labrecque, kristen Leroy, James Goldie, Eric Louis, Daniel Swerdlow and Kevin Cleary

Abstract

Ultrasound imaging is frequently used in medicine. The quality of ultrasound images is often dependent on the skill of the sonographer. Several researchers have proposed robotic systems to aid in ultrasound image acquisition. In this paper we first provide a short overview of robot-assisted ultrasound imaging (US). We categorize robot-assisted US imaging systems into three approaches: autonomous US imaging, teleoperated US imaging, and human-robot cooperation. For each approach several systems are introduced and briefly discussed. We then describe a compact six degree of freedom parallel mechanism telerobotic system for ultrasound imaging developed by our research team. The long-term goal of this work is to enable remote ultrasound scanning through teleoperation. This parallel mechanism allows for both translation and rotation of an ultrasound probe mounted on the top plate along with force control. Our experimental results confirmed good mechanical system performance with a positioning error of < 1 mm. Phantom experiments by a radiologist showed promising results with good image quality.

Robotic Arm–Assisted Sonography:

Review of Technical Developments and Potential Clinical Applications

Daniel R. Swerdlow, Kevin Cleary, Emmanuel Wilson, Bamshad Azizi-Koutenaei and Reza Monfaredi

Abstract

OBJECTIVE. Ultrasound imaging requires trained personnel. Advances in robotics and data transmission create the possibility of telesonography. This review introduces clinicians to current technical work in and potential applications of this developing capability.

CONCLUSION. Telesonography offers advantages in hazardous or remote environments. Robotically assisted ultrasound can reduce stress injuries in sonographers and has potential utility during robotic surgery and interventional procedures.

Shoulder-Mounted Robot for MRI-guided arthrography: Accuracy and mounting study

R Monfaredi, E Wilson, R Sze, K Sharma, B Azizi, I Iordachita, K Cleary

Abstract

A new version of our compact and lightweight patient-mounted MRI-compatible 4 degree-of-freedom (DOF) robot for MRI-guided arthrography procedures is introduced. This robot could convert the traditional two-stage arthrography procedure (fluoroscopy-guided needle insertion followed by a diagnostic MRI scan) to a one-stage procedure, all in the MRI suite. The results of a recent accuracy study are reported. A new mounting technique is proposed and the mounting stability is investigated using optical and electromagnetic tracking on an anthropomorphic phantom. Five volunteer subjects including 2 radiologists were asked to conduct needle insertion in 4 different random positions and orientations within the robot's workspace and the displacement of the base of the robot was investigated during robot motion and needle insertion. Experimental results show that the proposed mounting method is stable and promising for clinical application.

Appendix B: A comparison of related works on CAOS

Table 1. A comparison of related works on CAOS.

Method	Year	Technology	Anatomy	Data	Human Use	University/ Company
[94]	2014	Robotic	Femur	CT ***	No	TUM
[95]	2015	Single IMU	Femur	Fluoroscopy images	No	TUM
Bamshad	2018	Dual IMU	Femur	Fluoroscopy images	No	TUM
[59]	2010	CAMC	Pedicle, vertebra, intramedular	X-ray image Video image	No	TUM
[96]	Arxiv	HMD-C_ARM	Femur	X-ray image	No	Johns Hopkins University
[97]	2013	2 Cross-Sectional Laser-Beams, 1 3D optical localizer	total hip arthroplasty (THA), PLIF spine	2 X-ray images	Yes	University of Tokyo
[98]	2016	3D IV display, optical tracking system	bones of hand, wrist and part of the arm	CT for bone reconstruction	Yes	Tsinghua University, China
[78]	2017	3-D Image Marker-based Tracking Tools	Bones of hand	CT	Yes	Tsinghua University
[99]	2018	Auto-stereoscopic 3D image overlay	Bone phantom	*******	No	Tsinghua University
[83]	2018	Multiple Monocular Modules and a Sensor Fusion Approach	Cadaver Head	CT	No	The Chinese University of Hong Kong
[102]	2016	combination of locally positioned markers and a small camera placed on the surgical instrument	Bone phantom, forearm cadaver	2 X-ray images	No	Siemens Healthcare GmbH

[103]	2012	dual-laser-guided fluoro- laser navigation system	Bone phantom	2 X-ray images	No	University of Tokyo
[105]	2010	3D autostereoscopic image overlay system integrated with a laser guidance device	Knee	CT	Yes	University of Tokyo
[108]	2015	Optical See-through Head Mounted Display (HMD)	Pelvis	CT	No	Shanghai Jiao Tong University
[109]	2016	3D printing and pararectus approach	Acetabular	CT	Yes	Southern Medical University of China
[110]	2017	IMU	thoracic, lumbar, sacral pedicle	CT	Human Cadaver	University of Basel
[111]	2015	3D haptic-based patient-specific pre-operative planning	Pelvic, bone	CT	No	Hebrew University of Jerusalem
[112]	2015	Fluoroscopy-based laser guidance system	Bone phantom	2 X-ray images	No	University of Tokyo
[113]	2018	ADAPT	Femur	CT and X-ray	Yes	Kumamoto Kinoh Hospital
[114], [115]	2016	2 IMUs	Pelvis, acetabular fragments	CT	No	University of Bern
[116]	2016	HMD and Optical Tracking	Pelvis	CT	No	Shanghai Jiao Tong University
[117]	2018	AR-HIP	hip	CT	Yes	Nissan Tamagawa Hospital, Tokyo
[118]	2019	ADAPT	Femur	CT	Yes	University Medical Centre Lübeck
[119]	2018	IMU	Spine	CT	Human	University of Basel

					Cadaver	
[120]	2019	Laser beam and C-Arm (SAVN)	Thoracic spine	CT, MRI	Yes	China Second Military Medical University
[121]	2019	Stereo camera navigation system with AR technology	Maxilla	CT	Yes	Sungkyunkwan University School of Medicine, Korea
[122]	2017	combination of locally positioned markers and a small camera placed on the surgical instrument	Forearm, bone	2 X-ray images	No	Friedrich-Alexander University
[87]	2017	Hybrid optical and EM tracking	Tibia and leg phantom	Fluoroscopy images	No	Tsinghua University
[123]	2019	Variable angle drill guide with attached markers and a camera	Sawbones model	CT	No	Heidelberg University
[53]	2018	optical see-through headsets (HMD)	Femur	----------	No	Imperial College
[125]	2019	HMD	Spine	CT	No	University of Zurich
[128]	2019	Microscope-based AR	Spine	CT	Yes	University of Marburg
[129]	2019	HMD	Lumbar	CT	No	George Washington University
[130]	2019	Optical Camera	Spine	CT	Yes	Karolinska Institutet, Sweden
[131]	2018	Electromechanical Tracking Device	Spine	CT	No	University of Navarra, Spain